

Silicon Revisited: Understanding pure phonon
anharmonicity and the effects on thermophysical
properties

Thesis by
Dennis Sungtae Kim

In Partial Fulfillment of the Requirements for the
degree of
Doctor of Philosophy

The logo for the California Institute of Technology (Caltech), featuring the word "Caltech" in a bold, orange, sans-serif font.

CALIFORNIA INSTITUTE OF TECHNOLOGY
Pasadena, California

2018
Defended August 21, 2017

© 2018

Dennis Sungtae Kim
ORCID: 0000-0002-5707-2609

All rights reserved

ABSTRACT

Phonons, quantized lattice vibrations, govern most of the thermophysical properties of solid-state materials such that understanding the temperature dependent lattice dynamics is of great technological importance. I performed inelastic neutron scattering measurements at the Spallation Neutron Source on ARCS, a wide-angular chopper spectrometer, to measure phonon dispersions and density of states over a wide range of temperatures. Large phonon anharmonicities manifested by phonon energy shifts and broadenings were observed in both measured phonon dispersions and phonon density of states. The sources of deviations from the simple harmonic model with temperature were elucidated using experimentally assessed lattice dynamics coupled with *ab initio* methods. Pure anharmonicity dominates the changes in lattice dynamics with temperature and therefore drive the entropy and thermophysical properties of thermal expansion and thermal conductivity. Crystal structure, anharmonicity, and nuclear quantum effects all play important roles in the thermal expansion of silicon, and a simple mechanical explanation is inappropriate. The quantum effect of nuclear vibrations is also expected to be important for thermal expansion of many materials. My experimental techniques capture the linewidth broadenings from phonon anharmonicity needed to calculate thermal conductivity. The methods developed for data reduction on single crystal inelastic neutron scattering data and predicting macroscopic quantities should also be useful for understanding microscopic mechanisms behind thermophysical properties for materials.

PUBLISHED CONTENT AND CONTRIBUTIONS

- ¹D. S. Kim, H. L. Smith, J. L. Niedziela, C. W. Li, D. L. Abernathy, and B. Fultz, “Phonon anharmonicity in silicon from 100 to 1500 K”, *Phys. Rev. B* **91**, 014307 (2015) [10.1103/PhysRevB.91.014307](https://doi.org/10.1103/PhysRevB.91.014307),
D.S.K participated in the conception of the project, prepared sample and conducted the experiment, reduced and analyzed the data, calculated the computational analysis, and conducted the writing of the manuscript.
- ²T. Lan, C. W. Li, O. Hellman, D. S. Kim, J. A. Muñoz, H. Smith, D. L. Abernathy, and B. Fultz, “Phonon quarticity induced by changes in phonon-tracked hybridization during lattice expansion and its stabilization of rutile TiO₂”, *Phys. Rev. B* **92**, 054304 (2015) [10.1103/PhysRevB.92.054304](https://doi.org/10.1103/PhysRevB.92.054304),
D.S.K participated and performed inelastic neutron scattering experiments on TiO₂ samples, as well as reduced and analyze low incident energy data.
- ³H. L. Smith, C. W. Li, A. Hoff, G. R. Garrett, D. S. Kim, F. C. Yang, M. S. Lucas, T. Swan-Wood, J. Y. Y. Lin, M. B. Stone, D. L. Abernathy, M. D. Demetriou, and B. Fultz, “Separating the configurational and vibrational entropy contributions in metallic glasses”, *Nature Physics* **28**, 373 (2017) [10.1038/nphys4142](https://doi.org/10.1038/nphys4142),
D.S.K participated in sample preparation, data analysis, and commented on the manuscript.
- ⁴D. S. Kim, O. Hellman, J. Herriman, H. L. Smith, J. Y. Y. Lin, N. Shulumba, J. L. Niedziela, C. W. Li, D. L. Abernathy, and B. Fultz, “A nuclear quantum effect with pure anharmonicity and the anomalous thermal expansion of silicon”, *Proc. Natl. Acad. Sci. U.S.A.* (2018) [10.1073/pnas.1707745115](https://doi.org/10.1073/pnas.1707745115),
D.S.K participated in the conception of the project, prepared sample and conducted the experiment, reduced and analyzed the data, calculated the computational analysis, and conducted the writing of the manuscript.

TABLE OF CONTENTS

Abstract	iii
Published Content and Contributions	iv
Table of Contents	v
List of Illustrations	vi
List of Tables	xiii
Chapter I: Introduction	1
Chapter II: Vibrational Entropy of Silicon	6
Chapter III: Thermal Expansion of Silicon	32
Chapter IV: Thermal Conductivity of Silicon	72
Chapter V: Final Remarks and Future Directions	96

LIST OF ILLUSTRATIONS

<i>Number</i>	<i>Page</i>
2.1 Phonon DOS curves of silicon, $g_T(\varepsilon)$, normalized to unity. Curves are offset for clarity.	8
2.2 Gaussian fitted 100 K measured DOS of silicon. Individual components are red, black curve is their sum.	10
2.3 Phonon dispersion and DOS of silicon at the quasiharmonic 100 K equilibrium volume (black solid line) scaled in energy to fit the experimental 100 K DOS (orange dotted line) from Fig. 2.1. The distinct features are labeled with their corresponding marker used in Fig. 2.4.	12
2.4 The negative of the fractional thermal shifts of the five features of the DOS: transverse acoustic (TA: red squares and purple circles), longitudinal acoustic (LA: blue pentagons), longitudinal acoustic and optical (LA/LO: green hexagons), and transverse and longitudinal optical modes (TO/LO: black triangles). The average between the shifts of the five features is shown by a dotted orange line.	14
2.5 Silicon phonon DOS of experimental measurements at 100 (blue) and 1500 (red) K (solid lines). A DOS at 1500 K (dotted line) is obtained from shifting and renormalizing the measured DOS at 100 K (Eq. 2.2).	16

- 2.6 Vibrational entropy of silicon from experimental phonon DOS curves (orange circles). Entropy from calculated DOS curves are also shown: harmonic (solid black line) and quasiharmonic (green triangle). The interpolated anharmonic approximation is shown (orange dotted line), as is the NIST JANAF entropy data (blue diamonds) [45]. Inset enlarges the high temperature region. 21
- 2.7 Enlargement of vibrational entropy from 1200 to 1500 K. The difference between experimental (orange circles) and quasiharmonic (green triangles) changes sign with temperature as quasiharmonic drifts further from the experimental points. 24
- 3.1 Experimental phonon dispersions of silicon. Inelastic neutron scattering data of silicon were measured on the ARCS time-of-flight spectrometer at (a) 100 K, (b) 200 K, (c) 300 K, (d) 900 K, (e) 1200 K, (f) 1500 K. The 4-D phonon dynamical structure factor, $S(\mathbf{q},\epsilon)$, were reduced, multiphonon subtracted, and “folded” into one irreducible wedge in the first Brillouin zone. Phonon dispersions are shown along high symmetry lines and through the zone (L–X). 34
- 3.2 Comparison between experimental, s-TDEP and quasiharmonic (QH) *ab initio* calculations throughout the Brillouin zone. (a)–(c), Phonon dispersions of silicon from harmonic, s-TDEP, and QH *ab initio* density functional theory calculations. The (0.75,0.25,0.25)-point is shown as a black circle marker for reference. (b),(c) Insets shows low-energy transverse acoustic modes. 35

- 3.3 Comparison between experimental, s-TDEP and quasiharmonic (QH) *ab initio* calculations throughout the Brillouin zone. (a) Density of fractional phonon energy shifts with temperature. The densities from all branches (s-TDEP: teal, QH: red) and densities from just the low transverse modes are offset and scaled for clarity. (b) The density of the 700 K s-TDEP. Notice the more negative peak consists of a majority of TA-modes. 39
- 3.4 Comparison between experimental, s-TDEP and quasiharmonic (QH) *ab initio* calculations throughout the Brillouin zone. Temperature-dependent phonon shifts, $(\varepsilon - \varepsilon_{100\text{K}})/\varepsilon_{100\text{K}}$, of the low-energy transverse modes at the (a) L, (b) X, (c) (0.75,0.25,0.25) r.l.u., and (d) K points. Experimental fits of phonon centroids with standard (1σ) error-bars from the present work are shown alongside calculated shifts and previously reported shifts [14]. 40
- 3.5 Phonon shifts and entropy differences from constant volume *ab initio* calculations. (a)–(f) Density of fractional shifts with temperature at constant volumes using the s-TDEP method. The mean (dashed color line), median (solid color line), and the 5th and 95th percentile (black solid lines) of the density are also shown. Calculations shown for: [(a),(d),(g)] 99% of 0 K volume, [(b),(h),(e)] 0 K volume, and [(c),(f),(i)] 101% of 0 K volume. Quasiharmonic predictions are the dashed zero-lines in (a)–(f). (g)–(i) Corresponding constant volume differences between the quasiharmonic (QH) and s-TDEP in free energies from vibrational entropy with temperature. 42

3.6	Calculated and experimental coefficients of linear thermal expansion in silicon. Calculated coefficients are from minimized free energies using Supporting Information Eq. 1 (s-TDEP: teal solid line, quasiharmonic (QH): red dashed line). Experimental values are shown as colored markers [7–10]. Inset shows calculations and experimental values at higher temperatures.	46
3.7	“Folded” inelastic neutron scattering data without (a) and with (b) multiphonon subtracted $S(\mathbf{q},\epsilon)$ at 300 K. (c) Scattering intensity and fitted spectrum at the X-point. Fitted peaks are shown as the red solid line. Grey circles are without [(a)] and black triangles with [(b)] multiphonon scattering subtracted. Black dashed line shows subtracted multiphonon scattering intensity.	48
3.8	Constant \mathbf{q} - $S(\mathbf{q},\epsilon)$ data at the X point for 100, 200, 300, 900, 1200, 1500 K. Data are black markers and fits are in orange.	50
3.9	Inelastic neutron scattering [(a)–(c)] and first principle calculations [(d)–(f)] of $S(\mathbf{q},\epsilon)$ at 300 K along momenta \mathbf{q} (X– Γ –X) in different Brillouin zones. Calculated $S(\mathbf{q},\epsilon)$ was corrected for instrument resolution and polarization effects to match the experiment conditions [25, 26].	52
3.10	Phonon DOS of Si from (thick line) experimental measurement at 100 K [21], and (thin line) approximated with Debye and Einstein models.	56

3.11	(a) Heat capacities from phonons approximated by Debye and Einstein models, using the six branches of Fig. 3.10. (b) Coefficient of thermal expansion, assuming all Grüneisen parameters were +1 except for TA modes set as -1.	57
3.12	a , Tetrahedral coordination around a central Si atom. b , four interconnected tetrahedra of the diamond cubic structure. Thick vertical lines are along a [111] direction.	61
3.13	Trends for silicons thermal expansion coefficient vs. temperature plotted for scalings of the ratio of transverse to longitudinal force constants between 0 and 2.8	62
3.14	Maximum negative thermal expansion coefficients taken from each trend in Fig. S5 plotted against the scaling factor, k , applied to the ratios of transverse to longitudinal force constants.	64
3.15	Volume as a function of temperature for silicon obtained from classical and quantum mechanical free energies.	65

- 4.1 Phonon linewidths from inelastic neutron scattering experiments.
 (a) Example of experimental phonon dispersions of silicon from inelastic neutrons scattering data of silicon. Data were measured on ARCS time-of-flight spectrometer at 300 K, and reduced, multiphonon subtracted and “folded” into one irreducible wedge in the first Brillouin zone. (b) Phonon scattering spectra determined at \mathbf{q} -point = (0.75, 0.25, 0.25) r.l.u.. Experimental data is shown as purple circle markers and best fit of peaks is in grey solid line. The longitudinal acoustic mode is highlighted as an example of phonon lineshape deconvolution. (c) Deconvoluted longitudinal acoustic mode phonon lineshape at \mathbf{q} -point = (0.75, 0.25, 0.25) r.l.u. at 300 K. 75
- 4.2 Temperature-dependence of phonon shifts and broadening of the (0.75,0.25,0.25) q -point with temperature. Experimental changes are shown as markers, and *ab initio* calculated linewidth thermal trends with anharmonicity in teal solid line, and quasi-harmonic approximation in red-dashed line. 77
- 4.3 *Ab initio* calculated phonon linewidths with temperature ($2\Gamma = 1/\tau$). (a) Temperature dependence of shifts and broadenings throughout the Brillouin zone. (b) A comparison between the s-TDEP and quasi-harmonic calculations at 300 K and 1500 K. 79

4.4	Brillouin zone averaged temperature-dependent phonon energies (a) and linewidths (b). Energies calculated from experimental fits from Table ?? are in purple circle markers and <i>ab initio</i> calculations of the s-TDEP (solid teal line) and quasiharmonic approximation (red dashed line) are also shown.	81
4.5	Spectral thermal conductivity ($\kappa(\epsilon)/\kappa_{\text{tot}}$) at 300 (a) and 1500 K (b). <i>Ab initio</i> calculated total spectral thermal conductivity of silicon at as a black dashed line. Mode dependent spectral functions are shown as the shaded area(TA: maroon and red, LA: blue, LO: green, and TO: black). (b) Comparison between s-TDEP (teal) and quasiharmonic (red) calculation of spectral thermal conductivity.	83
4.6	Temperature-dependent thermal conductivity of silicon. Phonon anharmonic <i>ab initio</i> calculations (s-TDEP) are shown as a solid teal line and the quasiharmonic model in red dashed line. Experimental points as markers [12, 34, 35].	84

LIST OF TABLES

<i>Number</i>	<i>Page</i>
2.1	
Calculated and measured Grüneisen parameters using constants at room temperature. See text for details on values and method of calculation.	18

Chapter 1

INTRODUCTION

Atoms, the building blocks for all materials, are always in motion, even at 0 K. The changes in the motion of nuclei affect the levels in energy and entropy of materials, which in turn change its properties. Due to an ever growing need for more efficient, cheaper, safer, and greener technologies, there is interest in understanding the relationship between the atomic motions and materials properties. The optimization of materials properties for a specific application will require a fundamental understanding of these relationships. Since all manufacturing processes or synthesis conditions are influenced by the presence of heat, the effect of atomic motion and their interactions on the materials properties will be profound.

Starting from the seminal Gibbs free energy ($G = E - TS + PV$) we can see that entropy, S , is always correlated to temperature, the heat. In many materials, especially for unary intrinsic semiconductors with a moderate band gap, atomic vibrations make up the majority of entropy as the atoms explore coordinate and momentum phase space [1]. Understanding how atomic vibrations affect bonding, electronic states, to bulk properties is the basis of this thesis. In other words, understanding the mechanisms behind changes in entropy, anomalous thermal expansion behavior, and thermal conductivity will result in a far greater control of the material's thermal engineering parameter space.

The work presented is important not only to understand thermal properties of silicon, but also to show experimental methods in understanding vibrational properties of materials in general. Validating computational methods to study thermal properties of materials could then lead to high throughput capabilities in developing and characterizing new materials.

The aim of this thesis work is to experimentally determine the temperature-dependent lattice dynamics and elucidate its effects on thermodynamic quantities and thermal transport properties. This work tests the limits of time-of-flight inelastic neutron scattering methods to determine all phonon central frequency shifts and linewidth broadenings with temperature in materials.

A first take on lattice dynamics is typically through an Einstein solid where a delta function for the density of states (DOS) is used to approximate the complexity of real solid-state materials. The Debye model, where phonon dispersions are assumed to have constant group velocity can predict the experimental low temperature T^3 -dependent heat capacity behavior. Due to the simplicity of this one fitting parameter model it is still heavily used today despite the lack of accuracy. The accuracy, however, can further be improved through a normal mode analysis. These harmonic phonons do capture significant portions of thermophysical properties, but are still non-interacting with infinite lifetimes. In this approximation phonons would never result in thermal expansion, thermal conductivity or any interactions with other quasiparticles. A popular approach to approximate temperature effects is through the quasiharmonic model (QH). This assume harmonic oscillators with frequencies renormalized to account for the thermal expansion. Generally, this is physically intuitive as large distances

between atomic nuclei may lead to decreased forces based on the electronic bonding. But intuition is not always evidence for reality. Until recently, the ability to accurately include pure anharmonicities, phonon-phonon interactions, through *ab initio* methods throughout the Brillouin zone were unavailable or difficult to assess. But by now in 2017, many systems including “highly” anharmonic systems can be simulated.

The material of study in this thesis is silicon. Silicon, is the third most abundant element on our Earths crusts and the stable phase at atmospheric pressures is the diamond-cubic crystal structure ($Fd\bar{3}m$). This material is known for its strong covalent atomic bonds and in-direct band-gap of 1.12 eV. This band-gap is the initial reason for silicon’s ubiquitous use in modern semiconductor technologies, photovoltaics, thermoelectrics, nanomechanics, and batteries. Understanding the thermal properties of silicon because of its wide use in modern technology is of great importance. It also serves as a perfect test case material for experimental and theoretical comparisons due to the plethora of measured thermal quantities and synthesis capabilities already available.

The title of this thesis emphasizes the need to reexamine revisit the “solved” problem of atomic vibration effects on the thermophysical properties of silicon. I found that silicon is more complex than previously explained. I show that inelastic neutron scattering coupled with *ab initio* methods are perfect complements to studying lattice dynamics of materials. I believe advancements in both experimental and computational methods create better opportunities for applications oriented materials discovery and optimization. With the un-

equivocal importance and impact silicon has had on our technologically centric society, it behooves us to fully understand this important material. For brevity, full derivations are not presented in this thesis nor are in-depth descriptions to neutron scattering, lattice dynamics, and *ab initio* methods. Rigorous and more thoughtful derivations can be found in classical and emerging textbooks and references therein [1–7].

References

- ¹B. Fultz, *Phase transitions in materials* (Cambridge Univ. Press, Cambridge, Jan. 2014).
- ²G. Grimvall, *The electron-phonon interaction in metals*, Selected topics in solid state physics 16 (North-Holland Pub. Co. : sole distributors for the U.S.A. and Canada, Elsevier North-Holland, Amsterdam ; New York, 1981).
- ³G. L. Squires, *Introduction to the Theory of Thermal Neutron Scattering* (Cambridge Univ. Press, Cambridge, Mar. 2012).
- ⁴J. M. Ziman, *Elements of Advanced Quantum Theory* (Cambridge University Press, 1969).
- ⁵M. T. Dove, *Introduction to Lattice Dynamics* (Cambridge University Press, Oct. 1993).
- ⁶D. Chandler, *Introduction to modern statistical mechanics* (Oxford University Press, 1987).
- ⁷H. B. Callen, *Thermodynamics and an introduction to thermostatistics* (Wiley, 1985).

Chapter 2

VIBRATIONAL ENTROPY OF SILICON

Abstract from “Phonon anharmonicity in silicon from 100 to 1500 K” [1]:

Inelastic neutron scattering was performed on silicon powder to measure the phonon density of states (DOS) from 100 to 1500 K. The mean fractional energy shifts with temperature of the modes were $\langle \Delta \varepsilon_i / \varepsilon_i \Delta T \rangle = -0.07$ giving a mean isobaric Grüneisen parameter of $+6.95 \pm 0.67$, significantly different from the isothermal parameter of $+0.98$. These large effects are beyond the predictions from quasiharmonic models using density functional theory (DFT) or experimental data, demonstrating large effects from phonon anharmonicity. At 1500 K the anharmonicity contributes $0.15 k_B$ /atom to the vibrational entropy, compared to the $0.03 k_B$ /atom from quasiharmonicity. Excellent agreement was found between the entropy from phonon DOS measurements and the reference JANAF thermodynamic entropy from calorimetric measurements.

Understanding finite-temperature thermodynamics requires the, at times elusive, entropy. Phonons are responsible for most of the entropy of materials at modest temperatures. The phonon entropy, or vibrational entropy, can be estimated with a set of fixed phonon frequencies in the harmonic approximation, but these results are usually too inaccurate for thermodynamic predictions of phase stability at elevated temperatures [1]. Changes in phonon frequencies with temperature are generally important for calculating thermodynamic functions [2], but our understanding of high temperature behavior is still emerging. Such studies require phonon spectra at high T , for which there are few experimental data.

The thermal properties of silicon are of importance for silicon-based electronics, nano-mechanics, photovoltaics, thermoelectrics, and batteries [3–11]. Some of the nonharmonic behavior of a material is expected to originate from “quasiharmonic” thermal softening (reduction in frequency) of phonons, where the phonon entropy increases as the material expands against its bulk modulus. Anharmonicity from phonon-phonon interactions causes further phonon softening without thermal expansion and can account for a substantial part of the entropy of materials at high temperatures. Anharmonic phonon-phonon interactions also shorten the lifetimes of phonons, causing broadenings in the phonon spectrum and a finite phonon mean free path for thermal transport.

The lattice dynamics of silicon has attracted ongoing attention owing to its anomalous thermal expansion, which changes from negative to positive at low temperatures. Phonon dispersions of silicon have been reported, as have phonon densities of states (DOS), thermal properties and mode Grüneisen pa-

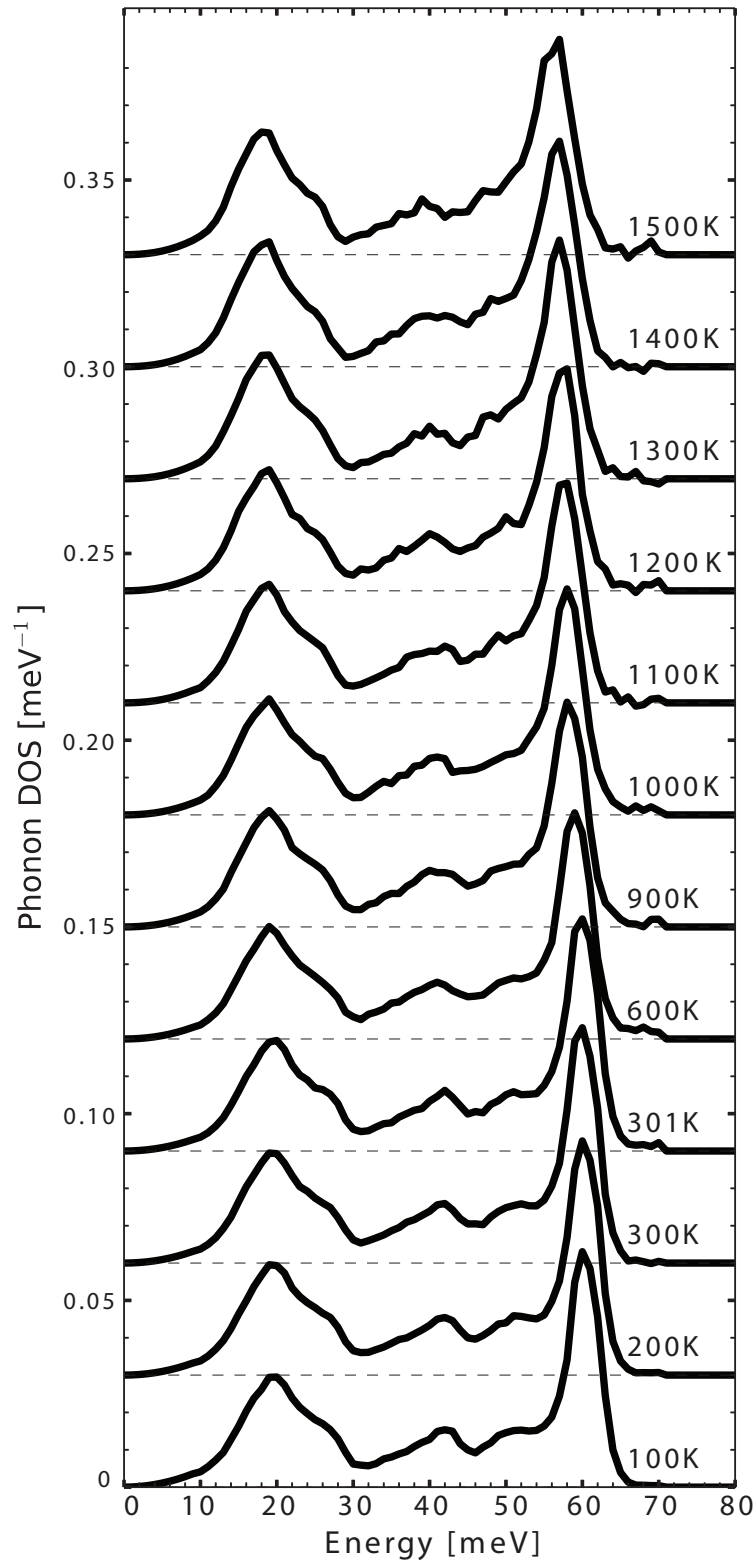


Figure 2.1: Phonon DOS curves of silicon, $g_T(\epsilon)$, normalized to unity. Curves are offset for clarity.

rameters [12–17]. The work with density functional theory (DFT) on silicon includes one of its earliest successes for determining the crystal structure of a solid at elevated temperatures [18]. Experimental work has employed inelastic neutron scattering (INS) and Raman spectroscopy up to 300 K and to high pressures [12–14, 19–23]. These studies assessed and correctly described the low temperature lattice dynamics, but to our knowledge there has not been a study of phonons above 700 K in silicon by inelastic neutron scattering. Measurements at higher temperatures are important for assessing phonon anharmonicity, which is also pertinent to thermal conductivity at all temperatures.

Inelastic neutron scattering (INS) spectra were obtained with ARCS [24] a time-of-flight Fermi chopper spectrometer at the Spallation Neutron Source at Oak Ridge National Laboratory, using an incident energy of 97.5 meV and an oscillating radial collimator to reduce background and multiple scattering [25]. Silicon of 99.9999% purity was pulverized, and 7.9 g of powder with an effective sample thickness of 6.0 mm was contained in an aluminum sachet and mounted in a closed-cycle helium refrigerator for measurements at temperatures 100, 200, and 300 K. Similar sachets made of niobium foil were mounted in a low-background electrical resistance vacuum furnace for measurements at temperatures 301, 600, 900, 1000, 1100, 1200, 1300, 1400, and 1500 K. Backgrounds were measured on empty sachets in the same sample environment at corresponding temperatures. Time-of-flight neutron data were reduced with the standard software packages in the procedures for the ARCS instrument as described previously [26–28]. Data reduction included subtraction of the background, and corrections for multiple scattering and multiphonon scatter-

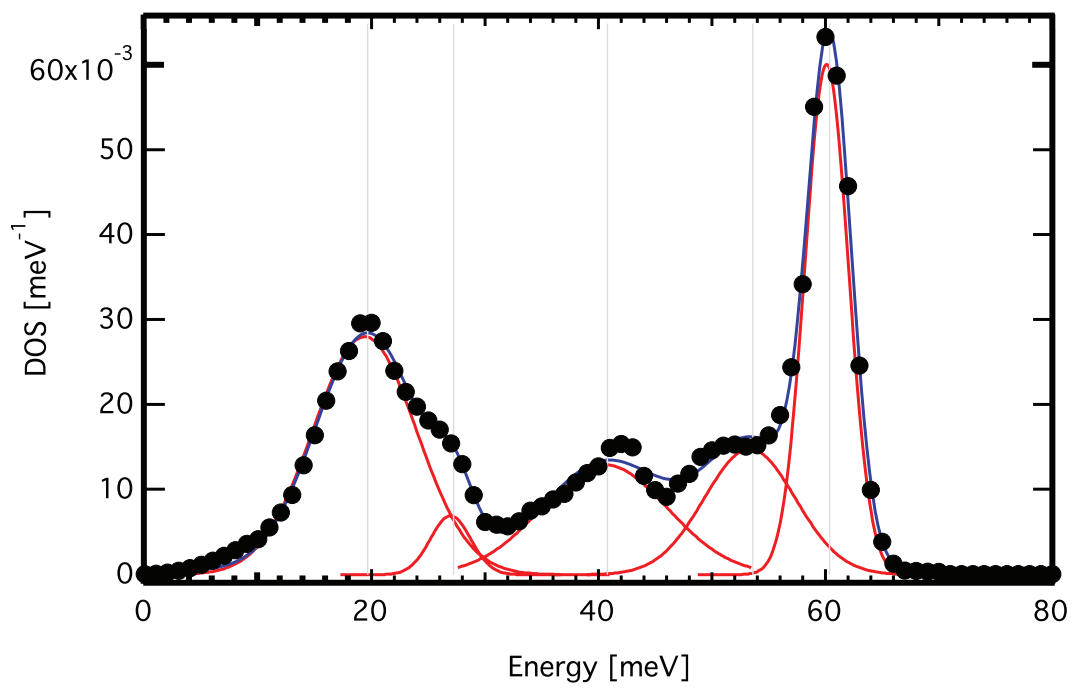


Figure 2.2: Gaussian fitted 100 K measured DOS of silicon. Individual components are red, black curve is their sum.

ing. Because silicon is a coherent scatterer, averages over a wide range of momentum transfer ($2\text{-}12 \text{ \AA}^{-1}$) were used to obtain the phonon DOS curves presented in Fig. 2.1. Successful background subtraction is indicated by the close similarity of the room temperature measurements in both the closed-cycle refrigerator and the electrical resistance furnace (300 and 301 K).

Ab-initio density functional theory (DFT) and density functional perturbation theory (DFPT) calculations were performed with the VASP package [29–33]. The generalized gradient method was used with PBE exchange correlation functionals [34, 35] for projector augmented wave pseudopotentials [36, 37] and a plane wave basis set. All calculations used a kinetic energy cutoff of 500 meV, a direct supercell of 216 atoms, and a $2 \times 2 \times 2$ k -point grid. The energy cutoffs, k -point density, and configurations were converged to within 5 meV/atom. The phonon eigenenergies were computed through DFPT [33, 38]. The free energy was calculated as

$$F(T, V) = E_0(V) + \int d\varepsilon g(\varepsilon) \left(\frac{\varepsilon}{2} + k_B T \ln(1 - e^{-\varepsilon/k_B T}) \right). \quad (2.1)$$

The quasiharmonic approximation (QHA) calculations were obtained by minimizing the free energy $F(T, V\{a_0\})$ of Eq. 2.1 with respect to the volume of the supercell. Ground state energies, $E_0(V)$, were calculated separately and self-consistently for each volume, and the DOS, $g(\varepsilon)$, were calculated with the specific lattice parameter, a_0 , that produced the minimized volume.

A sharp cutoff of the phonon spectrum occurs at 67 meV. The phonon DOS are near zero well above this cutoff, indicating the success of the cor-

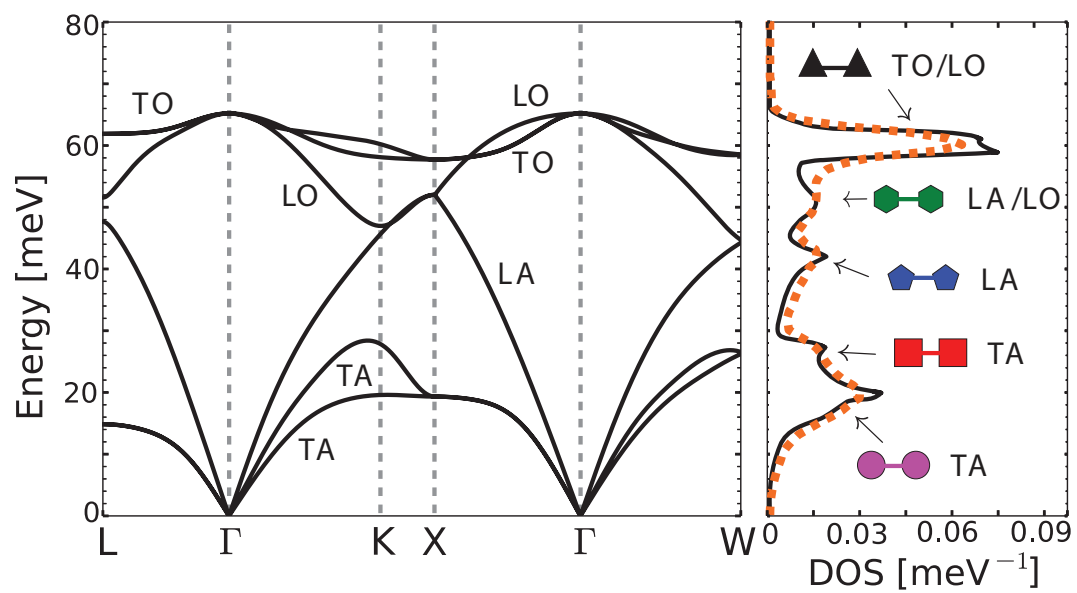


Figure 2.3: Phonon dispersion and DOS of silicon at the quasiharmonic 100 K equilibrium volume (black solid line) scaled in energy to fit the experimental 100 K DOS (orange dotted line) from Fig. 2.1. The distinct features are labeled with their corresponding marker used in Fig. 2.4.

rections for background, multiple scattering, and multiphonon scattering. Figure 2.1 shows that the phonon DOS go through a systematic thermal softening (decrease in phonon energy) and thermal linewidth broadening with increasing temperature. The DOS curves contain five distinct features caused by Van Hove singularities which were fitted to gaussians with temperature. An example of peak fits are shown in Fig. 2.2.

At 300 K, two transverse acoustic modes between 10 and 30 meV give the peak near 18 meV and the shoulder near 26 meV. The two features between 30 meV and 55 meV are from longitudinal acoustic and optical modes, respectively. Finally, the higher energy feature around 60 meV is from transverse and longitudinal optical modes. The high-energy optical modes centered around 60 meV show the largest thermal shift of approximately 4 meV between 100 and 1500 K, but the largest fractional changes, $\Delta\varepsilon_i/\varepsilon_i$, are found for the low-energy transverse acoustic modes from 10 to 30 meV. The negative fractional shifts of the five features are shown in Fig. 2.4. Fractional shifts agree within $\pm 1\%$ of the average fractional shift. This uniform trend might seem indicative of a simple quasiharmonic behavior, but the magnitude of the shift proves too large.

The measured DOS agree strongly with the calculations and allow for the identification of the five distinct features in the DOS corresponding to the specific branch or branches in the silicon dispersion relations as seen in Fig. 2.3. The phonon dispersion and DOS (Fig. 2.3) were calculated in the QHA at the 100 K equilibrium volume and scaled in energy to fit the 100 K measured DOS. Each branch was labeled and identified according to previously reported

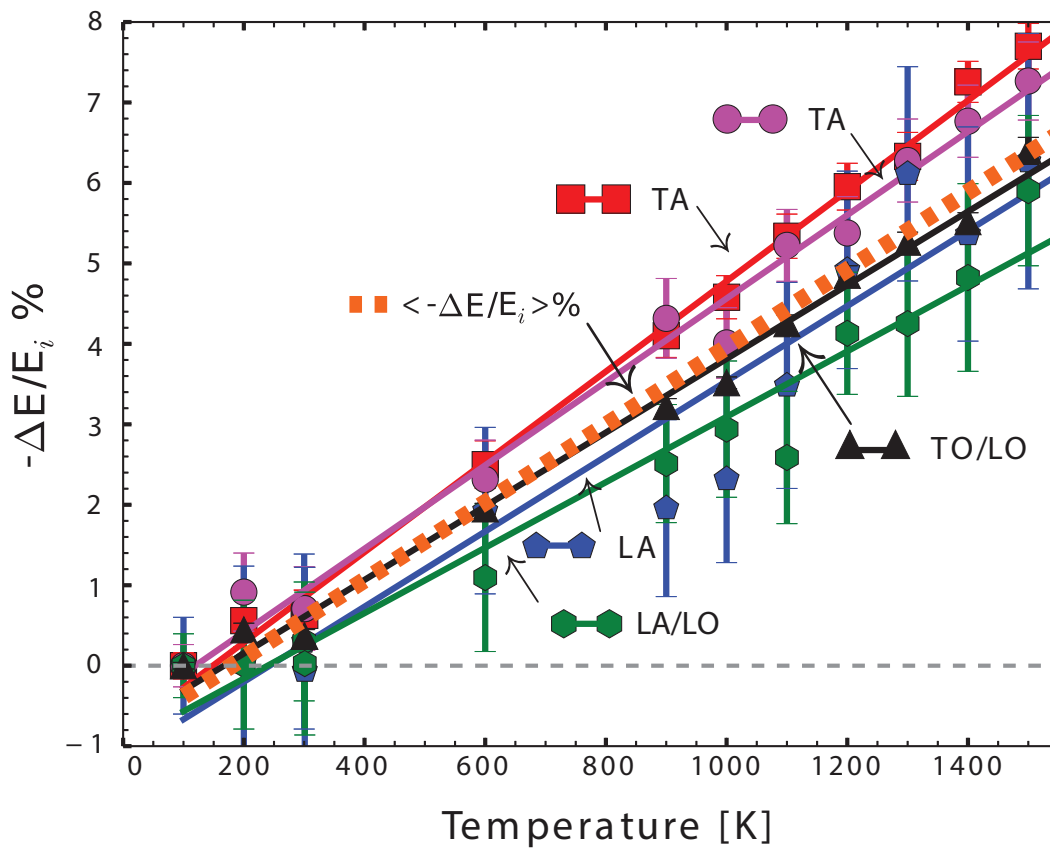


Figure 2.4: The negative of the fractional thermal shifts of the five features of the DOS: transverse acoustic (TA: red squares and purple circles), longitudinal acoustic (LA: blue pentagons), longitudinal acoustic and optical (LA/LO: green hexagons), and transverse and longitudinal optical modes (TO/LO: black triangles). The average between the shifts of the five features is shown by a dotted orange line.

methods and results [12, 39]. The self-similarity of the phonon DOS at elevated temperatures is shown in Fig. 2.5. Here the phonon DOS measured at 100 K was rescaled in energy and normalized to unity. The self-similarity of the phonon DOS at elevated temperatures is shown in Fig. 2.5. Here the phonon DOS measured at 100 K was rescaled in energy and normalized to unity.

$$g'(\varepsilon) = g_{100\text{K}}([1 - 3\alpha_T\bar{\gamma}_T(T - 100)]\varepsilon) \quad (2.2)$$

The rescaled phonon DOS, $g'(\varepsilon)$, is shown with the experimental DOS curve for 1500 K. The thermal expansion coefficient, α , and isobaric Grüneisen parameter are defined later in the text (Eq. 2.6). The two curves are in good coincidence, although the thermal broadening of the longitudinal peak at 56 meV is evident.

In the quasiharmonic approximation, the minimization of the free energy of Eq. 2.1 gives γ_i , the mode Grüneisen parameter

$$\gamma_i \equiv -\frac{V}{\varepsilon_i} \frac{\partial \varepsilon_i}{\partial V} \quad (2.3)$$

defined as the fractional shift of energy of phonon mode i per fractional shift in volume. There have been many studies defining the Grüneisen parameter as mode specific [14, 17, 40], but from the uniform thermal behavior of the phonons in the whole Brillouin zone, we present a mean Grüneisen parameter in Table. 2.1, defined as

$$\bar{\gamma} = -\left\langle \frac{V}{\varepsilon_i} \frac{\Delta \varepsilon_i}{\partial V} \right\rangle = -\left\langle \frac{\partial \ln \varepsilon_i}{\partial \ln V} \right\rangle \quad (2.4)$$

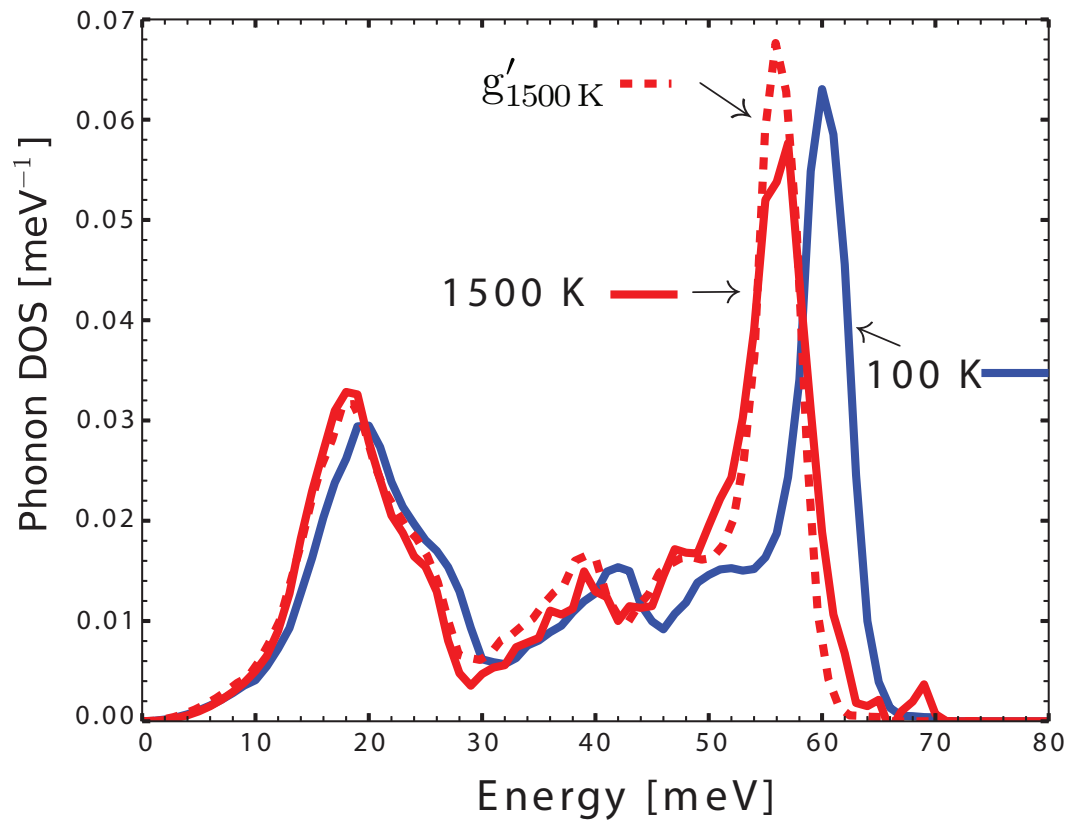


Figure 2.5: Silicon phonon DOS of experimental measurements at 100 (blue) and 1500 (red) K (solid lines). A DOS at 1500 K (dotted line) is obtained from shifting and renormalizing the measured DOS at 100 K (Eq. 2.2).

The isothermal ($\bar{\gamma}_P$) and isobaric ($\bar{\gamma}_T$) Grüneisen parameters are defined as

$$\bar{\gamma}_P = -\frac{1}{3\alpha(T)} \left\langle \frac{\partial \ln \varepsilon_i}{\partial V} \right\rangle \Big|_T \frac{\partial V}{\partial T} = B_T \left\langle \frac{\partial \ln \varepsilon_i}{\partial P} \right\rangle \Big|_T \quad (2.5)$$

$$\bar{\gamma}_T = -\frac{1}{3\alpha(T)} \left\langle \frac{\partial \ln \varepsilon_i}{\partial T} \right\rangle \Big|_P \quad (2.6)$$

$$\bar{\gamma}_T = -\frac{1}{3\alpha(T)} \left(\left\langle \frac{\partial \ln \varepsilon_i}{\partial V} \right\rangle \Big|_T \frac{\partial V}{\partial T} + \left\langle \frac{\partial \ln \varepsilon_i}{\partial T} \right\rangle \Big|_V \right) \quad (2.7)$$

$$\bar{\gamma}_T = \bar{\gamma}_P - \frac{1}{3\alpha(T)} \left\langle \frac{\partial \ln \varepsilon_i}{\partial T} \right\rangle \Big|_V \quad (2.8)$$

The isothermal and isobaric parameters describe the phonon energy shifts from effects of temperature and volume, where $\alpha(T)$ is the coefficient of linear thermal expansion and B_T is the bulk modulus. The experimental phonon shifts shown in Fig. 2.4 were used to obtain $\bar{\gamma}_T$ with Eq. 2.6, whereas all of the QHA parameters used phonon energy shifts from the differences in DFPT calculated DOS of the change in volume that minimized the free energy (Eq. 2.1). From Eq. 2.8, $\bar{\gamma}_T$ contains not only a contribution from the volume-dependent phonon frequency shifts, the “quasi-harmonic” contribution, but also a second term from a pure temperature dependence, the “anharmonic” contribution. The calculated isobaric and isothermal parameters were normalized with room temperature thermal expansion coefficients for consistency. Coefficients of linear thermal expansion, $\alpha(T)$, were obtained from reported values of thermal expansion and lattice constants [41, 42]. Our experimental isobaric parameter ($\bar{\gamma}_P$) was calculated using Eq. 2.5 with phonon shifts from high pressure Raman spectroscopy measurements reported by Weinstein and Piermarini [23].

Table 2.1: Calculated and measured Grüneisen parameters using constants at room temperature. See text for details on values and method of calculation.

	Experimental	Calculated in the QHA
$\bar{\gamma}$	-	1.00 ± 0.60
$\bar{\gamma}_T$	7.00 ± 0.67	1.102 ± 0.72
$\bar{\gamma}_P$	0.98	-
γ	0.367	-

Note: Errors bars were calculated from the differences in peak shifts of the five features.

The thermodynamic Grüneisen parameter γ is defined as

$$\gamma = \frac{3\alpha V_0 B_T}{C_V} \quad (2.9)$$

and is listed in Table 2.1. It was evaluated with $B_T = 0.9784 \times 10^{11}$ Pa [43], $\alpha = 2.59 \times 10^{-6}$ K⁻¹ [43], and the classical result of heat capacity [1], $C_V = 25$ J/(mol K). Table 2.1 shows a large discrepancy between the $\bar{\gamma}_T$ from the phonon measurements and the Grüneisen parameters from volume expansion.

In the present work we measured phonon DOS curves on high purity silicon powder using a direct geometry inelastic neutron spectrometer and investigated the phonon DOS with DFT. We found that the thermal changes in phonon frequencies were a factor of seven larger than expected from the quasi-harmonic model, indicating a large effect from phonon anharmonicity. The thermal broadening of features in the phonon spectrum also indicates anharmonicity.

To first order, the phonon DOS is the only function needed to obtain the vibrational entropy [1, 44]

$$S_{vib}(T) = 3k_B \int d\varepsilon g(\varepsilon) [(n+1) \ln(n+1) - n \ln(n)] \quad (2.10)$$

The entropy $S_{vib}(T)$ obtained from each measured DOS at temperature T , $g(\varepsilon)(T)$, is shown by orange circles in Fig. 2.6. To obtain a continuous curve, we also calculated the entropy with rescaled DOS curves from Eq. 2.2, using the experimental $\bar{\gamma}_T = 7.0$ from Table 2.1. An *ab initio* calculation of a DOS at 0 K is used with Eq. 3.8 to obtain a harmonic entropy for all temperatures. For the calculated results in the QHA, the *ab initio* DOS with thermal expansion were

evaluated. At the highest measured temperature of 1500 K, we find that the anharmonic contribution to entropy is $0.15 k_B/\text{atom}$, which is a factor of five larger than the quasiharmonic entropy contribution of $0.03 k_B/\text{atom}$. Finally, the total entropy from the NIST JANAF database [45] is shown in Fig. 2.6.

At all temperatures, the vibrational entropy $S_{vib}(T)$ obtained from the experimental phonon DOS measurements is in excellent agreement with the total entropy from the JANAF tables (Fig. 2.6). The agreement to within approximately 1% is striking, especially considering that the JANAF tables were assessed from calorimetric measurements, and our $S_{vib}(T)$ was obtained by counting phonons. The JANAF entropy is slightly higher than the phonon entropy at high temperatures suggesting an additional contribution, but the reliability of this difference is not yet understood. The contribution from electron excitations is probably negligible, and we also expect the phonon spectrum will be little affected by adiabatic electron-phonon coupling [1, 44, 46–48].

A harmonic model accounts for most of the entropy of silicon at modest temperatures, but the error at high temperatures is thermodynamically significant. The first correction from the quasiharmonic approximation is small because the bulk modulus is modest, and the thermal expansion is small for strongly covalently bonded atoms [14]. Both the measured and calculated mode-specific Grüneisen parameters have variations but are approximately 1 at elevated temperatures [17, 49]. Prior calculations of temperature-dependent Grüneisen parameters in the quasiharmonic approximation also do not exceed 1 [14]. Much of the previous interest in the lattice dynamics of silicon was centered on its peculiar thermal expansion at cryogenic temperatures. At low tem-

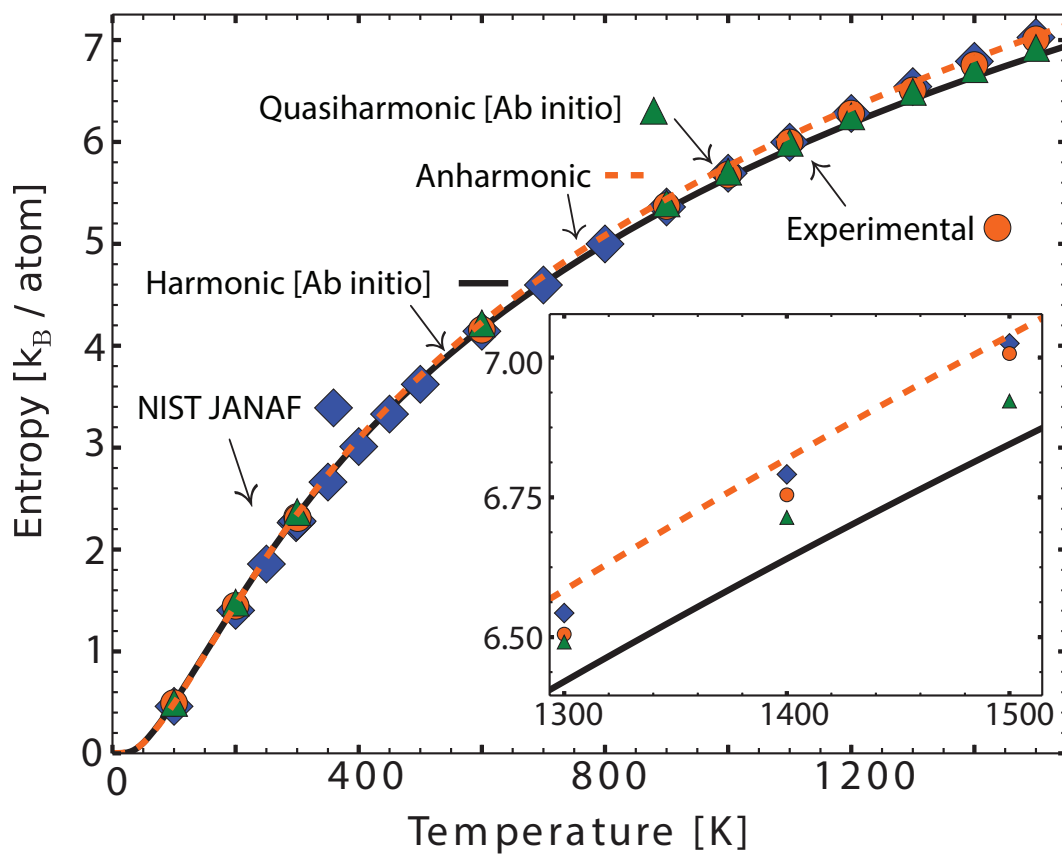


Figure 2.6: Vibrational entropy of silicon from experimental phonon DOS curves (orange circles). Entropy from calculated DOS curves are also shown: harmonic (solid black line) and quasiharmonic (green triangle). The interpolated anharmonic approximation is shown (orange dotted line), as is the NIST JANAF entropy data (blue diamonds) [45]. Inset enlarges the high temperature region.

peratures and high pressures, the quasiharmonic approximation has predicted accurate thermophysical behavior [14, 17, 20]. The quasiharmonic model can predict the thermal expansion at low temperatures and give results that are approximately accurate at high temperatures [50]. The low-energy transverse modes in the open diamond cubic crystal structure have been suggested as the source of the low temperature negative thermal expansion [20, 51, 52], but the mechanistic details were not fully understood, and are addressed in [cite] next chapter. Nevertheless, it is possible that the open-ness of the diamond cubic structure may also be responsible for the anharmonicity and low thermal expansion of silicon when all of the phonon modes are highly populated (above 800 K).

Thermal expansion is not a validation of the quasiharmonic model, as it predicts phonon shifts that are in error by an order of magnitude when actual values of thermal expansion are used, as seen by the discrepancy of the experimental and calculated $\bar{\gamma}_T$ in Table 2.1 and by the tiny phonon shifts predicted by the quasiharmonic model (e.g., [50]). The failure of the quasiharmonic approximation at high T stems from the assumptions that phonons are non-interacting. Thermal broadening is evident in the peak from longitudinal acoustic modes at 39 meV and longitudinal optic modes at 56 meV at high temperatures. Although lifetime broadening has no effect on the vibrational entropy to first order, we should expect that other anharmonic corrections to the phonon self energy from the cubic and quartic parts of the phonon potentials may be important [44]. This is most evident in the differences between $\bar{\gamma}_P$ and $\bar{\gamma}_T$ in Table 2.1. The second term in Eq. 2.8 for $\bar{\gamma}_T$, which gives the pure

temperature dependence of the phonon energy, is much larger than the first term from the quasiharmonic contribution. This pure anharmonicity dominates the non-harmonic thermodynamics of silicon at high temperatures, where 80% of the deviation from the harmonic model is from pure anharmonicity. If the phonon shifts (Fig. 2.4) were only dependent on volume changes and excluded temperature effects, the mode Grüneisen parameter ($\bar{\gamma}$) would have a value of around 4.4 when using experimental lattice parameters [41, 42]. This is more than a factor of four larger than the previously measured isothermal parameters (γ_P) found in Table 2.1 showing the need to differentiate the isothermal and isobaric parameters. The experimental points were obtained with Eq. 3.8, which was derived for non-interacting harmonic or quasi-harmonic phonons. With phonon lifetime broadening, there is a net shift of spectral weight to higher frequencies, lowering the apparent vibrational entropy. A small correction for this effect was suggested recently [2], and using this correction for the thermal broadening of the present data would give an upward shift of the experimental points in Fig. 2.6 by $0.015 k_B/\text{atom}$ at 1500 K, but less at lower temperatures.

At high temperatures (Fig 2.7) the problem is even less well understood because phonon spectra have only become available with the work reported in the present manuscript. What we show is that the quasiharmonic model is unreliable at high temperatures. Even though the quasiharmonic model gives thermal expansion results that are reasonable, the phonon energy shifts with temperature from anharmonicity are a factor of 7 larger than the thermal shifts from quasiharmonicity. This is new and is directly pertinent to both thermody-

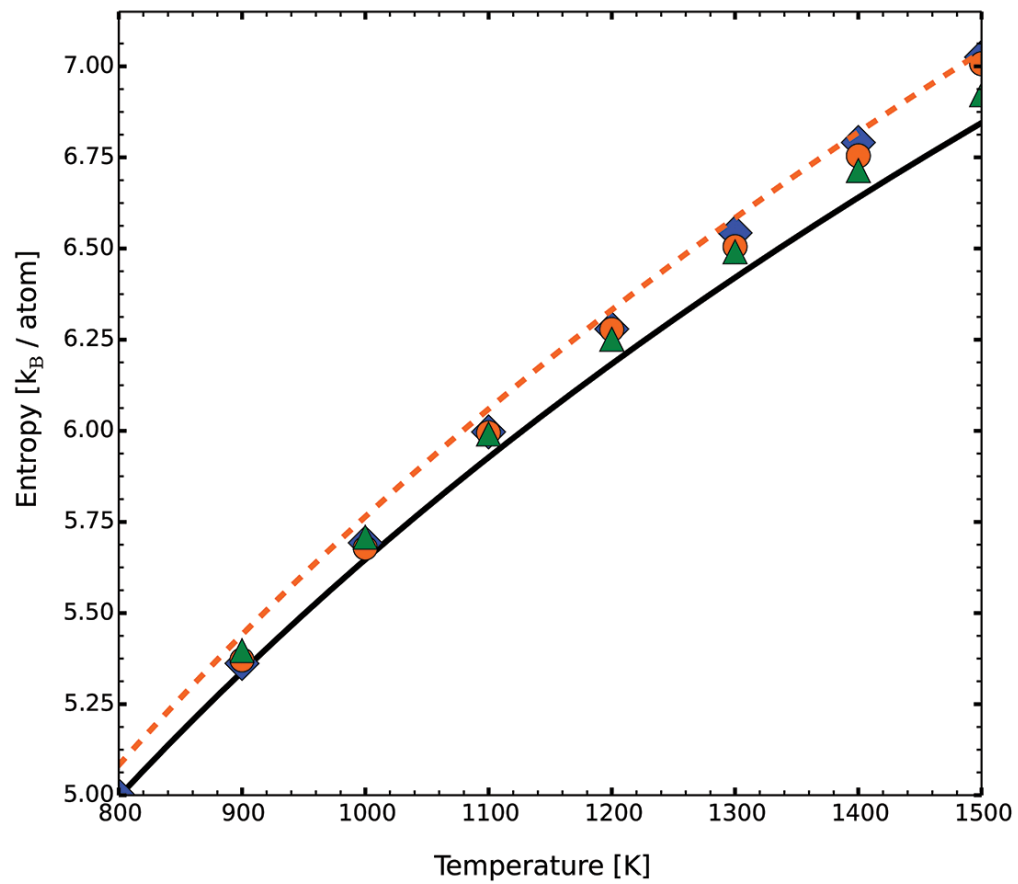


Figure 2.7: Enlargement of vibrational entropy from 1200 to 1500 K. The difference between experimental (orange circles) and quasiharmonic (green triangles) changes sign with temperature as quasiharmonic drifts further from the experimental points.

namics and thermal transport, which require anharmonic phonons. Although we report an experimental result that is not yet provable by theory, it is an important effect in an important material.

The phonon DOS of silicon shows a curious self-similarity. With increasing temperature the phonon DOS keeps approximately the same shape but is rescaled in energy. The simplest explanation is that all interatomic force constants decrease proportionately with temperature, but this explanation may be specious. At 1500 K the different features of the phonon DOS are broadened differently, reflecting differences in the imaginary part of the phonon self energy from cubic terms in the phonon potential [44]. Such differences were reported recently by Hellman, et al. [40], who showed large broadenings of the longitudinal and highest optical modes compared to the lower energy transverse acoustic modes. (Perhaps the lack of inversion symmetry at silicon atom sites allows for a relatively large cubic contribution to the potential energy of some phonons.) The different cubic anharmonicities also contribute different real shifts to the phonon self energies, so a thermal re-scaling of force constants would require compensating contributions from the quartic and quasiharmonic contributions of different phonons. It, therefore, seems unlikely that this self-similarity of the phonon DOS could be precisely accurate, and the different slopes in Fig. 2.4 suggest that it is only approximate.

Measurements of the phonon DOS of silicon from 100 to 1500 K showed significant thermal softening and some thermal broadening. From prior experimental studies of the effect of pressure on the phonons, and from the present computational study on the effect of volume on phonon frequencies, the quasi-

harmonic contribution to the non-harmonicity was obtained. At low temperatures, the quasiharmonic model works well to describe the phonon shifts but at high temperatures, all of the thermal broadening, and 80% of the thermal softening, were due to phonon anharmonicity. Nevertheless, the vibrational entropy calculated from the experimental phonon DOS curves of silicon was found to be within 1% of the total thermodynamic entropy reported by JANAF obtained from calorimetry data.

References

- ¹B. Fultz, “Vibrational thermodynamics of materials”, [Progress in Materials Science](#) **55**, 247–352 (2010).
- ²M. Palumbo, B. Burton, A. Costa e Silva, B. Fultz, B. Grabowski, G. Grimvall, B. Hallstedt, O. Hellman, B. Lindahl, A. Schneider, P. E. A. Turchi, and W. Xiong, “Thermodynamic modelling of crystalline unary phases: thermodynamic modelling of crystalline phases”, en, [physica status solidi \(b\)](#) **251**, 14–32 (2014) [10.1002/pssb.201350133](#).
- ³M. A. Green, J. Zhao, A. Wang, P. J. Reece, and M. Gal, “Efficient silicon light-emitting diodes”, [Nature](#) **412**, 805–808 (2001) [10.1038/35090539](#).
- ⁴A. I. Hochbaum, R. Chen, R. D. Delgado, W. Liang, E. C. Garnett, M. Najarian, A. Majumdar, and P. Yang, “Enhanced thermoelectric performance of rough silicon nanowires”, [Nature](#) **451**, 163–167 (2008) [10.1038/nature06381](#).
- ⁵Y. Cui, Z. Zhong, D. Wang, W. U. Wang, and C. M. Lieber, “High performance silicon nanowire field effect transistors”, en, [Nano Letters](#) **3**, 149–152 (2003) [10.1021/n10258751](#).
- ⁶J. Graetz, C. C. Ahn, R. Yazami, and B. Fultz, “Highly reversible lithium storage in nanostructured silicon”, en, [Electrochemical and Solid-State Letters](#) **6**, A194 (2003) [10.1149/1.1596917](#).
- ⁷A. I. Boukai, Y. Bunimovich, J. Tahir-Kheli, J.-K. Yu, W. A. Goddard III, and J. R. Heath, “Silicon nanowires as efficient thermoelectric materials”, [Nature](#) **451**, 168–171 (2008) [10.1038/nature06458](#).
- ⁸K. D. Hirschman, L. Tsybeskov, S. P. Dutttagupta, and P. M. Fauchet, “Silicon-based visible light-emitting devices integrated into microelectronic circuits”, [Nature](#) **384**, 338–341 (1996) [10.1038/384338a0](#).
- ⁹H. A. Atwater and A. Polman, “Plasmonics for improved photovoltaic devices”, [Nature Materials](#) **9**, 205–213 (2010) [10.1038/nmat2629](#).
- ¹⁰B. Tian, X. Zheng, T. J. Kempa, Y. Fang, N. Yu, G. Yu, J. Huang, and C. M. Lieber, “Coaxial silicon nanowires as solar cells and nanoelectronic power sources”, [Nature](#) **449**, 885–889 (2007) [10.1038/nature06181](#).
- ¹¹K. E. Petersen, “Silicon as a mechanical material”, [Proceedings of the IEEE](#) **70**, 420–457 (1982).
- ¹²G. Nilsson and G. Nelin, “Study of the homology between silicon and germanium by thermal-neutron spectrometry”, [Phys. Rev. B](#) **6**, 3777 (1972).

- ¹³G. Dolling and R. A. Cowley, “The thermodynamic and optical properties of germanium, silicon, diamond and gallium arsenide”, [Proceedings of the Physical Society](#) **88**, 463 (1966).
- ¹⁴S. Wei, C. Li, and M. Y. Chou, “Ab initio calculation of thermodynamic properties of silicon”, [Phys. Rev. B](#) **50**, 14587–14590 (1994) [10.1103/PhysRevB.50.14587](#).
- ¹⁵C. Flensburg and R. F. Stewart, “Lattice dynamical debye-waller factor for silicon”, [Phys. Rev. B](#) **60**, 284 (1999).
- ¹⁶G. Lang, K. Karch, M. Schmitt, P. Pavone, A. P. Mayer, R. K. Wehner, and D. Strauch, “Anharmonic line shift and linewidth of the raman mode in covalent semiconductors”, [Phys. Rev. B](#) **59**, 6182 (1999).
- ¹⁷W. B. Gauster, “Low-temperature grüneisen parameters for silicon and aluminum”, [Phys. Rev. B](#) **4**, 1288 (1971).
- ¹⁸M. T. Yin and M. L. Cohen, “Theory of static structural properties, crystal stability, and phase transformations: application to si and ge”, [Phys. Rev. B](#) **26**, 5668 (1982).
- ¹⁹J. Kulda, D. Strauch, P. Pavone, and Y. Ishii, “Inelastic-neutron-scattering study of phonon eigenvectors and frequencies in si”, [Phys. Rev. B](#) **50**, 13347 (1994).
- ²⁰S. Biernacki and M. Scheffler, “Negative thermal expansion of diamond and zinc-blende semiconductors”, [Phys. Rev. Lett.](#) **63**, 290–293 (1989).
- ²¹P. Mishra and K. P. Jain, “Temperature-dependent raman scattering studies in nanocrystalline silicon and finite-size effects”, [Phys. Rev. B](#) **62**, 14790 (2000).
- ²²J. Menéndez and M. Cardona, “Temperature dependence of the first-order raman scattering by phonons in si, ge, and α -sn: anharmonic effects”, [Phys. Rev. B](#) **29**, 2051 (1984).
- ²³B. A. Weinstein and G. J. Piermarini, “Raman scattering and phonon dispersion in si and GaP at very high pressure”, [Phys. Rev. B](#) **12**, 1172 (1975).
- ²⁴D. L. Abernathy, M. B. Stone, M. J. Loguillo, M. S. Lucas, O. Delaire, X. Tang, J. Y. Y. Lin, and B. Fultz, “Design and operation of the wide angular-range chopper spectrometer ARCS atSpallation Neutron Source”, [Rev. Sci. Instrum.](#) **83**, 015114 (2012).

- ²⁵M. B. Stone, J. L. Niedziela, M. J. Loguillo, M. A. Overbay, and D. L. Abernathy, "A radial collimator for a time-of-flight neutron spectrometer", *Review of Scientific Instruments* **85**, 085101 (2014).
- ²⁶*Mantid*: <http://www.mantidproject.org/>, 2013.
- ²⁷M. Kresch, M. Lucas, O. Delaire, J. Y. Y. Lin, and B. Fultz, "Phonons in aluminum at high temperatures studied by inelastic neutron scattering", *Phys. Rev. B* **77**, 024301 (2008) [10.1103/PhysRevB.77.024301](https://doi.org/10.1103/PhysRevB.77.024301).
- ²⁸M. Kresch, O. Delaire, R. Stevens, J. Y. Y. Lin, and B. Fultz, "Neutron scattering measurements of phonons in nickel at elevated temperatures", *Phys. Rev. B* **75**, 104301 (2007) [10.1103/PhysRevB.75.104301](https://doi.org/10.1103/PhysRevB.75.104301).
- ²⁹G. Kresse and J. Furthmüller, "Efficiency of ab-initio total energy calculations for metals and semiconductors using a plane-wave basis set", en, *Computational Materials Science* **6**, 15–50 (1996).
- ³⁰G. Kresse and J. Hafner, "Ab initio molecular dynamics for liquid metals", *Phys. Rev. B* **47**, 558–561 (1993).
- ³¹G. Kresse and J. Hafner, "Ab initio molecular-dynamics simulation of the liquid-metal–amorphous-semiconductor transition in germanium", en, *Phys. Rev. B* **49**, 14251–14269 (1994) [10.1103/PhysRevB.49.14251](https://doi.org/10.1103/PhysRevB.49.14251).
- ³²G. Kresse and J. Furthmüller, "Efficient iterative schemes for ab initio total-energy calculations using a plane-wave basis set", *Phys. Rev. B* **54**, 11169 (1996).
- ³³X. Gonze and C. Lee, "Dynamical matrices, born effective charges, dielectric permittivity tensors, and interatomic force constants from density-functional perturbation theory", *Phys. Rev. B* **55**, 10355 (1997).
- ³⁴J. P. Perdew, K. Burke, and M. Ernzerhof, "Generalized gradient approximation made simple", *Phys. Rev. Lett.* **77**, 3865 (1996).
- ³⁵J. P. Perdew, K. Burke, and M. Ernzerhof, "Generalized gradient approximation made simple [phys. rev. lett. 77, 3865 (1996)]", en, *Phys. Rev. Lett.* **78**, 1396–1396 (1997) [10.1103/PhysRevLett.78.1396](https://doi.org/10.1103/PhysRevLett.78.1396).
- ³⁶G. Kresse and D. Joubert, "From ultrasoft pseudopotentials to the projector augmented-wave method", *Phys. Rev. B* **59**, 1758 (1999).
- ³⁷P. E. Blöchl, "Projector augmented-wave method", *Phys. Rev. B* **50**, 17953 (1994).

- ³⁸A. Togo, F. Oba, and I. Tanaka, "First-principles calculations of the ferroelastic transition between rutile-type and cacl₂-type sio₂ at high pressures", *Phys. Rev. B* **78**, 134106 (2008).
- ³⁹S. Wei and M. Y. Chou, "Phonon dispersions of silicon and germanium from first-principles calculations", *Phys. Rev. B* **50**, 2221–2226 (1994) [10.1103/PhysRevB.50.2221](#).
- ⁴⁰O. Hellman and I. A. Abrikosov, "Temperature-dependent effective third-order interatomic force constants from first principles", *Phys. Rev. B* **88**, 144301 (2013) [10.1103/PhysRevB.88.144301](#).
- ⁴¹Y. Okada and Y. Tokumaru, "Precise determination of lattice parameter and thermal expansion coefficient of silicon between 300 and 1500 k", en, *Journal of Applied Physics* **56**, 314 (1984) [10.1063/1.333965](#).
- ⁴²D. N. Batchelder and R. O. Simmons, "Lattice constants and thermal expansivities of silicon and of calcium fluoride between 6° and 322° k", *The Journal of Chemical Physics* **41**, 2324 (1964) [10.1063/1.1726266](#).
- ⁴³Hull, Robert, *Properties of crystalline silicon* (INSPEC, the Institution of Electrical Engineers, London, 1999).
- ⁴⁴D. C. Wallace, *Thermodynamics of crystals* (Dover Publications, Mineola, N.Y, 1998).
- ⁴⁵M. W. J. Chase, *NIST-JANAF Thermochemical Tables, 4th Edition* (American Institute of Physics, New York, 1998).
- ⁴⁶G. Grimvall, *The electron-phonon interaction in metals*, Selected topics in solid state physics 16 (North-Holland Pub. Co. : sole distributors for the U.S.A. and Canada, Elsevier North-Holland, Amsterdam ; New York, 1981).
- ⁴⁷O. Delaire, K. Marty, M. B. Stone, P. R. Kent, M. S. Lucas, D. L. Abernathy, D. Mandrus, and B. C. Sales, "Phonon softening and metallization of a narrow-gap semiconductor by thermal disorder", *Proceedings of the National Academy of Sciences* **108**, 4725–4730 (2011).
- ⁴⁸G. Grimvall, *Thermophysical properties of materials*, Enl. and Rev. (Elsevier, Amsterdam, Netherlands ; New York, 1999), 424 pp.
- ⁴⁹A. Beattie and J. Schirber, "Experimental determination of the low-temperature grüneisen parameter of silicon from pressure derivatives of elastic constants", *Phys. Rev. B* **1**, 1548–1551 (1970) [10.1103/PhysRevB.1.1548](#).

- ⁵⁰Z.-K. Liu, Y. Wang, and S. Shang, “Thermal Expansion Anomaly Regulated by Entropy”, *Scientific Reports* **4**, 7043 (2014).
- ⁵¹J. S. Shah and M. E. Straumanis, “Thermal expansion behavior of silicon at low temperatures”, *Solid State Communications* **10**, 159–162 (1972).
- ⁵²D. F. Gibbons, “Thermal Expansion of Some Crystals with the Diamond Structure”, *Phys. Rev.* **112**, 136–140 (1958).

Chapter 3

THERMAL EXPANSION OF SILICON

Abstract from “A nuclear quantum effect with pure anharmonicity causes the anomalous thermal expansion of silicon” [2]:

Despite the widespread use of silicon in modern technology, its peculiar thermal expansion is not well-understood. Adapting harmonic phonons to the specific volume at temperature, the quasiharmonic approximation, has become accepted for simulating the thermal expansion, but has given ambiguous interpretations for microscopic mechanisms. To test atomistic mechanisms, we performed inelastic neutron scattering experiments from 100–1500 K on a single-crystal of silicon to measure the changes in phonon frequencies. Our state-of-the-art *ab initio* calculations, which fully account for phonon anharmonicity and nuclear quantum effects, reproduced the measured shifts of individual phonons with temperature, whereas quasiharmonic shifts were mostly of the wrong sign. Surprisingly, the accepted quasiharmonic model was found to predict the thermal expansion owing to a fortuitous cancellation of contributions from individual phonons.

A quantized harmonic oscillator was Einstein's seminal idea for understanding atom vibrations in solids. Better accuracy for crystalline solids is achieved when the vibrations are resolved into normal modes. Each normal mode is quantized, with a zero-point energy and excitations called phonons. However, harmonic models are limited to quadratic terms in the interatomic potential, and it is well-known that higher order terms are necessary to describe properties of real solids such as thermal conductivity and thermal expansivity. Despite this knowledge, the necessary and sufficient contributions to non-harmonic effects remain less clear. A popular approach is the quasi-harmonic model (QH), which assumes harmonic oscillators, but with frequencies renormalized to account for the thermal expansion. In a quasiharmonic model, the energy of the phonon mode i changes with crystal volume, V . Changes to phonon energies are usually described by a mode Grüneisen parameter, $\gamma_i = -(V \partial \varepsilon_i) / (\varepsilon_i \partial V)$, where $\varepsilon_i = \hbar \omega_i$ is the phonon energy (and $\omega_i / 2\pi$ is the frequency). A positive γ gives a reduction in mode energy with thermal expansion, increasing the vibrational entropy ΔS_{vib} . At finite temperature, the extra elastic energy from thermal expansion, ΔE_{el} , is offset by the term $-T \Delta S_{vib}$ in the free energy $\Delta F = \Delta E_{el} - T \Delta S_{vib}$ [1, 2]. For positive γ , ΔF is minimized with a positive thermal expansion; for negative γ , a negative thermal expansion is expected.

The cubic and quartic terms of the interatomic potential cause the normal modes to interact and exchange energy. This is pure anharmonicity, where the energy of a phonon is altered by the presence of other phonons irrespective of the volume of the solid. Phonon anharmonicity is essential for thermal

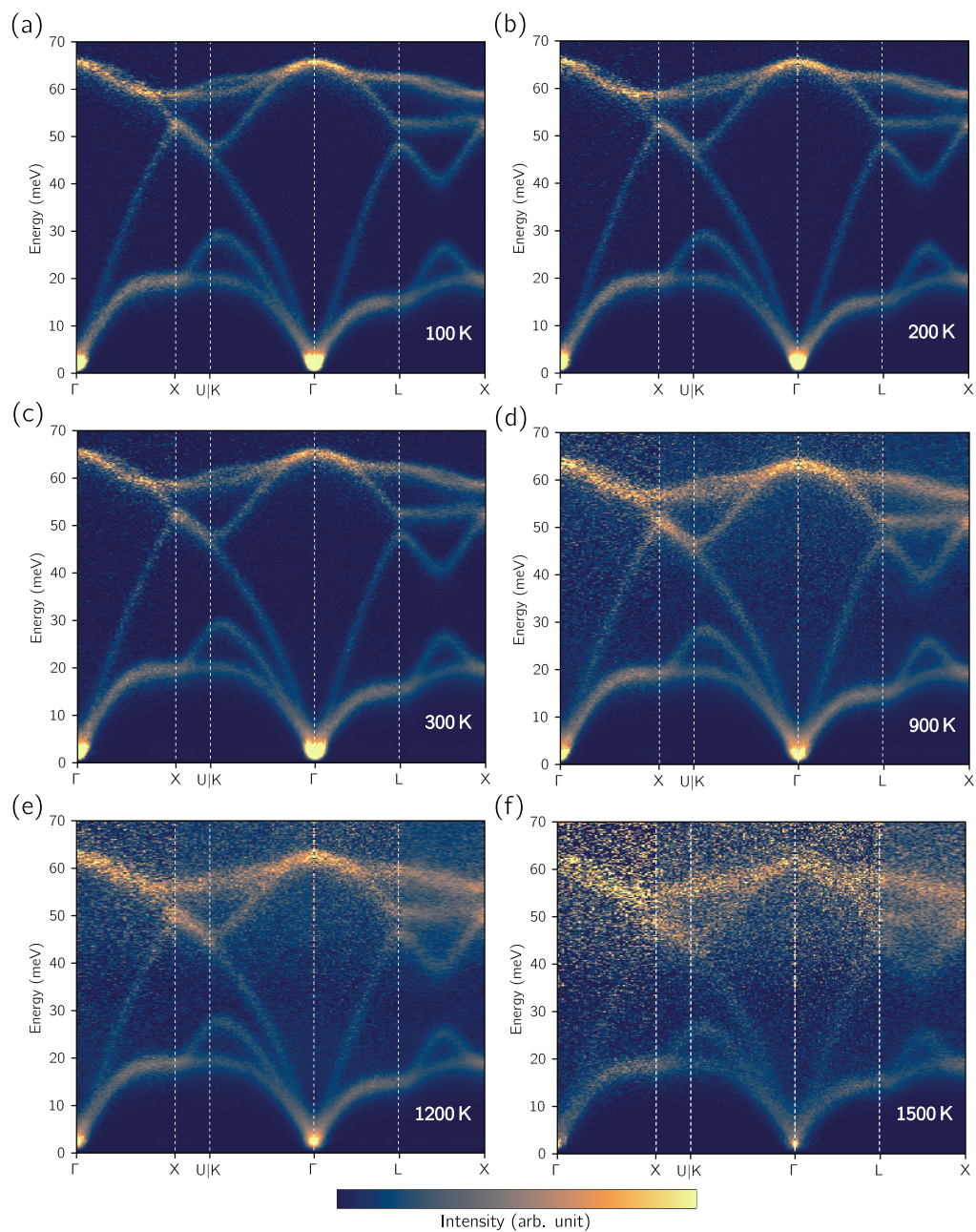


Figure 3.1: Experimental phonon dispersions of silicon. Inelastic neutron scattering data of silicon were measured on the ARCS time-of-flight spectrometer at (a) 100 K, (b) 200 K, (c) 300 K, (d) 900 K, (e) 1200 K, (f) 1500 K. The 4-D phonon dynamical structure factor, $S(\mathbf{q}, \varepsilon)$, were reduced, multiphonon subtracted, and “folded” into one irreducible wedge in the first Brillouin zone. Phonon dispersions are shown along high symmetry lines and through the zone (L–X).

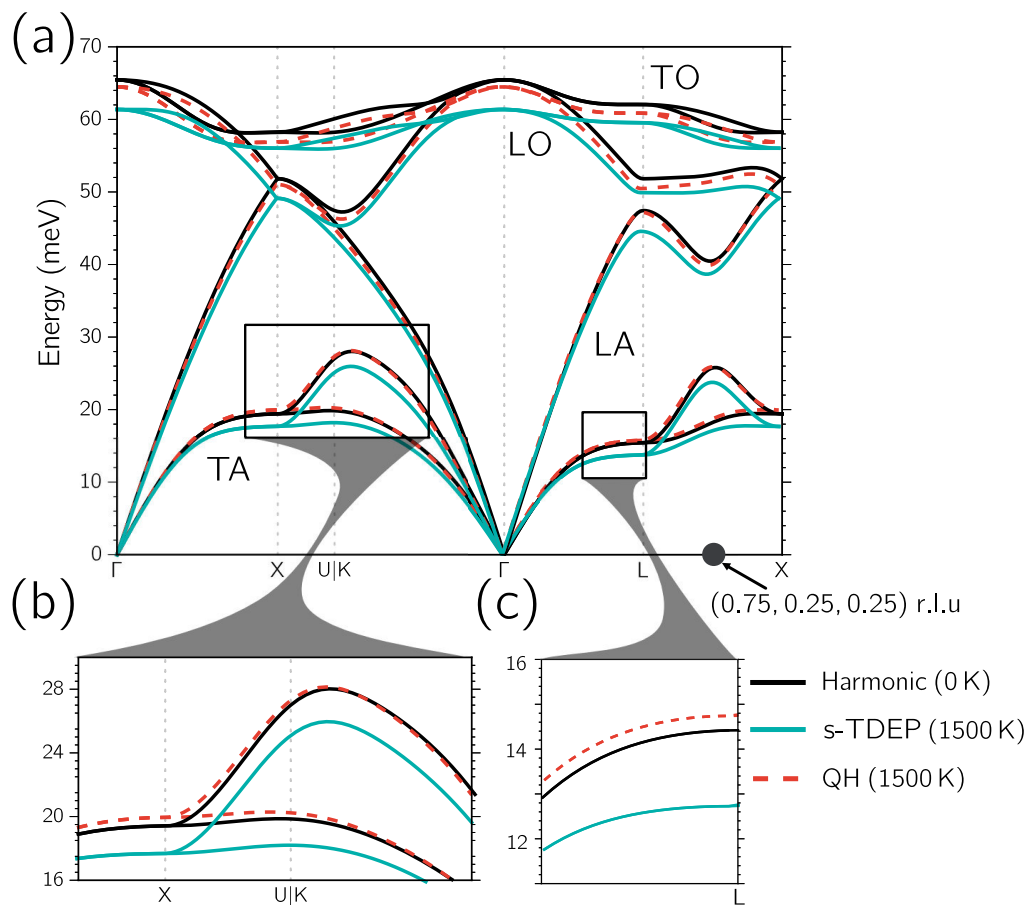


Figure 3.2: Comparison between experimental, s-TDEP and quasiharmonic (QH) *ab initio* calculations throughout the Brillouin zone. (a)–(c), Phonon dispersions of silicon from harmonic, s-TDEP, and QH *ab initio* density functional theory calculations. The (0.75,0.25,0.25)-point is shown as a black circle marker for reference. (b),(c) Insets shows low-energy transverse acoustic modes.

conductivity and other thermophysical properties. Anharmonic effects increase with larger thermal atomic displacements. Sometimes this causes a misperception that pure anharmonicity is important only at high temperatures, and quasiharmonic models may be valid at low and moderate temperatures owing to low phonon populations. However, the leading-order terms of both quasiharmonicity and anharmonicity are linear in temperature [3], so if anharmonicity is important at high temperatures, it can have the same relative importance at low temperatures, too. Furthermore, at low temperatures the “zero-point” energy gives atom displacements that allow a nuclear quantum effect to engage the high-energy phonon modes that are half occupied.

Finding the relative importances of quasiharmonicity and anharmonicity should be done by quantitative analysis, but to date the dominance of quasiharmonicity for silicon has been assumed in part because quasiharmonic models predict the thermal expansion with reasonable accuracy [4–6]. The quasiharmonic model predicts the anomalous negative thermal expansion of silicon from 10 K to 125 K and the low thermal expansion up to the melting temperature [7–11]. The positive thermal expansion coefficients observed at moderate and high temperatures are anomalous in their own right – they are small compared to diamond and other materials with zincblende structures [9]. Further validation of the quasiharmonic approximation was provided by measurements of the Raman mode and a few second-order Raman modes of silicon under pressure, which were accurately predicted by volume-dependent density functional theory (DFT) calculations at low temperature [12, 13]. The negative Grüneisen parameters of the low-energy transverse acoustic (TA) modes have

received considerable attention and have been attributed to the “open-ness” of the diamond cubic structure [11], the stability of angular forces [6], or entropy in general [5]. Nevertheless, the precise role of the TA modes in thermal expansion remains unclear [4, 6]. With increasing temperature, phonons are excited in higher-energy phonon branches, and their positive Grüneisen parameters are expected to cause the overall thermal expansion to change sign (as discussed in the [Supporting Information](#)). Today this quasiharmonic model is the workhorse for predicting thermal expansion.

“Non-trivial” phonon shifts that were not accounted for by thermal expansion were reported in an earlier experimental paper on phonon dispersions in silicon up to 300 K [14]. The importance of pure anharmonicity in temperature-dependent phonon shifts at moderate and high temperatures was also found in work based on molecular dynamics, many-body perturbation theory, and *ab initio* calculations on silicon [15–21]. The uncertainty principle and quantum distributions of nuclear positions influence the exploration of atomic potential landscapes. The zero-point motion was shown to be important, but does not by itself reproduce the correct thermal expansion coefficients [22, 23]. (More information on quantum and zero-point effects are in the [Supporting Information](#).) Temperature-dependent phonon shifts from pure phonon anharmonicity with zero-point energy could give a nuclear quantum effect that alters thermophysical properties. A more detailed study of the temperature dependence of phonons in silicon is therefore appropriate because very few modes were previously assessed [14, 19, 20, 24].

We report the first inelastic neutron scattering measurements of phonon

dispersions of silicon above 300 K along with fully anharmonic *ab initio* calculations. These measurements discredit the quasiharmonic theory, which predicts the wrong sign for phonon shifts with temperature, and we show that the crystal structure, pure anharmonicity, and nuclear quantum effects of silicon all play important roles in the thermal expansion of silicon.

The experiments used a high-purity single crystal of silicon (mass \approx 28.5 g) with $\langle 110 \rangle$ -orientation, machined into a tube for optimal neutron scattering properties. The sample was rotated in a furnace on a direct geometry time-of-flight inelastic neutron scattering spectrometer (ARCS) [25] at the Spallation Neutron Source at Oak Ridge National Laboratory. For each temperature the 4-dimensional $S(\mathbf{q}, \epsilon)$ data were reduced and multiphonon scattering subtracted to give all phonon dispersions in the irreducible wedge of the first Brillouin zone. The multiphonon scattering produces a relatively smooth background between the phonon dispersions and was determined to produce the majority of the background intensity (Supporting Information) [26]. Our “folding” technique of summing all of the $S(\mathbf{q}, \epsilon)$ data (from >100 Brillouin zones) into an irreducible wedge increases the signal strength, suppresses polarization effects that alter intensities in some Brillouin zones [26], and averages out any possible effects of “anharmonic interference” [27].

Figure 3.1 shows phonon dispersions as bright intensities. The dispersions at low temperatures are in excellent agreement with previous work that used triple-axis spectrometers [14, 24]. With increasing temperature, the majority of phonon modes, including the low-energy transverse acoustic modes, soften in proportion to their energy, i.e., the mode Grüneisen parameters are

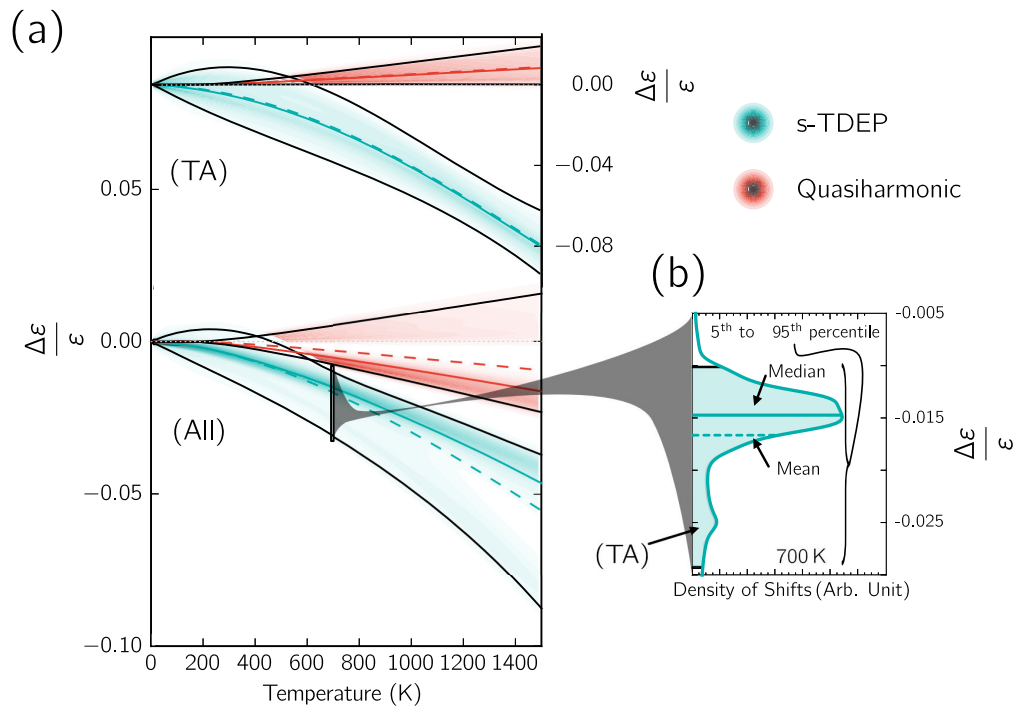


Figure 3.3: Comparison between experimental, s-TDEP and quasiharmonic (QH) *ab initio* calculations throughout the Brillouin zone. (a) Density of fractional phonon energy shifts with temperature. The densities from all branches (s-TDEP: teal, QH: red) and densities from just the low transverse modes are offset and scaled for clarity. (b) The density of the 700 K s-TDEP. Notice the more negative peak consists of a majority of TA-modes.

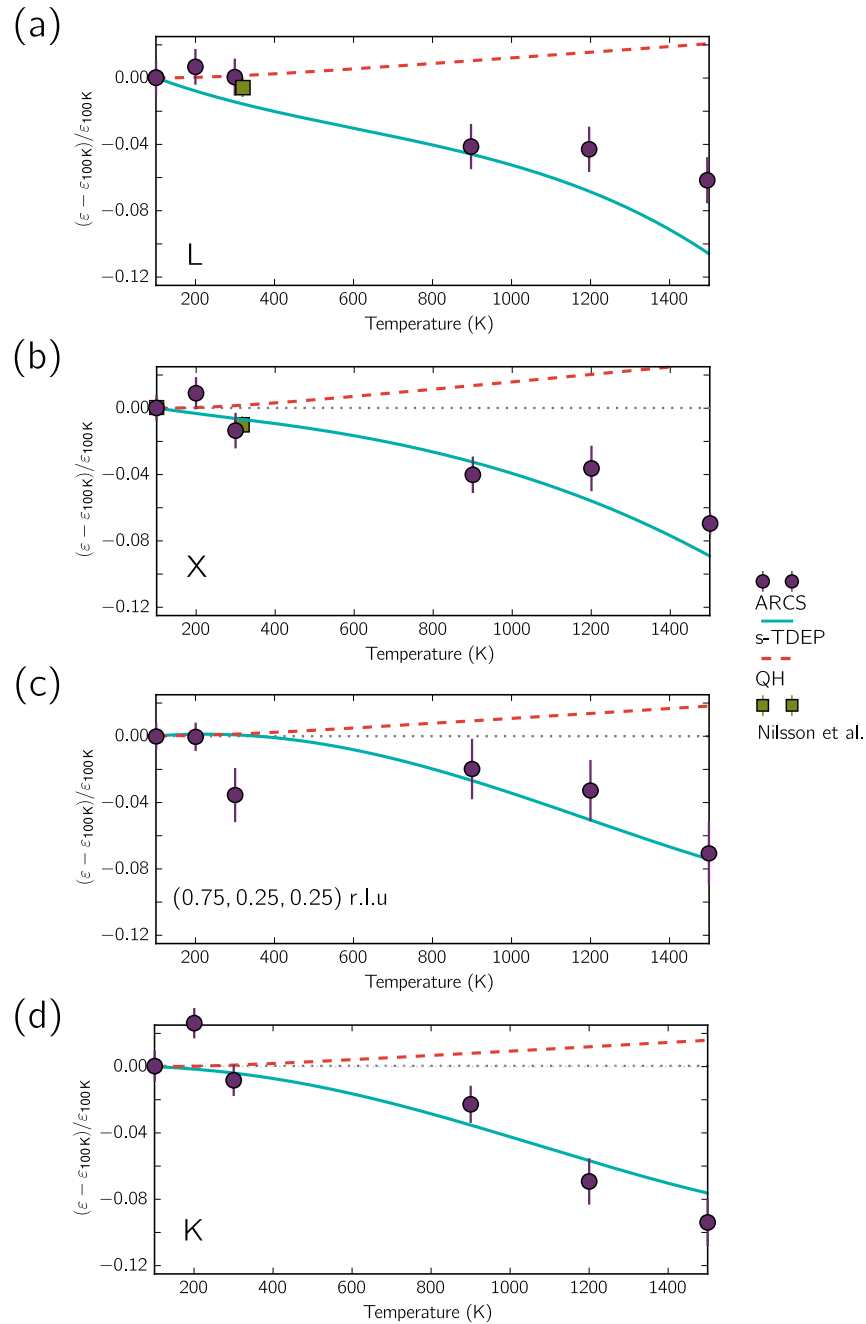


Figure 3.4: Comparison between experimental, s-TDEP and quasiharmonic (QH) *ab initio* calculations throughout the Brillouin zone. Temperature-dependent phonon shifts, $(\epsilon - \epsilon_{100K})/\epsilon_{100K}$, of the low-energy transverse modes at the (a) L, (b) X, (c) (0.75,0.25,0.25) r.l.u., and (d) K points. Experimental fits of phonon centroids with standard (1σ) error-bars from the present work are shown alongside calculated shifts and previously reported shifts [14].

similar. This self-similar behavior of phonon softening was reported previously [21].

All *ab initio* calculations were performed with the VASP package [28–34]. A stochastically-initialized temperature-dependent effective potential method (s-TDEP) [12, 35–37] was implemented to obtain phonon shifts with temperature, including intrinsic phonon anharmonicities and nuclear quantum effects. Quasiharmonic calculations were also conducted as described previously [21]. Methods for both the measurements and the calculations are described in the [Supporting Information](#).

Results from calculations by the s-TDEP method (with anharmonicity and thermal expansion) and conventional quasiharmonic *ab initio* calculations (with no anharmonicity) are shown in Fig. 3.2 through Fig. 3.4. There are large discrepancies in the signs and magnitudes of phonon energy shifts between the two models. Most interestingly, Fig. 3.2 (b),(c) show that the s-TDEP calculations predict a reduction in phonon energy, a thermal “softening”, in the transverse modes (roughly <35 meV), whereas the quasiharmonic calculations predict an increase in phonon energy, “stiffening”, at 1500 K (with negative Grüneisen parameters as reported previously [4–6]).

We calculated the fractional shifts of energies, $\Delta\varepsilon/\varepsilon(T)$, for all phonon modes in the first Brillouin zone. The energies of all phonons were calculated using a $50\times 50\times 50$ grid of \mathbf{q} -points. Figure 3.3 (a) compares the density of fractional phonon shifts from quasiharmonic and anharmonic (s-TDEP) calculations. The density of fractional shifts, $\rho(\Delta\varepsilon/\varepsilon)$, is shown in Fig. 3.3 (b) from

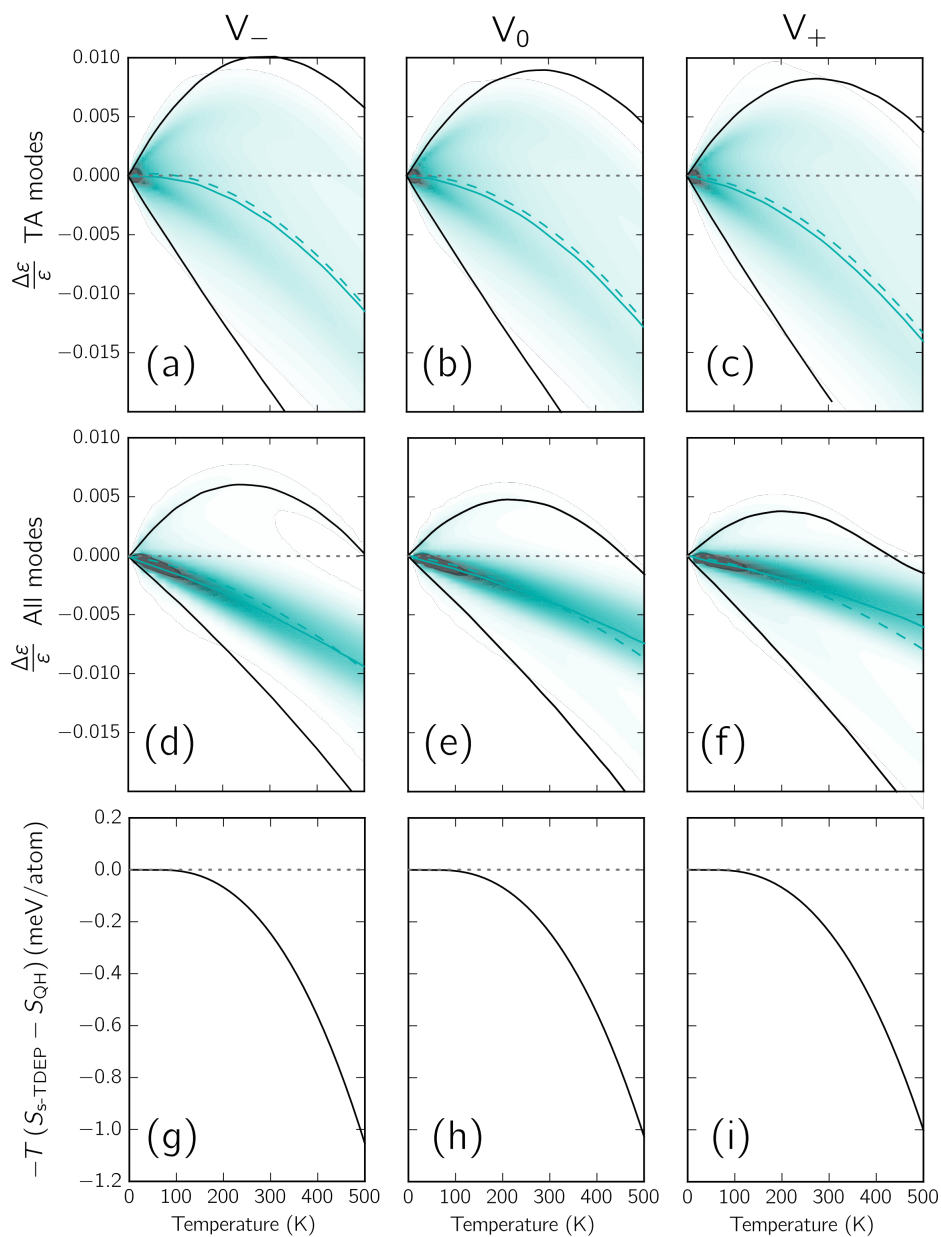


Figure 3.5: Phonon shifts and entropy differences from constant volume *ab initio* calculations. (a)–(f) Density of fractional shifts with temperature at constant volumes using the s-TDEP method. The mean (dashed color line), median (solid color line), and the 5th and 95th percentile (black solid lines) of the density are also shown. Calculations shown for: [(a),(d),(g)] 99 % of 0 K volume, [(b),(h),(e)] 0 K volume, and [(c),(f),(i)] 101 % of 0 K volume. Quasiharmonic predictions are the dashed zero-lines in (a)–(f). (g)–(i) Corresponding constant volume differences between the quasiharmonic (QH) and s-TDEP in free energies from vibrational entropy with temperature.

the s-TDEP method at 700 K. Compared to the quasiharmonic predictions for the TA modes (shown at top of Fig. 3.3 (a)), the anharmonic shifts are an order-of-magnitude larger, have opposite signs, and follow opposite thermal trends. Such large discrepancies allow for definitive experimental tests.

Individual phonon energies were obtained from constant- \mathbf{q} fits to the measured $S(\mathbf{q},\epsilon)$, as shown in the [Supporting Information](#). Fig. 3.4 (a)–(d) show that the trends from the anharmonic s-TDEP calculations are in far better agreement with experiment than the quasiharmonic trends. Thermal trends for individual phonons at the L,X,K-points (Fig. 3.4 (a), (b), (d)) are presented for their importance in the interpretation of quasiharmonic results [4]. Another example for a phonon mode located away from a high-symmetry line is shown in Fig. 3.4 (d).

Additional s-TDEP calculations of densities of thermal shifts suggest why the quasiharmonic theory has been so apparently successful. Calculations were performed for volumes that were 1% larger and 1% smaller than the 0 K harmonic volume calculated for Fig. 3.2 (a), and the results are shown on the left and right sides of Fig. 3.5 for the TA modes (top three panels) and all phonon modes (middle three panels). For all three volumes, at low temperatures there is a wide spread in the thermal phonon shifts, both stiffening and softening. At low temperatures, the average thermal shift from anharmonicity at a fixed volume is surprisingly nearly zero. At fixed volume, the shifts of all quasiharmonic phonons are zero, of course, so the two methods agree on the average owing to the cancellation of anharmonic stiffenings and softenings. This approximate cancellation is seen in Fig. 3.5 (a)–(c) for the TA

modes and in Fig. 3.5 (d)–(f) for all modes. Nevertheless, the average phonon energies from the s-TDEP method show an ordinary softening with increased volume and temperature, inconsistent with the negative Grüneisen parameters from quasiharmonic calculations. At high temperatures, Fig. 3.5 (d)–(f) show that all the modes tend to soften at similar rates. Differences in vibrational entropies from the s-TDEP and quasiharmonic methods were calculated using equations in the [Supporting Information](#). The difference in entropies ΔS from the quasiharmonic and anharmonic calculations was used to obtain the $-T\Delta S$ shown in Fig. 3.5 (g)–(i). For all volumes, the differences are negligible up to 125 K but increase at higher temperatures (Fig. 3.6). The success of the quasiharmonic theory may be an indicator that the diamond cubic structure is intrinsically prone to anomalies in thermal expansion, but the quasiharmonic model is not physically correct.

An independent concern about the quasiharmonic model is the elastic energy of thermal expansion, $\Delta E_{el} = 1/2Bv(\beta T)^2$, where B is the bulk modulus, β is the volume coefficient of thermal expansion, and v is the atomic volume. This ΔE_{el} should be comparable to the $-T\Delta S_{vib}$ contribution to the free energy from finite temperature phonons including pure anharmonicity and nuclear quantum effects. The maximum negative linear expansion at atmospheric pressure is 0.003 %, and the maximum positive linear expansion is 0.5% near the melting temperature [7, 8, 10]. The corresponding elastic energy per atom for the negative thermal expansion is in the μeV range, and the positive thermal expansion gives approximately 0.2 meV at 500 K [7, 8, 10, 38]. These quasiharmonic energies are orders of magnitude smaller than

the correct entropic contributions to the free energy. A quasiharmonic model with negative Grüneisen parameters gives a physically incorrect explanation of thermal expansion, although some of its predictions of average properties are preserved by gross cancellations of errors.

The zero-point energy proves important for thermal expansion in silicon [22, 23], where the (fractional) population of the higher energy phonons alters the self-energies of the TA phonons that change their population at low temperatures. Without this nuclear quantum effect, our anharmonic calculations predict significantly different thermal expansion at low temperatures ([Supporting Information](#)). Classical mechanical models based on the “open-ness” of the structure, classical springs, force constant ratios, and negative Grüneisen parameters may contribute to the general behavior as discussed in the [Supporting Information](#), but a classical picture of thermal expansion is not reliable. Nuclear quantum effects give an anharmonic coupling between phonons of all energies, even modes of higher energy that are not excited at low temperature, and these couplings are essential for correct predictions of thermal expansion. Nuclear quantum effects with pure anharmonicity should also alter thermal conductivity and other thermophysical properties at low temperatures.

Measurements of the phonon dispersions of single crystal silicon from 100 to 1500 K showed thermal shifts that contradict the trends predicted by the widely accepted quasiharmonic model, even at low temperatures. Pure phonon anharmonicity, i.e., phonon-phonon interactions, dominate the phonons in silicon from low to high temperatures, altering the effective interatomic potential and causing both positive and negative shifts of phonon energies. At

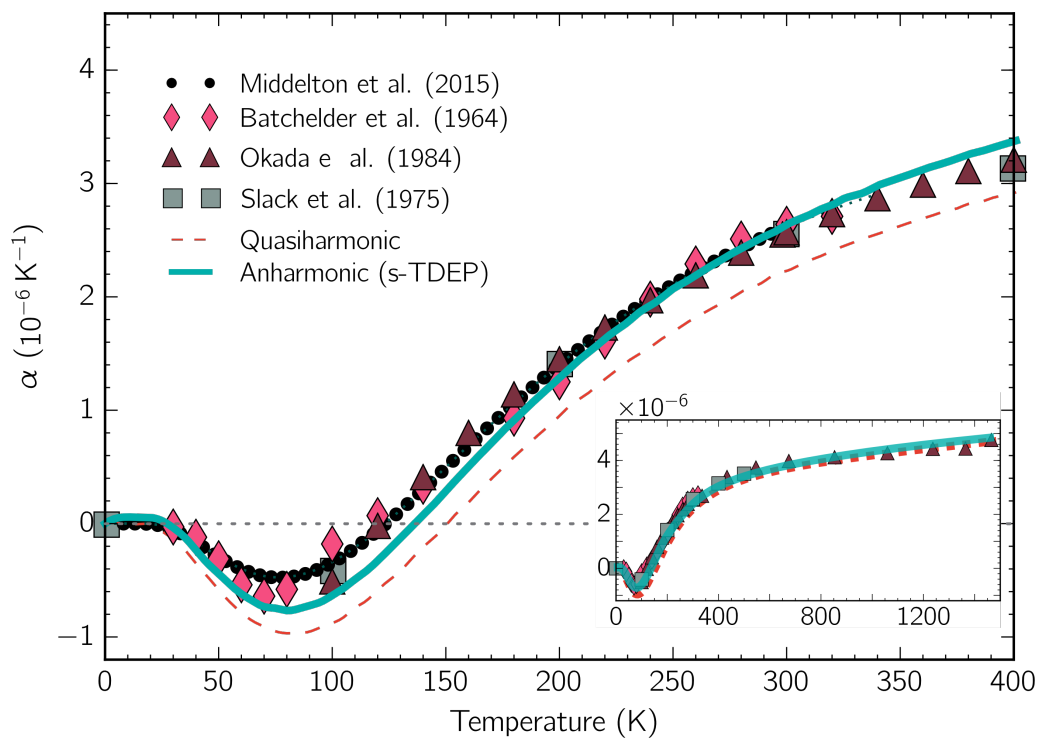


Figure 3.6: Calculated and experimental coefficients of linear thermal expansion in silicon. Calculated coefficients are from minimized free energies using Supporting Information Eq. 1 (s-TDEP: teal solid line, quasiharmonic (QH): red dashed line). Experimental values are shown as colored markers [7–10]. Inset shows calculations and experimental values at higher temperatures.

low temperatures the zero-point quantum occupancy of high-energy vibrational modes alter the energies of low-energy modes through anharmonic coupling. This nuclear quantum effect with anharmonicity is the essential cause of the negative thermal expansion of silicon. The crystal structure, anharmonicity, and nuclear quantum effects of silicon all play important roles in the thermal expansion of silicon, and could be essential in other technologically important materials.

Supporting Information (SI)

Inelastic Neutron Scattering

Inelastic neutron scattering measurements were performed on a single crystal of silicon of 99.999% purity that was highly-oriented ($<2^\circ$), purchased from Virginia Semiconductor, Inc. The [110] oriented single crystal was further machined into a cylinder of 3.8 cm in height, 2.54 cm in outer diameter and a 1.59 cm inner diameter to minimize multiple scattering. The crystal was suspended in an aluminum holder and then mounted into a closed-cycle helium refrigerator for the 100 and 200 K measurements, and a similar holder made from niobium was mounted into a low-background electrical resistance vacuum furnace for measurements at 300, 900, 1200 and 1500 K. For all measurements the incident energy was 97.5 meV, and an oscillating radial collimator was used to reduce background and multiple scattering [25, 39].

The time-of-flight neutron data included multiple datasets from 200 rotations in increments of 0.5° about the vertical [110]-axis, reduced to create the

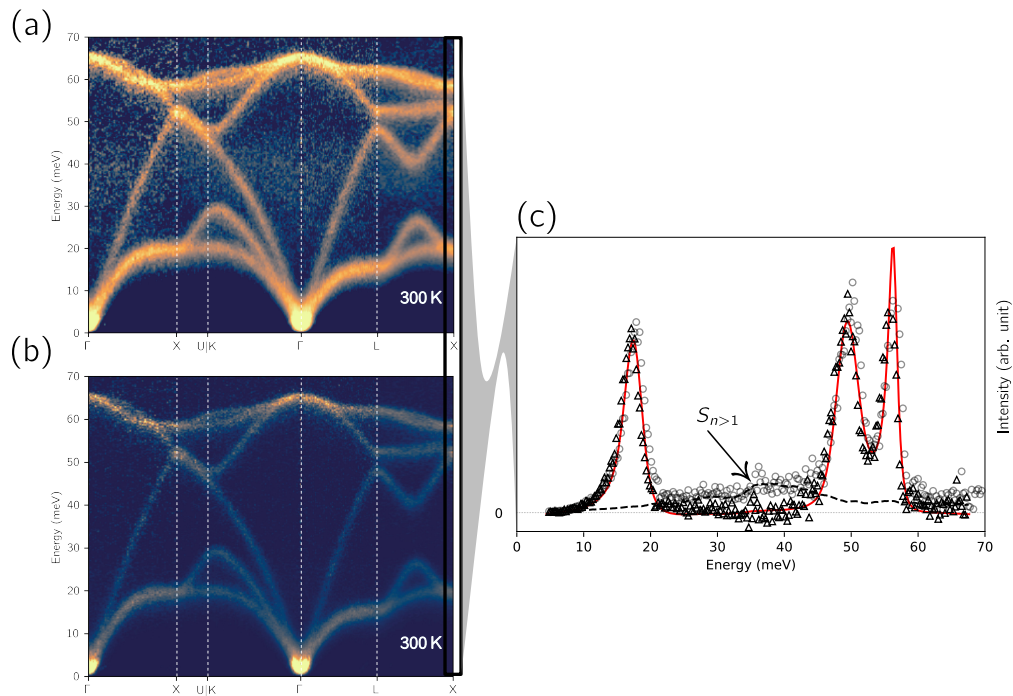


Figure 3.7: “Folded” inelastic neutron scattering data without (a) and with (b) multiphonon subtracted $S(\mathbf{q}, \epsilon)$ at 300 K. (c) Scattering intensity and fitted spectrum at the X-point. Fitted peaks are shown as the red solid line. Grey circles are without [(a)] and black triangles with [(b)] multiphonon scattering subtracted. Black dashed line shows subtracted multiphonon scattering intensity.

4-dimensional $S(\mathbf{q}, \varepsilon)$ [40, 41]. A secondary data reduction process consisted of ‘folding’ the entire $S(\mathbf{q}, \varepsilon)$ data set into an irreducible wedge in the first Brillouin zone. Non-linear offsets of the \mathbf{q} -grid were corrected by fitting typically 50 *in situ* Bragg diffractions in an energy transfer range of $\Delta\varepsilon = \pm 4$ meV by a transformation to the positions of the theoretical diffraction peaks for a diamond cubic structure. The multiphonon scattering was then subtracted, and the data ‘folded back’ and corrected for the phonon creation thermal factor [26].

The multiphonon scattering was determined with \mathbf{q} -dependence through the incoherent approximation and calculated from Eq. 3.1 [26],

$$S_{n>1}(\vec{q}, \varepsilon) = \sum_{n=2}^{10} e^{-2W} \frac{(2W)^n}{n!} A_1 \otimes A_{n-1}, \quad (3.1)$$

where the $2W$ is the well-known Debye-Waller factor calculated from the experimental temperature-dependent phonon density of states (DOS) [21, 26]. The single and n -phonon scattering spectrum are,

$$A_1 = \frac{g(\varepsilon)}{\varepsilon} \langle n + 1 \rangle, \quad (3.2)$$

$$A_n = A_1 \otimes A_{n-1}. \quad (3.3)$$

The $g(\varepsilon)$ is the experimental phonon DOS [21], and n is the Planck distribution. We find that even at temperatures > 1000 K the contributions above the 5th multiphonon spectrum (S_5) are negligible. A global scaling factor

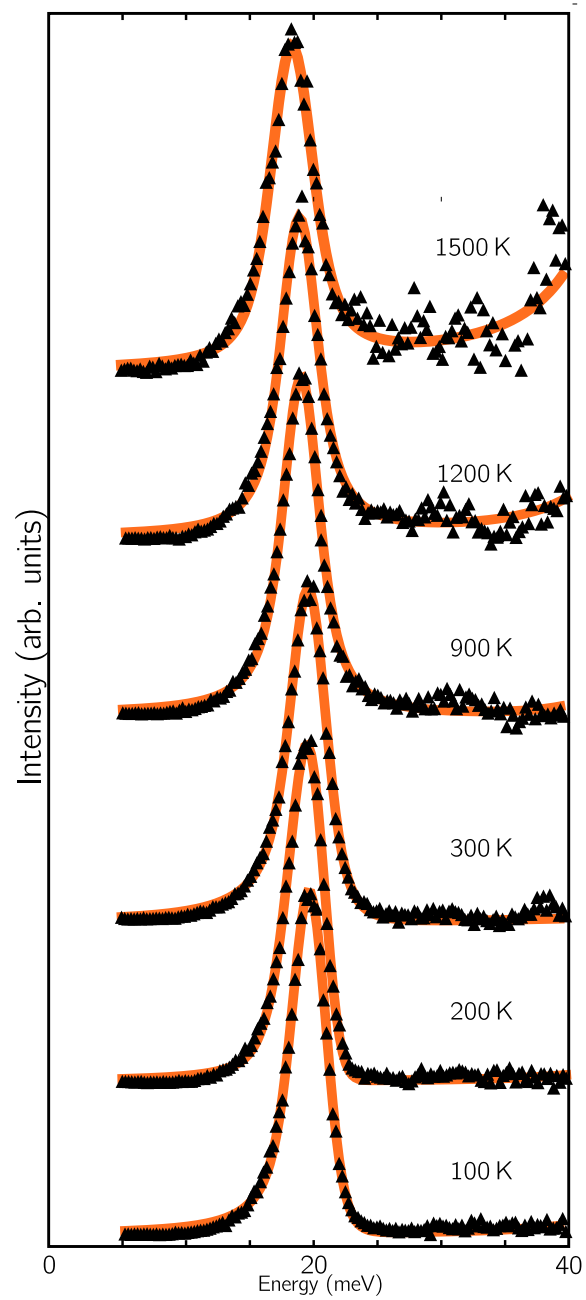


Figure 3.8: Constant \mathbf{q} - $S(\mathbf{q},\epsilon)$ data at the X point for 100, 200, 300, 900, 1200, 1500 K. Data are black markers and fits are in orange.

($b * S_{n>1}$) was applied to the total multiphonon scattering function throughout the Brillouin zone after “folding” to correct for normalization. The multiphonon scattering accounted for most of the background intensity as seen clearly in Fig 3.7.

The correct alignment of the data in reciprocal space and multiphonon subtraction produced $S(\mathbf{q}, \epsilon)$ of high statistical quality. Thermal shifts of phonons reported previously, when available, were in good agreement [14, 15, 20].

Energy spectra at specific \mathbf{q} -points mentioned were evaluated by integrating over 0.0025 \AA^{-3} . Phonon centroids were then fitted using the Levenberg-Marquardt non-linear least square method for multiple skewed-Voigt functions. The skewed-Voigt functions gave the best fits to the known asymmetric lineshape of the ARCS time-of-flight spectrometer. Examples of the scattered intensities at a constant- \mathbf{q} , with fits, are shown for the X-point in Fig. 3.8.

For comparison, a “slice” of “unfolded” 4-D $S(\mathbf{q}, \epsilon)$ along a momentum direction is shown in Fig. 3.9. The data were processed using standard software and corrected for the phonon creation thermal factor [26, 42]. First principles calculations were performed using the s-TDEP method described below and elsewhere [12, 43]. The experimental results are in good agreement with first principles calculations throughout reciprocal space. There are benefits of assessing phonon intensities over multiple Brillouin zones, but these are not essential for a study of thermal expansion.

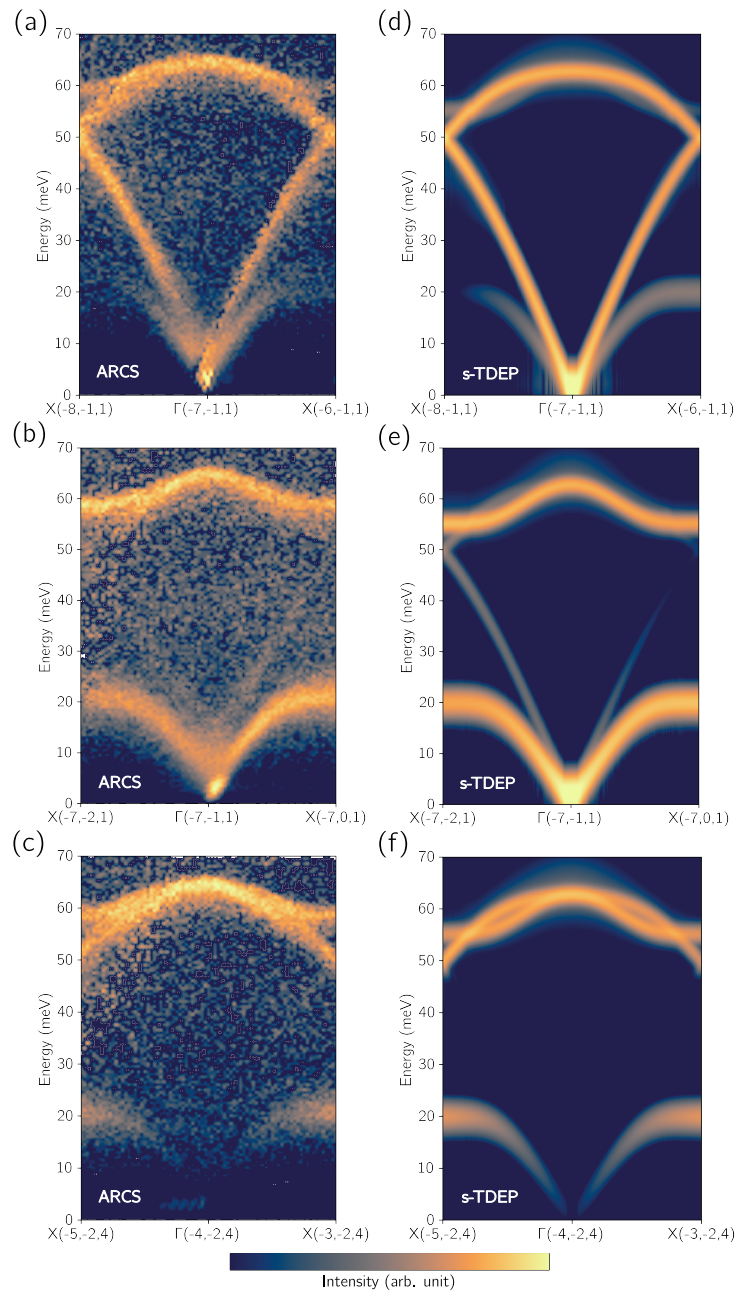


Figure 3.9: Inelastic neutron scattering [(a)–(c)] and first principle calculations [(d)–(f)] of $S(\mathbf{q}, \varepsilon)$ at 300 K along momenta \mathbf{q} (X– Γ –X) in different Brillouin zones. Calculated $S(\mathbf{q}, \varepsilon)$ was corrected for instrument resolution and polarization effects to match the experiment conditions [25, 26].

Ab-initio Calculations

Ab initio DFT calculations were performed with the projector augmented wave [44] formalism as implemented in VASP [28–30, 45]. All calculations used a $5 \times 5 \times 5$ supercell and a 500 eV plane wave energy cutoff. The Brillouin zone integrations used a $3 \times 3 \times 3$ k -point grid, and the exchange-correlation energy was calculated with the AM05 functional [32–34]. All calculations were converged to within 1 meV/atom.

Finite temperature phonon dispersions of silicon were calculated by fitting first-principles forces to a model hamiltonian,

$$H = U_0 + \sum_i \frac{\mathbf{p}_i^2}{2m} + \frac{1}{2} \sum_{ij\alpha\beta} \Phi_{ij}^{\alpha\beta} u_i^\alpha u_j^\beta + \frac{1}{3!} \sum_{ijk\alpha\beta\gamma} \Phi_{ijk}^{\alpha\beta\gamma} u_i^\alpha u_j^\beta u_k^\gamma. \quad (3.4)$$

The forces on atoms were generated using DFT with various configurations of displaced atoms by a stochastic sampling of a canonical ensemble, with cartesian displacements (u_i^α) normally distributed around the mean thermal displacement using

$$u_i^\alpha = \sum_k \frac{\epsilon_k^{i\alpha} c_k}{\sqrt{m_i}} \sqrt{-2 \ln \xi_1} \sin(2\pi \xi_2). \quad (3.5)$$

The thermal factor, c_k , is based on thermal amplitudes of normal mode k , with eigenvector ϵ_k and frequency ω_k [36, 46, 47]

$$c_k = \sqrt{\frac{\hbar(2n_k + 1)}{2\omega_k}}, \quad (3.6)$$

and ξ_1 and ξ_2 are stochastically sampled numbers between 0 and 1. The phonon distribution follows the Planck distribution, $n_k = (e^{\beta \hbar \omega_k} - 1)^{-1}$, where the nuclear quantum effect can be turned off by taking the high-temperature

limit of Eq. 4.3. The fitting to the model Hamiltonian used the temperature-dependent effective potential method (TDEP) [12, 35]. With thermal displacements from Eq. 4.2 and Eq. 4.3, we refer to our temperature-dependent calculations as the stochastically-initialized temperature-dependent effective potential method (s-TDEP). This method circumvents the issue of expensive computational resources required of *ab initio* molecular-dynamics (AIMD), replacing AIMD with a Monte Carlo sampling of atomic positions and momentum near equilibrium positions [12, 36]. The quasiharmonic model was calculated as described previously [21].

Thermodynamic Calculations

Temperature dependent coefficients of linear thermal expansion in silicon were calculated through the minimization of the free energy,

$$F(T, V) = E(T, V) + \sum_{\mathbf{q}, k} \left(\frac{\hbar\omega_k(\mathbf{q}, V, T)}{2} + k_B T \ln(1 - e^{-\hbar\omega_k(\mathbf{q}, T, V)/k_B T}) \right), \quad (3.7)$$

from quasiharmonic calculations, and from s-TDEP (main text Fig. 5). The quasiharmonic model implies the only temperature dependence of the entropy is from the volume expansion $\epsilon_i(V\{T\})$ and the Planck distribution (n_k), whereas the anharmonic s-TDEP method minimizes the free energy for temperature and volume simultaneously. The vibrational entropy from all phonon modes, \sum_k , was calculated as [1],

$$S_{vib}(T) = 3k_B \sum_k [(n_k + 1) \ln(n_k + 1) - n_k \ln(n_k)]. \quad (3.8)$$

Possible Contributions to the Thermal Expansion

As stated in the main text, a simple physical model for the anomalous thermal expansion of silicon is unlikely because different effects contribute to the thermal expansion. In particular, the anharmonicity and nuclear quantum effects are difficult to formulate as a simple 3D model. The thermal expansion of Si can be simulated properly with methods based on *ab initio* calculations that includes all these factors, but this seems unsatisfying for a “physical” understanding. A number of possible contributions and models are presented here, but any single model is insufficient by itself.

Negative Grüneisen Parameters as Fitting Parameters

If individual Grüneisen parameters are assigned to different parts of the phonon DOS, it is easy to make a model that predicts negative thermal expansion at low temperatures. An approximation for silicon is shown in Fig. 3.10, together with the experimental phonon DOS reported previously [21]. The six phonon branches were modeled as follows: acoustic branches were approximated by Debye models with cutoff energies of 20, 25, 42 meV, and optical branches were approximated as Einstein modes with energies of 52, 60, 60 meV. These curves were convoluted with a Gaussian function of standard deviation $\sqrt{3}$ meV, summed, and are compared to the experimental phonon DOS of Si [21] in Fig. 3.10.

The heat capacities of these six functions were calculated as shown in Fig. 3 (a). For simplicity, a Grüneisen parameter of -1 was assigned to the lowest-energy TA modes, and a Grüneisen parameter of $+1$ was assigned

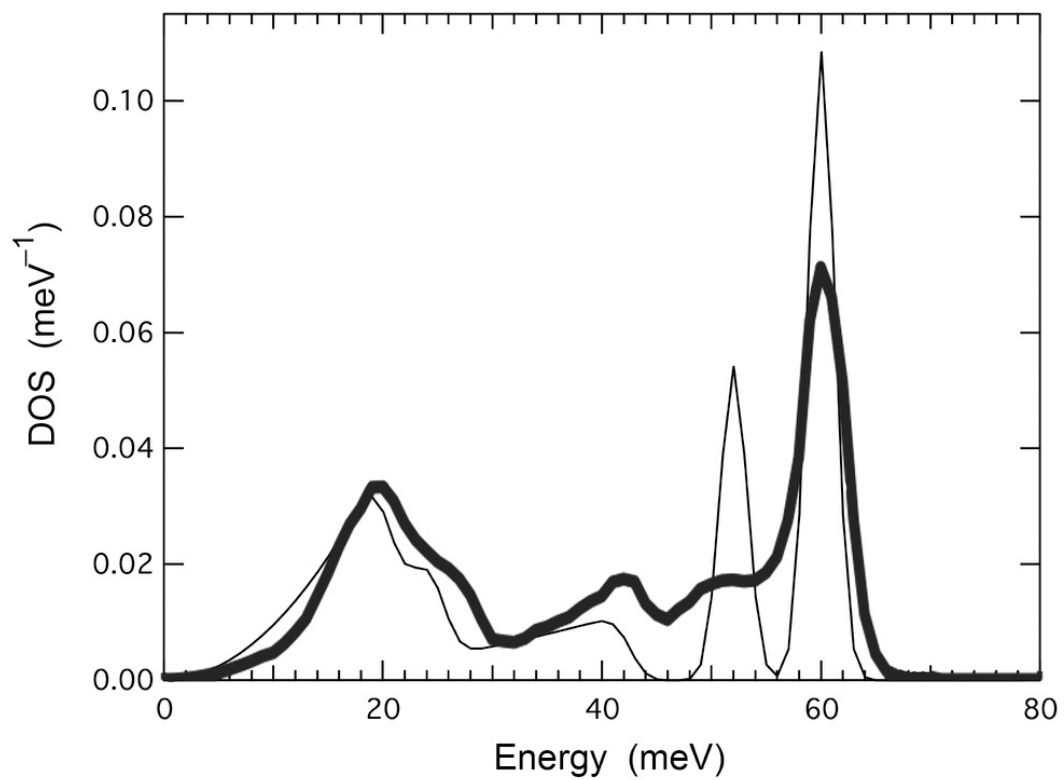


Figure 3.10: Phonon DOS of Si from (thick line) experimental measurement at 100 K [21], and (thin line) approximated with Debye and Einstein models.

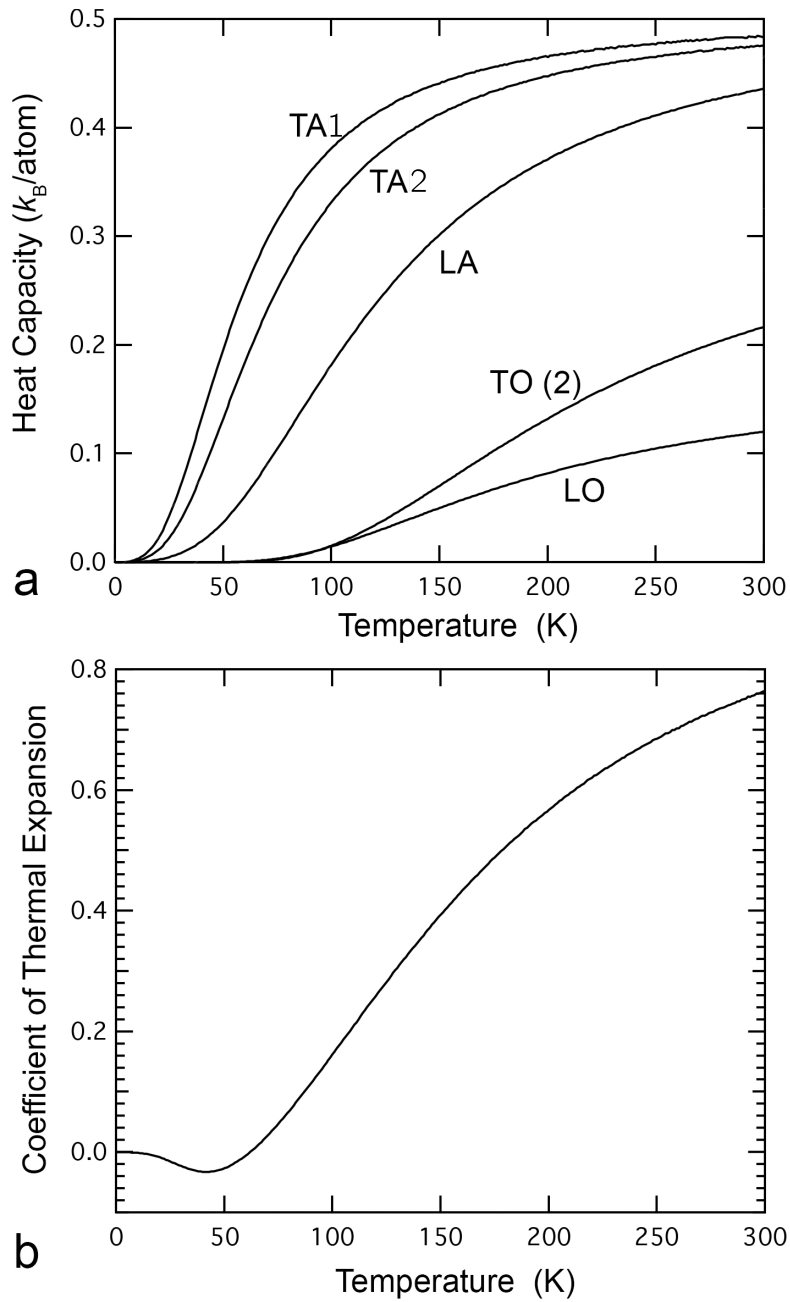


Figure 3.11: (a) Heat capacities from phonons approximated by Debye and Einstein models, using the six branches of Fig. 3.10. (b) Coefficient of thermal expansion, assuming all Grüneisen parameters were +1 except for TA modes set as -1.

to the other five phonon branches. The thermal expansion as a function of temperature, shown in Fig. 3.(b), has a shape that follows the heat capacity curves times their Grüneisen parameters. At low temperatures, the negative contribution from the TA1 modes overcomes the positive contribution from the TA2 modes, but the thermal expansion changes sign when the LA modes are sufficiently occupied. With six Grüneisen parameters, there are many ways to optimize the thermal expansion as a function of temperature, and the depth and breadth of the minimum can be tuned by appropriate parameter selection. We did not explore this further because the main text shows that this approach is physically incorrect.

Simple Springs and Angular Bonds

The simplest model of harmonic interatomic forces is useful for illustrating a geometrical source of phonon anharmonicity. Fig. 3.(a) shows a tetrahedron with a Si atom surrounded by its nearest neighbors. The four bonds are assumed to be harmonic springs, and it can be initially assumed that the neighbors remain fixed in position. As shown in Fig. 3.(a), the springs are relaxed, with no elastic energy. If the central Si atom is displaced vertically, the amount of elastic energy stored in the spring to the neighbor above is the same for positive and negative displacements of equal magnitude. This symmetry does not hold for the lower three springs. Upwards displacements are more along the directions of the springs, and generate more elastic energy than downwards displacements. The elastic energy is straightforward to calculate for harmonic springs in a tetrahedral coordination with angles of 109.5° and a nearest-neighbor separation of a . For vertical displacements, x , a numerical fit to the elastic energy in

all four springs gives

$$E_{el}(x) \propto \left(\frac{x}{a}\right)^2 + 0.666 \left(\frac{x}{a}\right)^3, \quad (3.9)$$

so negative x (downwards) displacements are more favorable energetically. The lengthening of the vertical bond in Fig. 3.(a) gives positive thermal expansion, and it is likely important at high temperatures when numerous short wavelength phonons disrupt the cooperative displacements between adjacent tetrahedra.

For long wavelength phonons, however, displacements along the [111] direction can provide for negative thermal expansion. Figure 3.(a) helps to illustrate a phonon mode where the vertical Si pairs along [111] maintain a fixed separation, and vibrate as a unit along the [111] direction. For the case shown in Fig. 3.(b), the cubic anharmonicity of Eq. 3.9 will cause a decrease in separations between planes of atoms, illustrated by the arrows. For a 1% mean-squared displacement, Eq. 3.9 predicts that the cubic term is approximately 1% of the magnitude of the quadratic. We might expect the lattice parameter to decrease by approximately one part in 10^{-4} if such modes dominate. The complexity of accounting for all different modes and their thermal occupancies makes further analysis impractical, however. These examples show

- When atom displacements are not along the directions of the springs, phonon modes can be anharmonic even when the springs are harmonic.
- These geometrically-induced anharmonicities can change sign with the wavevector of the phonon mode.

The influence of anharmonicity may also be expected because the geo-

metrical structure of silicon does not have inversion symmetry at each atom. This allows cubic phonon-phonon interactions in first order [3, 48], making vibrational modes more free to exchange energy.

Transverse Bonds

The diamond cubic structure is not stable under longitudinal forces alone, and transverse forces are required to prevent its collapse into a denser structure. Xu, et al., argue that the negative thermal expansion of silicon depends on the relative strengths of the first-nearest-neighbor bond-bending and bond-stretching forces [6]. For two specific phonon modes ($TA(\mathbf{q}=X)$ and $TA(\mathbf{q}=L)$), they develop a mechanical model that predicts negative Grüneisen parameters when both central forces and non-central forces are of comparable strength. They note that the relative strength of the non-central forces plays a major role in setting the thermal expansion of silicon [6].

We decomposed pairwise interactions between silicon atoms, quantified as force constant tensors, into components that are transverse and longitudinal to the relevant bond. Interestingly, we found that with a model quasi-harmonic system there is some optimal scaling of the transverse to longitudinal force constants that results in maximal negative thermal expansion in Si. (Although the simple modes described previously in Section B have no transverse forces but have negative Grüneisen parameters, there are many other modes that contribute to the thermal expansion.) To do this, we began with force constant tensors that describe pairwise interactions between the atom at each of the two distinct symmetry positions in silicon and its closest 123 neighbors as a

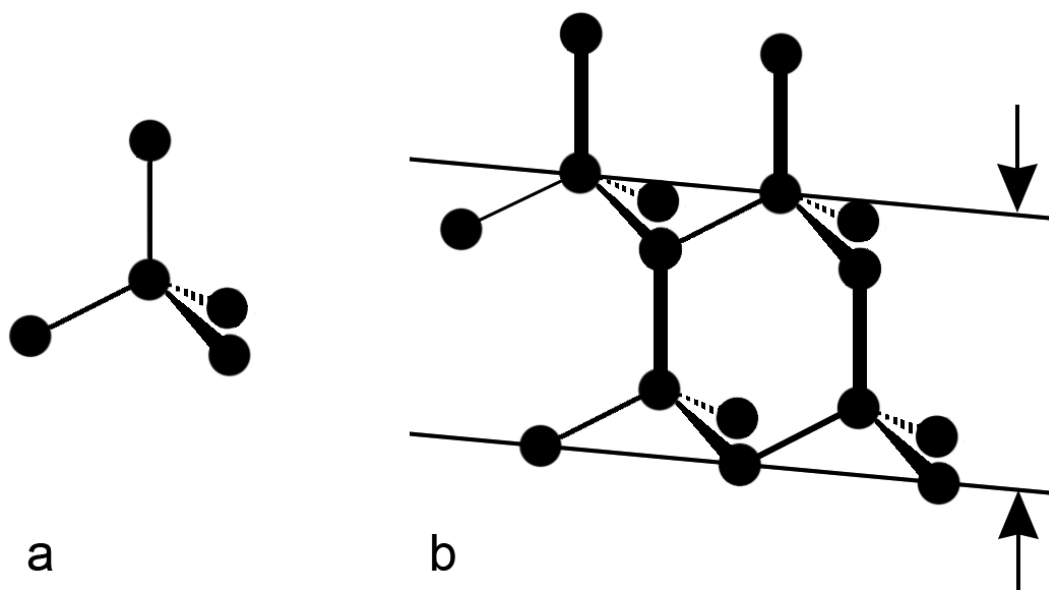


Figure 3.12: **a**, Tetrahedral coordination around a central Si atom. **b**, four interconnected tetrahedra of the diamond cubic structure. Thick vertical lines are along a $[111]$ direction.

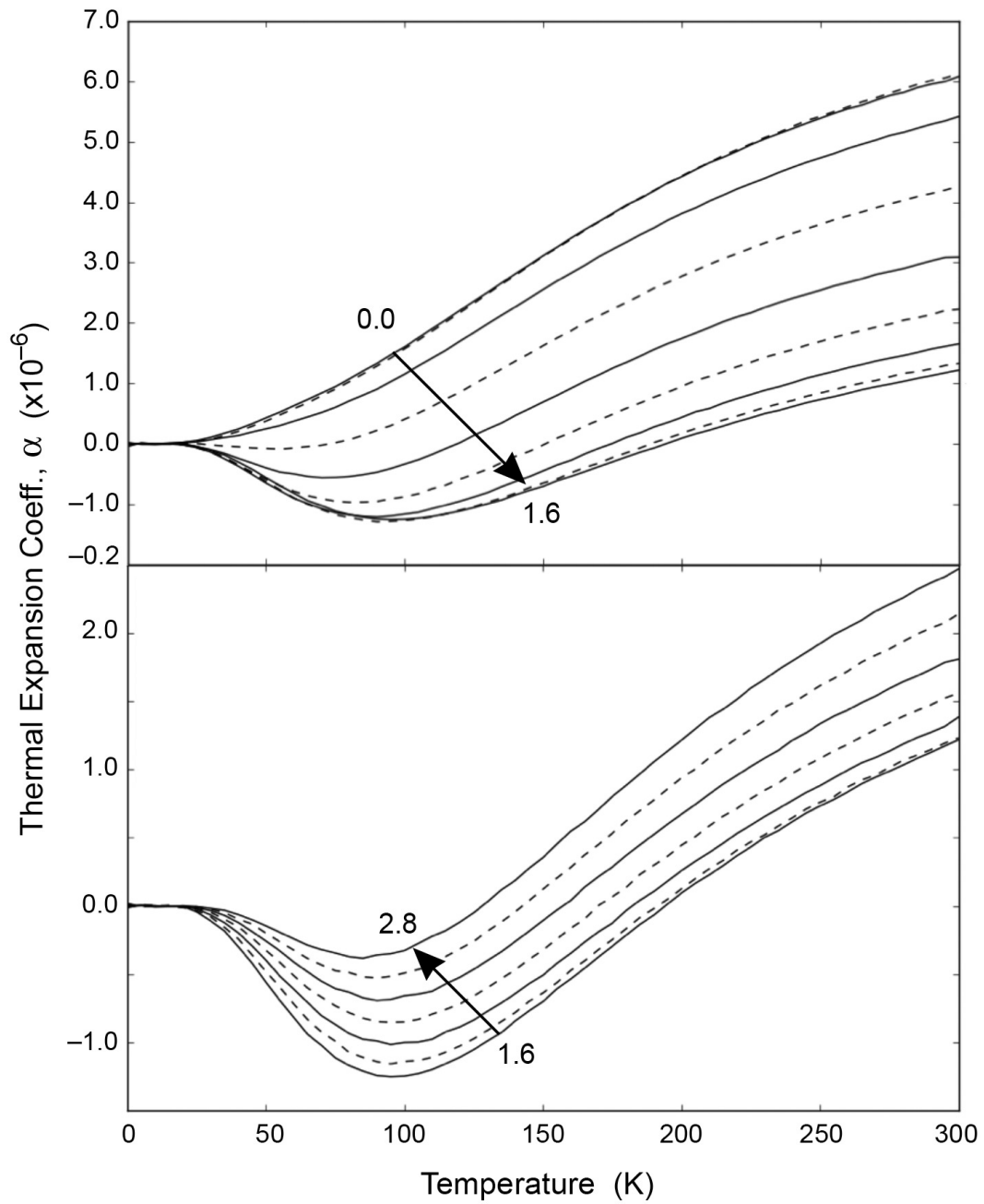


Figure 3.13: Trends for silicon's thermal expansion coefficient vs. temperature plotted for scalings of the ratio of transverse to longitudinal force constants between 0 and 2.8

function of volume at 0 K. For each pairwise interaction between each of the atoms at distinct symmetry positions and its neighbors, we decomposed the force constant tensor into components transverse and longitudinal to the bond between the pair of atoms. We scaled the ratio of transverse to longitudinal force constants by a constant, k , while holding fixed the norm of the force constant tensor. We then calculated the thermal expansion in silicon for values of k between 0 and 2.8. In Fig. 3.13, we show that increasing the ratios of transverse to longitudinal force constants in the system for values of k between 0 and about 1.6 increases the amount of negative thermal expansion, and that increasing k beyond 1.6 decreases negative thermal expansion. In Fig. 3.14, we illustrate the dependence of the negative thermal expansion on the ratios of transverse to longitudinal force constants by plotting the minimum value of thermal expansion exhibited by the system (one metric for quantifying the degree of NTE) against the scaling constant k . Although the quasiharmonic approximation should not be used to predict how negative Grüneisen parameters give the negative thermal expansion of silicon, the ratio of forces should influence on the thermal expansion of diamond cubic structures.

Quantum and Zero-point Effects

Models with transverse bonds and simple springs, like many other previous models, can be understood with classical mechanics. There is evidence that this is inadequate [22, 23]. For lattice dynamics, the difference between quantum and classical particles are evident in the governing distributions. Classical molecular dynamics or even Born-Oppenheimer *ab initio* molecular dynamics are still classical depictions of nuclear dynamics, and do not provide the correct

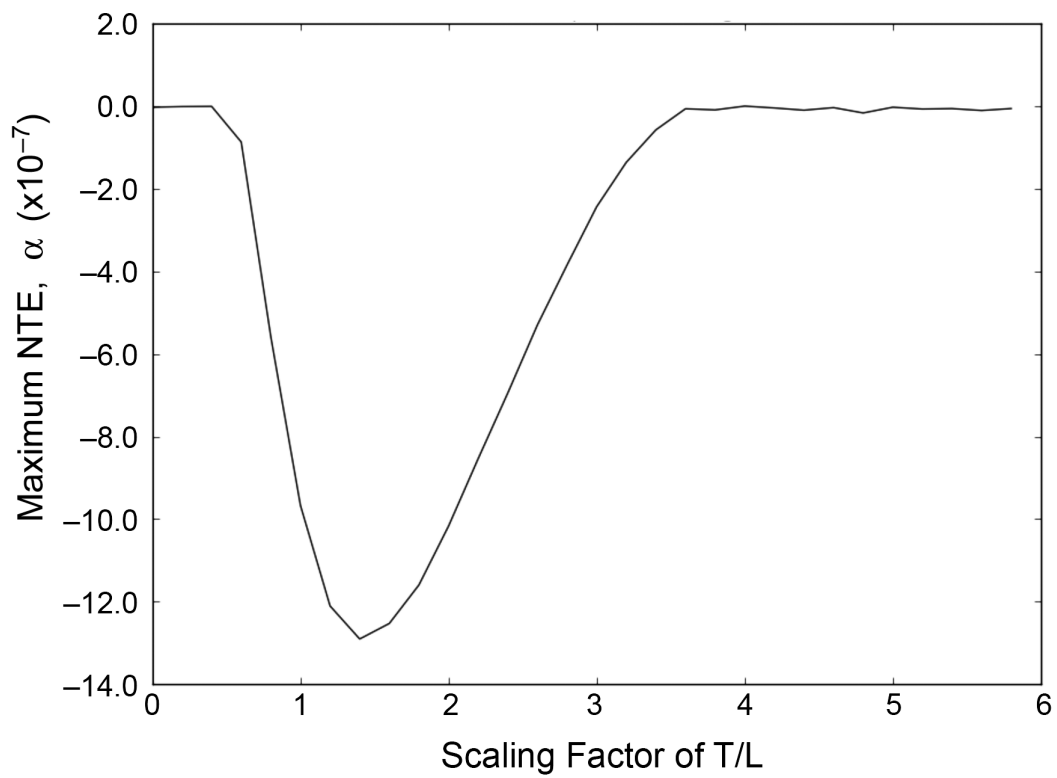


Figure 3.14: Maximum negative thermal expansion coefficients taken from each trend in Fig. S5 plotted against the scaling factor, k , applied to the ratios of transverse to longitudinal force constants.

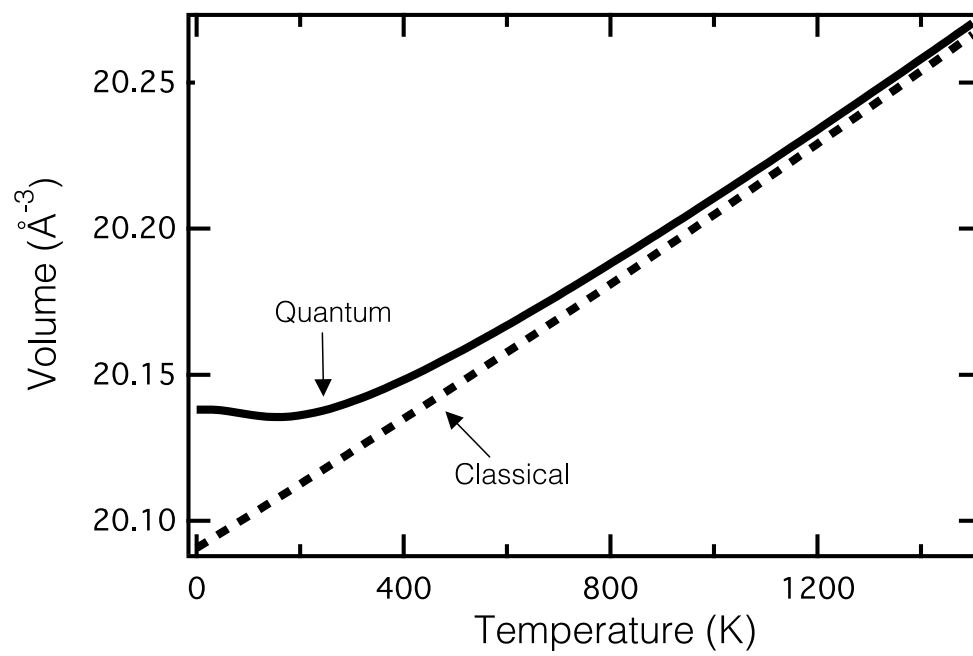


Figure 3.15: Volume as a function of temperature for silicon obtained from classical and quantum mechanical free energies.

quantum distributions. There have been great advances in overcoming this by utilizing path-integral methods to include nuclear quantum effects including zero-point motion [23], but a full *ab initio* path-integral molecular dynamics of solid materials is computationally expensive. We have addressed these limitations through our stochastic method as described above which includes the zero-point energy ($\hbar\omega_x/2$) in Eq. 4.3, giving nuclear quantum effects with the anharmonicity.

Using Eq. 3.8 for classical or quantum distributions in Eq. 3.7 for the free energy give major differences in thermal expansion in silicon, as shown in Fig. 3.15. Even at lower temperatures, the zero-point energy brings importance to all the phonon modes. Not only are quantum effects essential at lower temperatures, but differences persist up to melting temperatures. Varying the zero-point motion from changes in nuclear mass allow for an interesting engineering opportunity, too [23, 49–51]

In general, all of the models explained above are effective for a pedagogical thought exercise for a “physical interpretation” of the negative thermal expansion of silicon, but no single simple model is able to capture the full behavior. A simple model has not yet been provided, as there is none.

References

- ¹Fultz, B., “Vibrational thermodynamics of materials”, *Prog. Mater. Sci.* **55**, 247–352 (2010).
- ²B. Fultz, *Phase transitions in materials* (Cambridge Univ. Press, Cambridge, Jan. 2014).
- ³A. A. Maradudin and A. E. Fein, “Scattering of Neutrons by an Anharmonic Crystal”, *Phys. Rev.* **128**, 2589–2608 (1962).
- ⁴S. Wei, C. Li, and M. Y. Chou, “Ab initio calculation of thermodynamic properties of silicon.”, *Phys. Rev. B* **50**, 14587–14590 (1994).
- ⁵Z.-K. Liu, Y. Wang, and S. Shang, “Thermal Expansion Anomaly Regulated by Entropy”, *Scientific Reports* **4**, 7043 (2014).
- ⁶C. H. Xu, C. Z. Wang, C. T. Chan, and K. M. Ho, “Theory of the thermal expansion of Si and diamond.”, *Phys. Rev. B* **43**, 5024–5027 (1991).
- ⁷T. Middelmann, A. Walkov, G. Bartl, and R. Schödel, “Thermal expansion coefficient of single-crystal silicon from 7 K to 293 K”, *Phys. Rev. B* **92**, 174113–7 (2015).
- ⁸Y. Okada and Y. Tokumaru, “Precise determination of lattice parameter and thermal expansion coefficient of silicon between 300 and 1500 K”, *J. Appl. Phys.* **56**, 314–8 (1984).
- ⁹G. A. Slack and S. F. Bartram, “Thermal expansion of some diamondlike crystals”, *J. Appl. Phys.* **46**, 89 (1975).
- ¹⁰D. N. Batchelder and R. O. Simmons, “Lattice Constants and Thermal Expansivities of Silicon and of Calcium Fluoride between 6° and 322° K”, *J. Chem. Phys.* **41**, 2324–7 (1964).
- ¹¹J. S. Shah and M. E. Strauman, “Thermal expansion behavior of silicon at low temperatures”, *Solid state Commun.* **10**, 159–162 (1972).
- ¹²O. Hellman, P. Steneteg, I. A. Abrikosov, and S. I. Simak, “Temperature dependent effective potential method for accurate free energy calculations of solids”, *Phys. Rev. B* **87**, 104111 (2013).
- ¹³B. A. Weinstein and G. J. Piermarini, “Raman scattering and phonon dispersion in Si and GaP at very high pressure”, *Phys. Rev. B* **12**, 1172–1186 (1975).

- ¹⁴G. Nilsson and G. Nelin, "Study of the Homology between Silicon and Germanium by Thermal-Neutron Spectrometry", *Phys. Rev. B* **6**, 3777–3786 (1972).
- ¹⁵A. Debernardi, S. Baroni, and E. Molinari, "Anharmonic Phonon Lifetimes in Semiconductors from Density-Functional Perturbation Theory", *Phys. Rev. Lett.* **75**, 1819–1822 (1995).
- ¹⁶S. Narasimhan and D. Vanderbilt, "Anharmonic self-energies of phonons in silicon.", *Phys. Rev. B* **43**, 4541–4544 (1991).
- ¹⁷M. Balkanski, R. F. Wallis, and E. Haro, "Anharmonic effects in light scattering due to optical phonons in silicon", *Phys. Rev. B* **28**, 1928–1934 (1983).
- ¹⁸C. Z. Wang, C. T. Chan, and K. M. Ho, "Empirical tight-binding force model for molecular-dynamics simulation of Si.", *Phys. Rev. B* **39**, 8586–8592 (1989).
- ¹⁹J. Menéndez and M. Cardona, "Temperature dependence of the first-order Raman scattering by phonons in Si, Ge, and α -Sn: Anharmonic effects", *Phys. Rev. B* **29**, 2051–2059 (1984).
- ²⁰R. Tsu and J. G. Hernandez, "Temperature dependence of silicon Raman lines", *Appl. Phys. Lett.* **41**, 1016–1018 (1982).
- ²¹D. S. Kim, H. L. Smith, J. L. Niedziela, C. W. Li, D. L. Abernathy, and B. Fultz, "Phonon anharmonicity in silicon from 100 to 1500 K", *Phys. Rev. B* **91**, 014307 (2015).
- ²²P. B. Allen, "Anharmonic phonon quasiparticle theory of zero-point and thermal shifts in insulators: heat capacity, bulk modulus, and thermal expansion", *Phys. Rev. B* **92**, 064106 (2015) [10.1103/PhysRevB.92.064106](https://doi.org/10.1103/PhysRevB.92.064106).
- ²³C. P. Herrero and R. Ramírez, "Path-integral simulation of solids", *J. Phys.: Condens. Matter* **26**, 233201–36 (2014).
- ²⁴B. N. Brockhouse, "Lattice Vibrations in Silicon and Germanium", *Phys. Rev. Lett.* **2**, 256–258 (1959).
- ²⁵D. L. Abernathy, M. B. Stone, M. J. Loguillo, M. S. Lucas, O. Delaire, X. Tang, J. Y. Y. Lin, and B. Fultz, "Design and operation of the wide angular-range chopper spectrometer ARCS at Spallation Neutron Source", *Rev. Sci. Instrum.* **83**, 015114 (2012).
- ²⁶G. L. Squires, *Introduction to the Theory of Thermal Neutron Scattering* (Cambridge Univ. Press, Cambridge, Mar. 2012).

- ²⁷H. R. Glyde, “Interference Effects in Neutron and X Ray Scattering”, *Can. J. Phys.* **52**, 2281 (1974).
- ²⁸G. Kresse and J. Hafner, “Ab initio molecular dynamics for liquid metals”, *Phys. Rev. B* **47**, 558–561 (1993).
- ²⁹G. Kresse and J. Hafner, “Ab initio molecular-dynamics simulation of the liquid-metal-amorphous-semiconductor transition in germanium”, *Phys. Rev. B* **49**, 14251–14269 (1994) [10.1103/PhysRevB.49.14251](https://doi.org/10.1103/PhysRevB.49.14251).
- ³⁰G. Kresse and J. Furthmüller, “Efficiency of ab-initio total energy calculations for metals and semiconductors using a plane-wave basis set”, *Comput. Mater. Sci.* **6**, 15–50 (1996).
- ³¹G. Kresse and J. Furthmüller, “Efficient iterative schemes for ab initio total-energy calculations using a plane-wave basis set”, *Phys. Rev. B* **54**, 11169–11186 (1996) [10.1103/PhysRevB.54.11169](https://doi.org/10.1103/PhysRevB.54.11169).
- ³²A. E. Mattsson, R. Armiento, J. Paier, G. Kresse, J. M. Wills, and T. R. Mattsson, “The AM05 density functional applied to solids”, *The Journal of Chemical Physics* **128**, 084714–12 (2008).
- ³³A. E. Mattsson and R. Armiento, “Implementing and testing the AM05 spin density functional”, *Phys. Rev. B* **79**, 155101–13 (2009).
- ³⁴R. Armiento and A. E. Mattsson, “Functional designed to include surface effects in self-consistent density functional theory”, *Phys. Rev. B* **72**, 085108–5 (2005).
- ³⁵O. Hellman and I. A. Abrikosov, “Temperature-dependent effective third-order interatomic force constants from first principles”, *Phys. Rev. B* **88**, 144301 (2013) [10.1103/PhysRevB.88.144301](https://doi.org/10.1103/PhysRevB.88.144301).
- ³⁶I. Errea, M. Calandra, and F. Mauri, “Anharmonic free energies and phonon dispersions from the stochastic self-consistent harmonic approximation: Application to platinum and palladium hydrides”, *Phys. Rev. B* **89**, 064302–16 (2014).
- ³⁷N. Shulumba, O. Hellman, and A. J. Minnich, “Intrinsic localized mode and low thermal conductivity of pbse”, *Phys. Rev. B* **95**, 014302 (2017) [10.1103/PhysRevB.95.014302](https://doi.org/10.1103/PhysRevB.95.014302).
- ³⁸S. P. Nikanorov, Y. A. Burenkov, and A. V. Stepanov, “Elastic Properties of Si”, *Sov. Phys. Solid State* **13**, 2516–2518 (1972).

- ³⁹M. B. Stone, J. L. Niedziela, M. J. Loguillo, M. A. Overbay, and D. L. Abernathy, "A radial collimator for a time-of-flight neutron spectrometer", *Review of Scientific Instruments* **85**, 085101 (2014).
- ⁴⁰*Mantid (2013): manipulation and analysis toolkit for instrument data.; mantid project*, 2013.
- ⁴¹O. Arnold, J. C. Bilheux, J. M. Borreguero, A. Buts, S. I. Campbell, L. Chapon, M. Doucet, N. Draper, R. F. Leal, M. A. Gigg, V. E. Lynch, A. Markvardsen, D. J. Mikkelson, R. L. Mikkelson, R. Miller, K. Palmen, P. Parker, G. Passos, T. G. Perring, P. F. Peterson, S. Ren, M. A. Reuter, A. T. Savici, J. W. Taylor, R. J. Taylor, R. Tolchenov, W. Zhou, and J. Zikovsky, "Mantid—Data analysis and visualization package for neutron scattering and μ SR experiments", *Nucl. Instrum. Meth. A* **764**, 156–166 (2014).
- ⁴²R. A. Ewings, A. Buts, M. D. Le, J. van Duijn, I. Bustinduy, and T. G. Perring, "Horace: Software for the analysis of data from single crystal spectroscopy experiments at time-of-flight neutron instruments", *Nuclear Instruments & Methods in Physics Research Section a-Accelerators Spectrometers Detectors and Associated Equipment* **834**, 132–142 (2016).
- ⁴³C. W. Li, J. Hong, A. F. May, D. Bansal, S. Chi, T. Hong, G. Ehlers, and O. Delaire, "Orbitally driven giant phonon anharmonicity in SnSe", *Nature Physics* **11**, 1063–1069 (2015).
- ⁴⁴P. E. Blochl, "Projector augmented-wave method", *Phys.Rev.* **B50**, 17953–17979 (1994).
- ⁴⁵X. Gonze and C. Lee, "Dynamical matrices, born effective charges, dielectric permittivity tensors, and interatomic force constants from density-functional perturbation theory", *Phys. Rev. B* **55**, 10355–10368 (1997).
- ⁴⁶D. C. Wallace, *Thermodynamics of Crystals* (Wiley, New York, 1972).
- ⁴⁷M. T. Dove, *Introduction to Lattice Dynamics* (Cambridge University Press, Oct. 1993).
- ⁴⁸J. L. Feldman, L. L. Boyer, Edwardson, P. J., and J. R. Hardy, "Calculation of Dielectric Susceptibility for Complex Ionic Systems - Application to a Predicted Superlattice", *Phys. Rev. B* **40**, 4105–4118 (1989).
- ⁴⁹C. P. Herrero, R. Ramírez, and M. Cardona, "Isotope effects on the lattice parameter of cubic SiC", *Physical Review B* **79**, 012301–4 (2009).

- ⁵⁰C. P. Herrero, “Dependence of the silicon lattice constant on isotopic mass”, *Solid State Communications* **110**, 243–246 (1999).
- ⁵¹J. C. Noya, C. P. Herrero, and R. Ramírez, “Isotope dependence of the lattice parameter of germanium from path-integral Monte Carlo simulations”, *Physical Review B* **56**, 237–243 (1997).

Chapter 4

THERMAL CONDUCTIVITY OF SILICON

Abstract:

Inelastic neutron scattering is vital for a fundamental understanding of materials. Measured temperature-dependent phonon spectrum contain phonon energies and scattering lifetime information; all the information needed to determine thermal properties. But the correct determination of phonon lifetimes (linewidths) throughout the Brillouin zone are difficult to assess due to beam brightness, interference effects, polarization, multiphonon scattering, and instrument resolution. We were able to overcome these limitations by deconvolving linewidths from scattering data that used a reduction process that “folds” and subtracts the multiphonon spectrum. We determined phonon linewidths and phonon centroids throughout the Brillouin zone and compared to *ab initio* calculations. This method advances experimental and *ab initio* methods for thermophysical property analysis. Phonon anharmonicities are required to obtain correct lattice dynamics shifts but do not significantly effect the total thermal conductivity.

Understanding thermal properties of materials is of the utmost importance for current and future development of technologies. One of these thermal properties is the thermal conductivity, a fundamental quantity in transport phenomena that describes how a crystal lattice conducts heat. The thermal properties of silicon are extensively studied due to the wide range of silicon-based technologies including thermoelectrics, semiconductors, electronics, nanomechanics, and photovoltaics [1–10]. Understanding the silicon lattice thermal conductivity through both calculations and experiment provides valuable insight for designing more efficient silicon-based technologies. Silicon is also a perfect model material to build more encompassing thermal lattice dynamics models.

Historically, the experimental lattice thermal conductivity of silicon was measured as a standard value due to the high purity and availability of the crystal. Initial silicon experiments used a radial heat flow apparatus to determine the lattice thermal conductivity [11, 12]. More modern experimental techniques include the time and frequency-domain transient thermoreflectance methods, and mean free path spectroscopy which are applicable for both bulk and thin film samples [13, 14]. Due to the abundance of experimental thermal conductivity of silicon, calculating the thermal conductivity via *ab initio* techniques has gained traction in recent years. In these methods the lattice thermal conductivity is calculated by iteratively solving the Boltzmann transport equation (BTE), or using the Green-Kubo method with either classical force field potentials or *ab initio* derived ones [15–20].

For semiconductors, like silicon, this theory traces back to the micro-

scopic model for phonon-phonon scattering developed by Peierls in 1929 [21]. The lattice thermal conductivity is largely dominated by phonon-phonon interactions, phonon anharmonicity, especially at high temperatures. The phonon-phonon couplings shorten phonon lifetimes and cause shifts in central frequencies, which results in a finite phonon mean free path in thermal transport. Although, in many materials, conductivity calculations are heavily dependent on volume/pressure and temperature, classical forces and many-body perturbation methods predict the correct temperature dependence of phonon lifetimes and thermal conductivity in silicon [16, 18, 22–24].

Previous studies on silicon show, however, that thermal trends of phonon frequency shifts in silicon are not accurately described by the quasiharmonic model, harmonic frequencies renormalized with thermal expansion [25, 26]. Due to the lack of experimental verification, a better understanding of both changes in phonon centers and linewidths, the phonon self-energy, is necessary. The phonon self-energy, ($\Sigma = \Delta + i\Gamma$), the anharmonic corrections to the harmonic frequencies, provide the necessary corrections through shifts and broadenings of finite temperature lattice dynamic behavior.

Difficulties in determining accurate thermal conductivity information from phonon lifetimes measured by inelastic neutron scattering measurements are due to instrument resolution, missing volumes of the Brillouin zones, or overall source brightness. Typically only a few modes are assessed through triple-axis experiments or Raman scattering [27–32]. Due to instrument resolution, although single crystals on chopper spectrometers have been used to determine trends, a quantitative linewidth determinations require complemen-

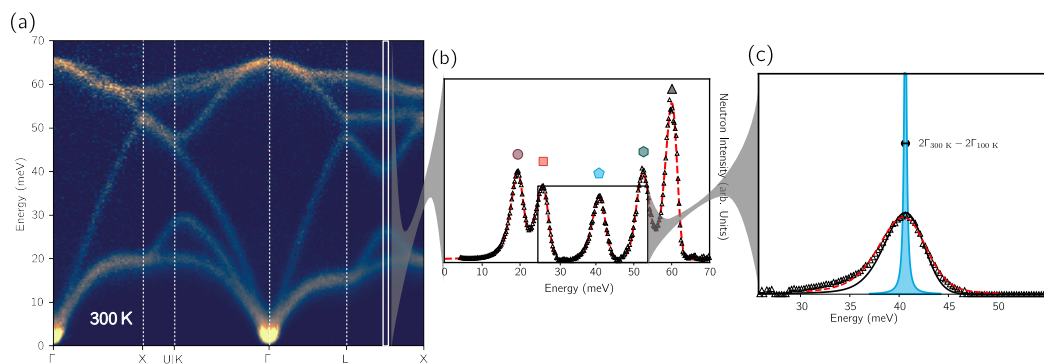


Figure 4.1: Phonon linewidths from inelastic neutron scattering experiments. (a) Example of experimental phonon dispersions of silicon from inelastic neutrons scattering data of silicon. Data were measured on ARCS time-of-flight spectrometer at 300 K, and reduced, multiphonon subtracted and “folded” into one irreducible wedge in the first Brillouin zone. (b) Phonon scattering spectra determined at \mathbf{q} -point = $(0.75, 0.25, 0.25)$ r.l.u.. Experimental data is shown as purple circle markers and best fit of peaks is in grey solid line. The longitudinal acoustic mode is highlighted as an example of phonon lineshape deconvolution. (c) Deconvoluted longitudinal acoustic mode phonon lineshape at \mathbf{q} -point = $(0.75, 0.25, 0.25)$ r.l.u. at 300 K.

tary model calculations. These hurdles were overcome through in this work through a “folding” and multiphonon subtraction data reduction scheme. To date we report the highest statistical quality of phonon dispersions of silicon with temperature. We report accurate measurements of phonon dispersions, frequencies and linewidths, from time-of-flight inelastic neutron scattering experiments and show the effects of anharmonicity on thermal conductivity.

Phonon spectrum (Fig. 4.1.a) show bright intensities at atomic vibration resonances. The widths of these peaks are the inverse of phonon lifetimes or scattering rates. Phonon dispersions with temperature were obtained through inelastic neutron scattering experiments on a time-of-flight chopper spectrometer, ARCS, at the SNS [33]. 4-dimensional scattering functions ($S(\mathbf{q}, \epsilon)$) with temperature were reduced and processed through standard reduction with “folding” and multiphonon background subtraction. Phonon linewidths, per mode (λ), were determined through the deconvolution of phonon difference lineshapes to determine the change in linewidths with temperature ($2\Gamma_T - 2\Gamma_{100K}$). Experimental methods are discussed in more detail in the Materials and Methods section. Changes in linewidths at 300, 900, 1200, 1500 K show broadening, decrease in lifetime, or decrease in lifetimes with temperature. An example of fitted phonon linewidths for the (0.75, 0.25, 0.25) \mathbf{q} -point longitudinal acoustic mode (LA) is shown in Fig. 4.2.c. Phonon centroid energies show self similar softening behavior, a decrease in energy, with temperature (Fig. 4.2.b). The observed thermal trends are in good agreement with previous results where available [12, 34, 35]. Previously, only Raman measurements of phonon linewidths at a few modes were observed and the thermal trends

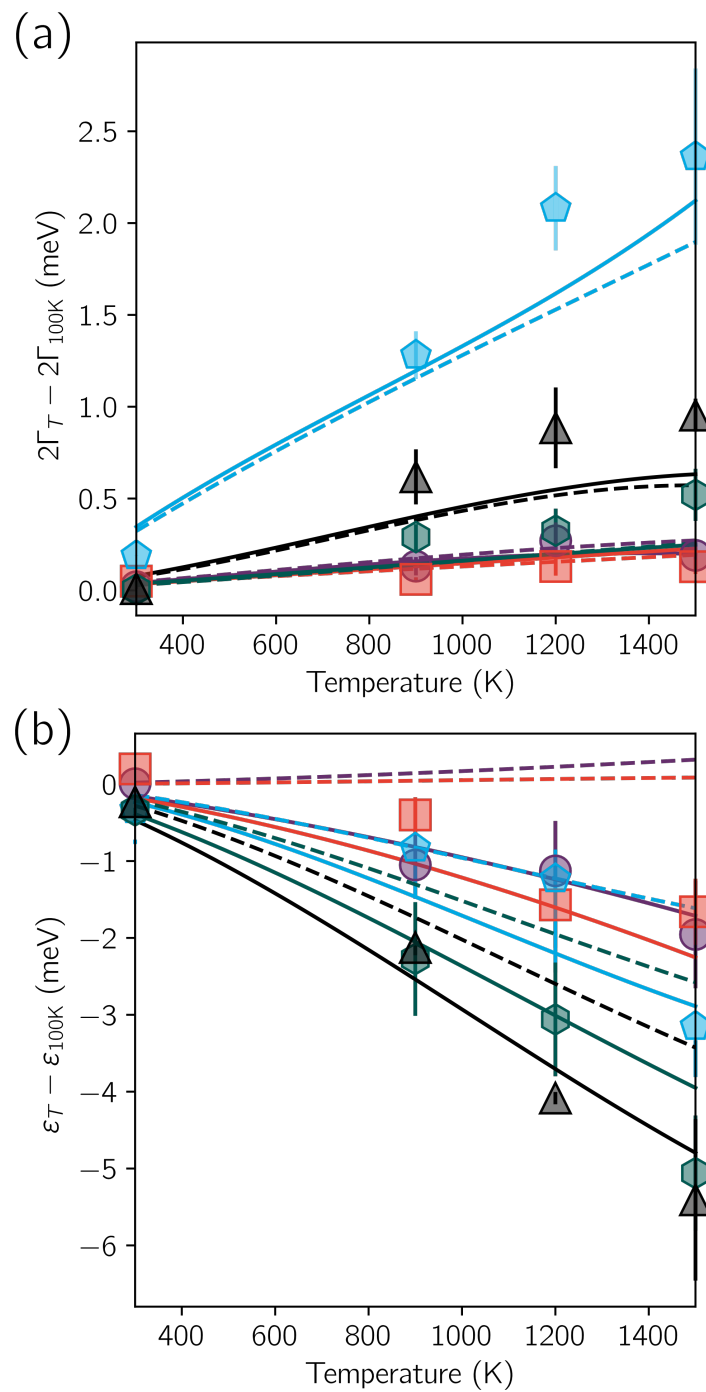


Figure 4.2: Temperature-dependence of phonon shifts and broadening of the $(0.75, 0.25, 0.25)$ q -point with temperature. Experimental changes are shown as markers, and *ab initio* calculated linewidth thermal trends with anharmonicity in teal solid line, and quasiharmonic approximation in red-dashed line.

coincide well with our results.

Recent advances in *ab initio* methods allow for direct comparisons to experimental shifts and broadenings. Equilibrium phonon dispersions and linewidths with phonon anharmonicities were calculated using DFT and the stochastically initialized temperature-dependent effective potential method (s-TDEP) [36–38]. The quasiharmonic phonon dispersions and linewidths were calculated as described in the Materials and Methods section. The quasiharmonic theory does not include phonon interactions and would not have any lifetimes associated with phonon and only scaled energies with respect to volume expansion. But the third-order forces on atoms can be determined from the 0 K force constants (harmonic model) in the TDEP framework (Materials and Methods) or even as the third derivatives using density functional perturbation theory [39] at various volumes. Both calculations inherently include pure anharmonicity, but the s-TDEP calculations include the temperature-dependence sampled through a stochastic canonical ensemble average.

We find good agreement with experimental shifts and broadenings with our phonon anharmonicity included *ab initio* calculations. The quasiharmonic shifts with temperature are heavily underestimated for softening in the higher energy modes [40].

Both the s-TDEP and quasiharmonic calculations are in good agreement with measured broadenings throughout the Brillouin zone (Table ??). We have assessed over 950 modes and phonon centroids and linewidths and can be found in the Supplemental Information. For the longitudinal acoustic modes

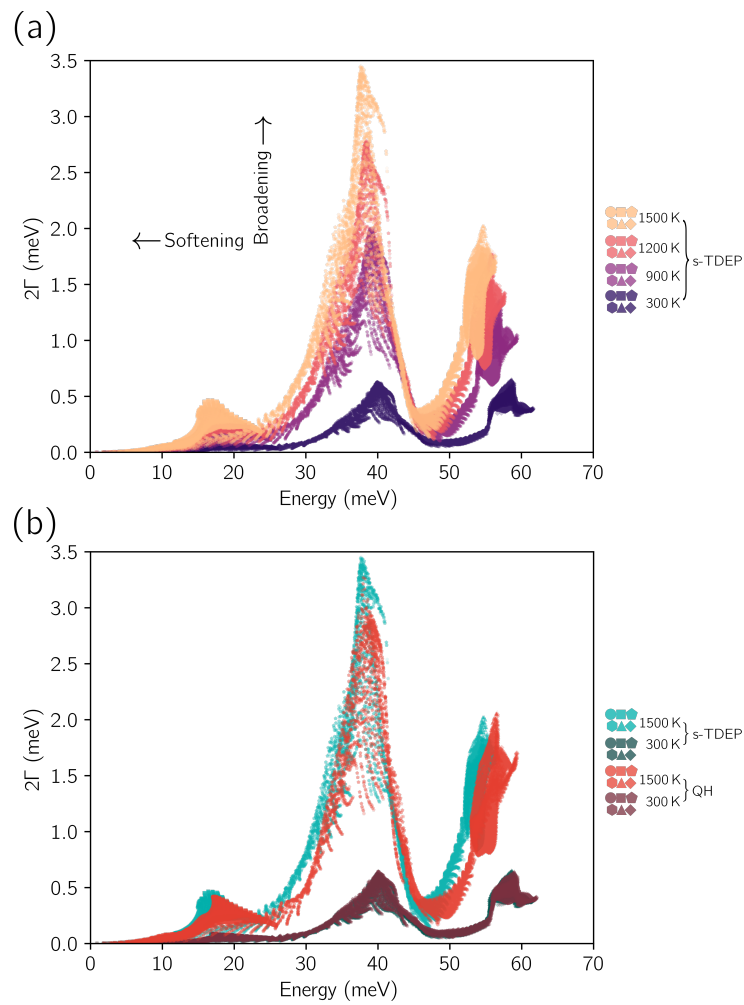


Figure 4.3: *Ab initio* calculated phonon linewidths with temperature ($2\Gamma = 1/\tau$). (a) Temperature dependence of shifts and broadenings throughout the Brillouin zone. (b) A comparison between the s-TDEP and quasiharmonic calculations at 300 K and 1500 K.

and optical phonons we find the s-TDEP calculations slightly underestimate the thermal broadenings in linewidths compared to s-TDEP and quasiharmonic calculated linewidths.

Phonon linewidths ($1/\tau$) throughout the Brillouin zone are shown in Fig. 4.3 for a better comparison between the quasiharmonic and s-TDEP calculations. Figure 4.3.a shows the temperature effects and resultant softening and broadening with temperature from a $50 \times 50 \times 50$. Although, the quasiharmonic model can produce a significant portion of broadening with temperature, the central frequencies are not. At 1500 K the s-TDEP calculated shifts are 65% and broadening 15% different than those of the quasiharmonic model. A comparison between the average phonon energy shifts and averaged broadening are shown in Fig. 4.3.a-b. The experimental points in purple are calculated from Table ???. Finite linewidths were determined by adding to 100 K calculated linewidths.

Using both the second and third order interatomic force constants we solved the Boltzmann transport equations with temperature as described in the Materials and Methods section. We calculated total and mode-dependent spectral thermal conductivity ($\kappa(\varepsilon)/\kappa_{tot}$) with temperature shown in Fig. 4.5 to show the amount of heat carried with phonon energy. The majority of heat is carried through low-energy phonons. Optical modes carry only 5 % of heat at 300 K and increases to roughly 8.5 % at 1500 K (Fig. 4.4). With temperature higher-modes increase in contribution to thermal conductivity. But, pure anharmonicity included s-TDEP calculations at 1500 K show higher heat carried by lower energies shown in Fig. 4.4. The quasiharmonic calculations show a greater

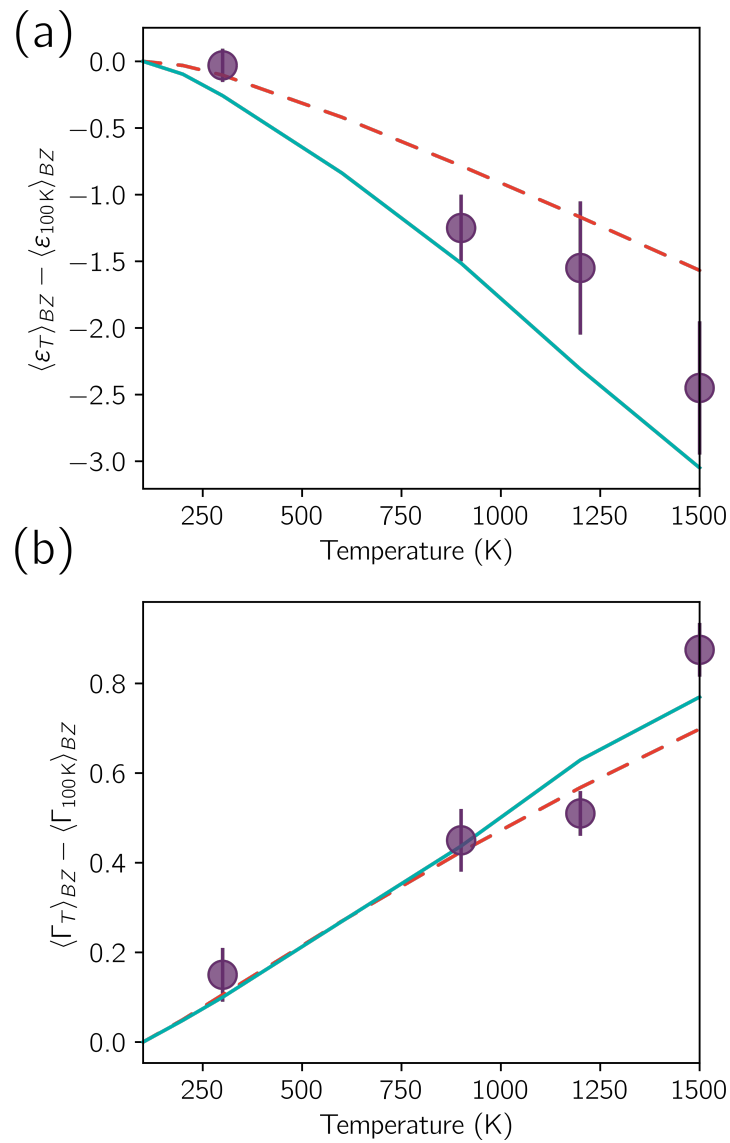


Figure 4.4: Brillouin zone averaged temperature-dependent phonon energies (a) and linewidths (b). Energies calculated from experimental fits from Table ?? are in purple circle markers and *ab initio* calculations of the s-TDEP (solid teal line) and quasiharmonic approximation (red dashed line) are also shown.

increase in heat carried by optical modes than s-TDEP calculation by an 11 % difference. The total thermal conductivity values are in good agreement with experimental values (Fig. 4.5). At higher temperatures (> 1200 K) we see a decrease in conductivity in both quasiharmonic and s-TDEP calculations.

At all temperatures the experimental linewidths, therefore phonon scattering lifetimes, are in agreement with *ab initio* calculations. Pure anharmonicity beyond perturbation calculations using quasiharmonic forces show changes in shifts of frequencies, but only small deviations of linewidth changes at elevated temperatures (> 800 K). The small frequency corrections from thermal expansion do not significantly alter calculations from constant volume calculations. Pure phonon anharmonicities with temperature are shown to affect the real part of phonon self-energy, the shifts in frequencies with temperature. The real part of the self-energy is consisted of third and fourth-order contributions, we expect a proper fourth-order calculations would increase the accuracy of temperature-dependent shifts. The s-TDEP method allows the sampling of all orders of anharmonicity contained to the second and third order forces.

The observed softening in all phonons with temperature, although thermodynamically significant [40], do not seem to affect the thermal transport calculations. The cause of this can be explained as follows. The kinematics of the anharmonic coupling between modes are essentially unchanged as softening is self-similar in all modes and the ratios between branches are not changed. Therefore the large acoustic optical mode gap or acoustic bunching [41] are not created and could be the cause for small differences between the quasiharmonicity and pure anharmonicity calculated phonon lifetimes. There are also

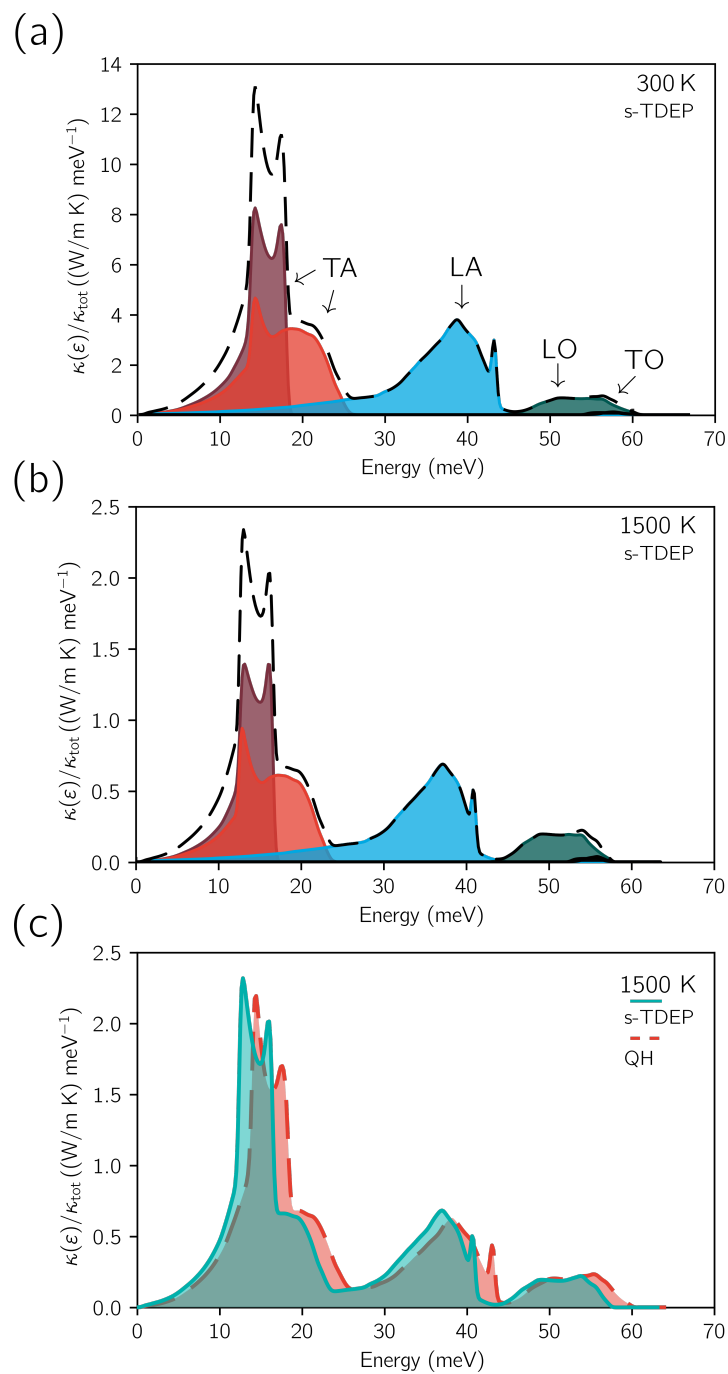


Figure 4.5: Spectral thermal conductivity ($\kappa(\epsilon)/\kappa_{\text{tot}}$) at 300 (a) and 1500 K (b). *Ab initio* calculated total spectral thermal conductivity of silicon at as a black dashed line. Mode dependent spectral functions are shown as the shaded area(TA: maroon and red, LA: blue, LO: green, and TO: black). (b) Comparison between s-TDEP (teal) and quasiharmonic (red) calculation of spectral thermal conductivity.

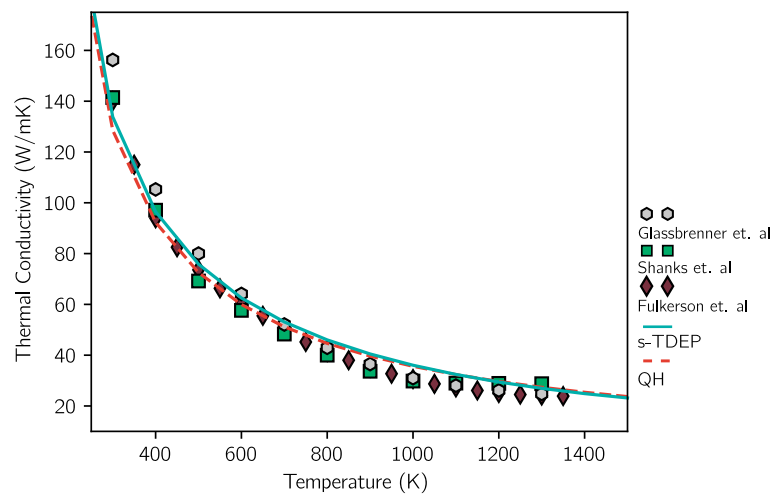


Figure 4.6: Temperature-dependent thermal conductivity of silicon. Phonon anharmonic *ab initio* calculations (s-TDEP) are shown as a solid teal line and the quasiharmonic model in red dashed line. Experimental points as markers [12, 34, 35].

no significant differences in the group velocities, and only significant differences in phonon lifetimes of higher energy modes ($> 30 \text{ meV}$). But the contribution from the higher energy modes are decreased as the overall softening heightens the low transverse mode contributions to the overall thermal conductivity. Generally, the heat capacity per mode would not change with softening alone as the decrease in energy is compensated by the increase in population [42].

These methods for determining phonon lifetimes and centroid frequencies in materials extends beyond a study of silicon. The exact phonon spectrum with temperature, energy, and momentum dependence contains all of the information necessary to fit second and third order force constants for systems where *ab initio* methods are intractable. As inelastic neutron scattering experiments are not limited to simple solids and can be extended to more complex systems in other applied fields. In silicon pure anharmonicity appears mostly in the shifts with temperature throughout the Brillouin zone.

MATERIALS AND METHODS

Inelastic Neutron Scattering

Inelastic neutron scattering measurements were performed on a single crystal of silicon of 99.999% purity that was highly-oriented. The [110] oriented single crystal was machined into a cylinder of 3.8 cm in height, 2.54 cm in outer diameter and a 1.59 cm inner diameter to minimize multiple scattering. The crystal was suspended in an aluminum holder and then mounted into a closed-cycle helium refrigerator for the 100 K measurements, and a similar holder made from niobium was mounted into a low-background electrical resistance vacuum furnace for measurements at 300, 900, 1200 and 1500 K. For all measurements the incident energy was 97.5 meV, and an oscillating radial collimator was used to reduce background and multiple scattering [33, 43].

The time-of-flight neutron data included multiple datasets from 200 rotations in increments of 0.5° about the vertical [110]-axis, reduced to create the 4-dimensional $S(\mathbf{q},\epsilon)$ using standard software [44, 45]. A secondary data reduction process consisted of ‘folding’ the entire $S(\mathbf{q},\epsilon)$ data set into an irreducible wedge in the first Brillouin zone as previously mentioned [cite_me]. Phonon centroids were then fitted using the Levenberg-Marquardt non-linear least square method for multiple skewed-voigt functions. Changes in phonon linewidths ($\text{FWHM} \propto 2\Gamma$) were determined from isolating each peak at a specific \vec{q} -point and deconvoluting the finite temperature phonon lineshape from the fixed resolution approximated as the shape of the 100 K corresponding

peak. The energy resolution from the 100 K data [cite:me_alpha] corresponds well to previously reported ARCS resolution [33, 43].

Ab initio calculations

Ab initio calculations were completed with the VASP package [46–49]. The projector augmented-wave formalism with the exchange-correlation energy calculated with the AM05 functional were used [50–52]. All calculations used $5 \times 5 \times 5$ supercell with a kinetic-energy cutoff of 500 eV and a $3 \times 3 \times 3$ k -point grid. Phonon dispersions with fully anharmonic phonons with nuclear quantum effects with temperature were calculated from stochastically initialized temperature-dependent effective potential method (s-TDEP) described previously [37, 53]. All calculations were converged to within 1 meV/atom.

Finite temperature phonon dispersions of silicon were calculated by fitting first-principles forces to a model hamiltonian,

$$H = U_0 + \sum_i \frac{\mathbf{p}_i^2}{2m} + \frac{1}{2} \sum_{ij\alpha\beta} \Phi_{ij}^{\alpha\beta} u_i^\alpha u_j^\beta + \frac{1}{3!} \sum_{ijk\alpha\beta\gamma} \Phi_{ijk}^{\alpha\beta\gamma} u_i^\alpha u_j^\beta u_k^\gamma. \quad (4.1)$$

The forces on atoms were generated using DFT with various configurations of displaced atoms by a stochastic sampling of a canonical ensemble, with cartesian displacements (u_i^α) normally distributed around the mean thermal displacement using

$$u_i^\alpha = \sum_\lambda \frac{\epsilon_\lambda^{i\alpha} c_\lambda}{\sqrt{m_i}} \sqrt{-2 \ln \xi_1} \sin(2\pi \xi_2). \quad (4.2)$$

The thermal factor, c_λ , is based on thermal amplitudes of normal mode λ , with eigenvector ϵ_λ and frequency ω_λ [54–56]

$$c_\lambda = \sqrt{\frac{\hbar(2n_\lambda + 1)}{2\omega_\lambda}}, \quad (4.3)$$

and ξ_1 and ξ_2 are stochastically sampled numbers between 0 and 1. The phonon distribution follows the Planck distribution, $n_\lambda = (e^{\beta\hbar\omega_\lambda} - 1)^{-1}$, where the nuclear quantum effect can be turned off by taking the high-temperature limit of Eq. 4.3. The fitting to the model Hamiltonian used the temperature-dependent effective potential method (TDEP) [37, 53]. With thermal displacements from Eq. 4.2 and Eq. 4.3, we refer to our temperature-dependent calculations as the stochastically-initialized temperature-dependent effective potential method (s-TDEP). This method circumvents the issue of expensive computational resources required of *ab initio* molecular-dynamics (AIMD), replacing AIMD with a Monte Carlo sampling of atomic positions and momentum near equilibrium positions [53, 54]. The quasiharmonic model was calculated with 0 K configurations at the respective volumes for a minimized quasiharmonic free energy [40].

Phonon self-energies

The phonon self-energy part, correction to phonon energies from many-body interactions, is comprised of real and imaginary contributions,

$$\Sigma_\lambda = \Delta_\lambda + i\Gamma_\lambda. \quad (4.4)$$

Phonon scattering rates, their lifetimes, are related to the imaginary part of the self-energy ($\frac{1}{\tau_\lambda} = 2\Gamma_\lambda$) for mode λ evaluated at the harmonic fre-

quency $[\omega]$. The imaginary part of the self-energy from many-body perturbation theory is

$$\begin{aligned} \Gamma_\lambda(\Omega) &= \frac{\hbar\pi}{16} \sum_{\lambda\lambda'} |\Phi_{\lambda\lambda\lambda'}|^2 \\ &\times \left\{ (n_\lambda + n_{\lambda'} + 1) \delta(\Omega - \omega_\lambda - \omega_{\lambda'}) + (n_\lambda - n_{\lambda'}) \right. \\ &\times \left. [\delta(\Omega - \omega_\lambda + \omega_{\lambda'}) - \delta(\Omega + \omega_\lambda - \omega_{\lambda'})] \right\}. \end{aligned} \quad (4.5)$$

The $\Omega (= E/\hbar)$ is the probing energy and the delta functions conserve energy and momentum and sum over all possible three-phonon interactions between modes. The $\Phi_{\lambda\lambda\lambda'}$ is the three-phonon matrix elements the Fourier transform of the third-order component of the interatomic potential (Eq. 4.6),

$$\begin{aligned} \Phi_{\lambda\lambda\lambda'} &= \sum_{ijk} \sum_{\alpha\beta\gamma} \frac{\epsilon_\lambda^{i\alpha} \epsilon_{\lambda'}^{j\beta} \epsilon_{\lambda''}^{k\gamma}}{\sqrt{m_i m_j m_k} \sqrt{\omega_\lambda \omega_{\lambda'} \omega_{\lambda''}}} \\ &\times \Phi_{ijk}^{\alpha\beta\gamma} e^{i\vec{q}\cdot\vec{r}_i + i\vec{q}'\cdot\vec{r}_j + i\vec{q}''\cdot\vec{r}_k}, \end{aligned} \quad (4.6)$$

where the constants are as previously described and \vec{r}_i is the lattice vector associated with atom i . The real part of the self-energy is calculated through a Kramers-Kronig transformation of the imaginary part

$$\Delta(\Omega) = \frac{1}{\pi} \int d\omega \frac{\Gamma(\omega)}{\omega - \Omega}. \quad (4.7)$$

Ab initio calculated phonon-self energies used second and third order force constants with temperature (s-TDEP) and at 0 K for the quasi-harmonic

model (4). Note, this quasiharmonic model, still incorporates pure anharmonicity through the third-order force constants, but is different in nature from DFT calculations which include the true temperature-dependent forces on atoms.

Thermal conductivity

Using perturbation theory, thermal conductivities for both force constants from experimental data and *ab initio* calculated force constants were obtained by iteratively solving the full Boltzmann transport equation (BTE) on a $90 \times 90 \times 90$ q -point grid [18]. The only inputs are the second and third order force constants. The momentum conservation is exactly fulfilled, and energy conservation was employed with the tetrahedron method [57]. Thermal conductivity was converged with respect to q -point grid density to within 0.01%. Pure anharmonicity, from phonon-phonon interactions, and isotope scattering in the natural distribution were included [58].

$$\kappa_{\alpha\alpha} = \frac{1}{V} \sum_{\vec{q}s} C_{\vec{q}s} v_{\alpha\vec{q}s}^2 \tau_{\alpha\vec{q}s} \quad (4.8)$$

References

- ¹L.-D. Zhao, S.-H. Lo, Y. Zhang, H. Sun, G. Tan, C. Uher, C. Wolverton, V. P. Dravid, and M. G. Kanatzidis, "Ultralow thermal conductivity and high thermoelectric figure of merit in SnSe crystals", *Nature* **508**, 373–377 (2014).
- ²M. A. Green, J. Zhao, A. Wang, P. J. Reece, and M. Gal, "Efficient silicon light-emitting diodes.", *Nature* **412**, 805–808 (2001).
- ³A. I. Hochbaum, R. Chen, R. D. Delgado, W. Liang, E. C. Garnett, M. Najarian, A. Majumdar, and P. Yang, "Enhanced thermoelectric performance of rough silicon nanowires", *Nature* **451**, 163–167 (2008).
- ⁴J. Graetz, C. C. Ahn, R. Yazami, and B. Fultz, "Highly Reversible Lithium Storage in Nanostructured Silicon", *Electrochemical and Solid-State Letters* **6**, A194–4 (2003).
- ⁵Y. Cui, Z. Zhong, D. Wang, W. U. Wang, and C. M. Lieber, "High Performance Silicon Nanowire Field Effect Transistors", *Nano Letters* **3**, 149–152 (2003).
- ⁶A. I. Boukai, Y. Bunimovich, J. Tahir-Kheli, J.-K. Yu, W. A. Goddard III, and J. R. Heath, "Silicon nanowires as efficient thermoelectric materials", *Nature* **451**, 168–171 (2008).
- ⁷H. A. Atwater and A. Polman, "Plasmonics for improved photovoltaic devices", *Nature Publishing Group* **9**, 205–213 (2010).
- ⁸B. Tian, X. Zheng, T. J. Kempa, Y. Fang, N. Yu, G. Yu, J. Huang, and C. M. Lieber, "Coaxial silicon nanowires as solar cells and nanoelectronic power sources", *Nature* **449**, 885–889 (2007).
- ⁹L. Tsybeskov, S. P. Dutttagupta, K. D. Hirschman, P. M. Fauchet, K. L. Moore, and D. G. Hall, "Room-temperature photoluminescence and electroluminescence from Er-doped silicon-rich silicon oxide", *Applied Physics Letters* **70**, 1790–1792 (1997).
- ¹⁰A. J. Minnich, M. S. Dresselhaus, Z. F. Ren, and G. Chen, "Bulk nanostructured thermoelectric materials: current research and future prospects", *Energy & Environmental Science* **2**, 466–14 (2009).
- ¹¹P. D. Maycock, "Thermal conductivity of silicon, germanium, III-V compounds and III-V alloys", *Solid-State Electronics* **10**, 161–168 (1967).

- ¹²C. J. Glassbrenner and G. A. Slack, “Thermal conductivity of silicon and germanium from 3 K to the melting point”, *Physical Review* **134**, A1058–A1069 (1964).
- ¹³D. G. Cahill, P. V. Braun, G. Chen, D. R. Clarke, S. Fan, K. E. Goodson, P. Keblinski, W. P. King, G. D. Mahan, A. Majumdar, H. J. Maris, S. R. Phillpot, E. Pop, and L. Shi, “Nanoscale thermal transport. II. 2003–2012”, *Applied Physics Reviews* **1**, 011305–46 (2014).
- ¹⁴A. J. Minnich, “Determining Phonon Mean Free Paths from Observations of Quasiballistic Thermal Transport”, *Physical Review Letters* **109**, 141–5 (2012).
- ¹⁵G. Chen, “Thermal conductivity and ballistic-phonon transport in the cross-plane direction of superlattices”, *Physical Review B* **57**, 14958–14973 (1998).
- ¹⁶D. A. Broido, A. Ward, and N. Mingo, “Lattice thermal conductivity of silicon from empirical interatomic potentials”, *Physical Review B* **72**, 13521–8 (2005).
- ¹⁷J. Garg, N. Bonini, B. Kozinsky, and N. Marzari, “Role of Disorder and Anharmonicity in the Thermal Conductivity of Silicon-Germanium Alloys: A First-Principles Study”, *Physical Review Letters* **106**, 045901–4 (2011).
- ¹⁸D. A. Broido, M. Malorny, G. Birner, N. Mingo, and D. A. Stewart, “Intrinsic lattice thermal conductivity of semiconductors from first principles”, *Applied Physics Letters* **91**, 231922–4 (2007).
- ¹⁹N. Shulumba, O. Hellman, and A. J. Minnich, “Intrinsic localized mode and low thermal conductivity of PbSe”, *Physical Review B* **95**, 781–9 (2017).
- ²⁰A. Henry and G. Chen, “High Thermal Conductivity of Single Polyethylene Chains Using Molecular Dynamics Simulations”, *Physical Review Letters* **101**, 235502–4 (2008).
- ²¹R. Peierls, “Zur kinetischen Theorie der Wärmeleitung in Kristallen”, *Annalen der Physik* **395**, 1055–1101 (1929).
- ²²T. Feng and X. Ruan, “Quantum mechanical prediction of four-phonon scattering rates and reduced thermal conductivity of solids”, *Physical Review B* **93**, 045202–10 (2016).
- ²³K. Esfarjani, G. Chen, and H. T. Stokes, “Heat transport in silicon from first-principles calculations”, *Physical Review B* **84**, 141–11 (2011).

- ²⁴S. G. Volz and G. Chen, “Molecular-dynamics simulation of thermal conductivity of silicon crystals”, *Phys. Rev. B* **61**, 2651–2656 (2000).
- ²⁵D. S. Kim, O. Hellman, J. Herriman, H. L. Smith, J. Y. Y. Lin, N. Shulumba, J. L. Niedziela, C. W. Li, D. L. Abernathy, and B. Fultz, “A nuclear quantum effect with pure anharmonicity and the anomalous thermal expansion of silicon”, *Proc. Natl. Acad. Sci. U.S.A.* (2018) [10.1073/pnas.1707745115](https://doi.org/10.1073/pnas.1707745115),
- ²⁶D. S. Kim, H. L. Smith, J. L. Niedziela, C. W. Li, D. L. Abernathy, and B. Fultz, “Phonon anharmonicity in silicon from 100 to 1500 K”, *Phys. Rev. B* **91**, 014307 (2015) [10.1103/PhysRevB.91.014307](https://doi.org/10.1103/PhysRevB.91.014307),
- ²⁷O. Delaire, J. Ma, K. Marty, A. F. May, and M. A. McGuire, “Giant anharmonic phonon scattering in PbTe”, *Nature Materials* (2011).
- ²⁸G. Lang, K. Karch, M. Schmitt, P. Pavone, A. P. Mayer, R. K. Wehner, and D. Strauch, “Anharmonic line shift and linewidth of the raman mode in covalent semiconductors”, *Phys. Rev. B* **59**, 6182 (1999).
- ²⁹S. Narasimhan and D. Vanderbilt, “Anharmonic self-energies of phonons in silicon.”, *Phys. Rev. B* **43**, 4541–4544 (1991).
- ³⁰A. Debernardi, S. Baroni, and E. Molinari, “Anharmonic Phonon Lifetimes in Semiconductors from Density-Functional Perturbation Theory”, *Physical Review Letters* **75**, 1819–1822 (1995).
- ³¹J. H. Parker, D. W. Feldman, and M. Ashkin, “Raman Scattering by Silicon and Germanium”, *Physical Review* **155**, 712–714 (1967).
- ³²P. G. Klemens, “Anharmonic Decay of Optical Phonons”, *Physical Review* **148**, 845–848 (1966).
- ³³D. L. Abernathy, M. B. Stone, M. J. Loguillo, M. S. Lucas, O. Delaire, X. Tang, J. Y. Y. Lin, and B. Fultz, “Design and operation of the wide angular-range chopper spectrometer ARCS at Spallation Neutron Source”, *Rev. Sci. Instrum.* **83**, 015114 (2012).
- ³⁴H. R. Shanks, P. D. Maycock, P. H. Sidles, and G. C. Danielson, “Thermal conductivity of silicon from 300 to 1400 K”, *Physical Review* **130**, 1743–1748 (1963).
- ³⁵W. Fulkerson, J. P. Moore, R. K. Williams, R. S. Graves, and D. L. McElroy, “Thermal Conductivity, Electrical Resistivity, and Seebeck Coefficient of Silicon from 100 to 1300 K”, *Physical Review* **167**, 765–782 (1968).

- ³⁶O. Hellman, I. A. Abrikosov, and S. I. Simak, “Lattice dynamics of anharmonic solids from first principles”, *Physical Review B* **84**, 180301–4 (2011).
- ³⁷O. Hellman and I. A. Abrikosov, “Temperature-dependent effective third-order interatomic force constants from first principles”, *Phys. Rev. B* **88**, 144301 (2013) [10.1103/PhysRevB.88.144301](https://doi.org/10.1103/PhysRevB.88.144301).
- ³⁸N. Shulumba, O. Hellman, and A. J. Minnich, “Intrinsic localized mode and low thermal conductivity of PbSe”, *Physical Review B* **95**, 014302–9 (2017).
- ³⁹A. Debernardi and S. Baroni, “Third-order density-functional perturbation theory: A practical implementation with applications to anharmonic couplings in Si”, *Solid State Communications* **91**, 813–816 (1994).
- ⁴⁰D. S. Kim, H. L. Smith, J. L. Niedziela, C. W. Li, D. L. Abernathy, and B. Fultz, “Phonon anharmonicity in silicon from 100 to 1500 K”, *Phys. Rev. B* **91**, 014307 (2015).
- ⁴¹L. Lindsay, D. A. Broido, and T. L. Reinecke, “First-Principles Determination of Ultrahigh Thermal Conductivity of Boron Arsenide: A Competitor for Diamond?”, *Physical Review Letters* **111**, 025901–5 (2013).
- ⁴²“Phase Transitions in Materials Brent Fultz”, *MRS Bulletin* **41**, 261–261 (2016).
- ⁴³M. B. Stone, J. L. Niedziela, M. J. Loguillo, M. A. Overbay, and D. L. Abernathy, “A radial collimator for a time-of-flight neutron spectrometer”, *Review of Scientific Instruments* **85**, 085101 (2014).
- ⁴⁴*Mantid (2013): manipulation and analysis toolkit for instrument data.; mantid project*, 2013.
- ⁴⁵O. Arnold, J. C. Bilheux, J. M. Borreguero, A. Buts, S. I. Campbell, L. Chapon, M. Doucet, N. Draper, R. F. Leal, M. A. Gigg, V. E. Lynch, A. Markvardsen, D. J. Mikkelsen, R. L. Mikkelsen, R. Miller, K. Palmen, P. Parker, G. Passos, T. G. Perring, P. F. Peterson, S. Ren, M. A. Reuter, A. T. Savici, J. W. Taylor, R. J. Taylor, R. Tolchenov, W. Zhou, and J. Zikovsky, “Mantid—Data analysis and visualization package for neutron scattering and μ SR experiments”, *Nucl. Instrum. Meth. A* **764**, 156–166 (2014).
- ⁴⁶G. Kresse and J. Furthmüller, “Efficiency of ab-initio total energy calculations for metals and semiconductors using a plane-wave basis set”, *Comput. Mater. Sci.* **6**, 15–50 (1996).

- ⁴⁷G. Kresse and J. Hafner, “Ab initio molecular dynamics for liquid metals”, *Phys. Rev. B* **47**, 558–561 (1993).
- ⁴⁸G. Kresse and J. Hafner, “Ab initio molecular-dynamics simulation of the liquid-metal-amorphous-semiconductor transition in germanium”, *Phys. Rev. B* **49**, 14251–14269 (1994) [10.1103/PhysRevB.49.14251](https://doi.org/10.1103/PhysRevB.49.14251).
- ⁴⁹X. Gonze and C. Lee, “Dynamical matrices, born effective charges, dielectric permittivity tensors, and interatomic force constants from density-functional perturbation theory”, *Phys. Rev. B* **55**, 10355–10368 (1997).
- ⁵⁰R. Armiento and A. E. Mattsson, “Functional designed to include surface effects in self-consistent density functional theory”, *Phys. Rev. B* **72**, 085108–5 (2005).
- ⁵¹A. E. Mattsson and R. Armiento, “Implementing and testing the AM05 spin density functional”, *Phys. Rev. B* **79**, 155101–13 (2009).
- ⁵²A. E. Mattsson, R. Armiento, J. Paier, G. Kresse, J. M. Wills, and T. R. Mattsson, “The AM05 density functional applied to solids”, *The Journal of Chemical Physics* **128**, 084714–12 (2008).
- ⁵³O. Hellman, P. Steneteg, I. A. Abrikosov, and S. I. Simak, “Temperature dependent effective potential method for accurate free energy calculations of solids”, *Phys. Rev. B* **87**, 104111 (2013).
- ⁵⁴I. Errea, M. Calandra, and F. Mauri, “Anharmonic free energies and phonon dispersions from the stochastic self-consistent harmonic approximation: Application to platinum and palladium hydrides”, *Phys. Rev. B* **89**, 064302–16 (2014).
- ⁵⁵D. C. Wallace, *Thermodynamics of Crystals* (Wiley, New York, 1972).
- ⁵⁶M. T. Dove, *Introduction to Lattice Dynamics* (Cambridge University Press, Oct. 1993).
- ⁵⁷G. Lehmann and M. Taut, “On the Numerical Calculation of the Density of States and Related Properties”, *physica status solidi (b)* **54**, 469–477 (1972).
- ⁵⁸S. Tamura, “Isotope Scattering of Dispersive Phonons in Ge”, *Physical Review B (Condensed Matter)* **27**, 858–866 (1983).

Chapter 5

FINAL REMARKS AND FUTURE DIRECTIONS

This thesis work benefited from a synchronous approach to understanding the theoretical model needed to accurately determine entropy, thermal expansion, and thermal conductivity of silicon. Silicon, does not exhibit “giant” or “massive” anharmonicities in the absolute sense, but show property altering deviations from the harmonic and quasiharmonic approximated phonon frequency changes with temperature. Pure anharmonicities whether it be coupled to nuclear quantum effects at low temperatures, or as the dominant driving force for finite temperature changes should be important for thermal characterization of materials and optimal applications.

Without the systematic wide temperature range study, the majority of this work would have been overlooked. The possible error in calculating high temperature quasiharmonic entropy was not surprising initially. The surprise came from the mechanism behind these increasing errors. The microscopic mechanism of shifts in low energy modes of the wrong sign motivated us to revisit silicon’s anomalous thermal expansion behavior. The quasiharmonic theory predicts incorrect phonon frequency shifts and therefore is incorrect, at all temperatures. The leading-order terms of both quasiharmonicity and anharmonicity are linear in temperature [1], so if anharmonicity is important at high temperatures, it can have the same relative importance at low temperatures,

too. Thus, the accepted quasiharmonic model is incorrect, but it is shown that it predicts the macroscopic behavior correctly. For thermal expansion, the cancellation of shifts of various modes average out the differences in total entropy at lower temperatures as well as at high T.

The thermal conductivity at high temperatures is mediated on the other hand by large softening of phonons competing with their intrinsic increase of heat capacity. These pure anharmonicities, and nuclear quantum effects should prove to be important for many materials and its thermal properties. Macroscopic bulk properties may not always be a fail proof method for validating theoretical models alone. Precise inelastic neutron scattering experiments and state-of-the-art *ab initio* calculations will be a useful in thermal characterization of materials based on anharmonicities and nuclear quantum effects.

Recent progress in understanding complexities in vibrational entropy, and thermodynamic properties opens new ways to accurately describe thermal properties over a broad range of materials. Another problem to address is the temperature dependence of elasticity. Although simple explanations for temperature-dependent elastic constants seem trivial [2–5], due to the nature of silicon's strong covalent bonds, understanding how elasticity is effected by phonon-phonon interactions and any deviations from linearity will prove to be interesting especially for micro-mechanic applications [6, 7]. Single crystal inelastic neutron scattering data-sets could prove to be a perfect way to sample sound velocities in all directions especially anisotropic solids. Sampling all directions to study anisotropy could be a promising method of understanding strength of materials with temperature, pressure, or in other applied fields

through time-of-flight inelastic neutron scattering.

A closer look at neutron scattering with materials on these large data sets of accurate and high statistical quality allows for a better understanding of anharmonic interference. Anharmonic interference is from the constructive or destructive interference of scattered neutrons with itself as the cubic term of anharmonicity allows for either one phonon scattering to two created phonons or two phonons annihilated with the creation of one. This phase difference will cause a change in scattered intensity ($S(\mathbf{q}, \varepsilon)$) across various points in \mathbf{q} -space. Anharmonic interference has been theoretically solved previously with comparisons to historical scattering experiments [8–12]. But, the impact of these effects on the phonon spectrum intensity between various Brillouin zones are typically ignored and deserves a more deliberate examination.

In depth studies on nuclear quantum effects and its role in negative thermal expansion are also promising research directions. Real-space interpretations or mechanisms would prove to be interesting as can be levered for future quantitative analysis and high-throughput engineering. Other materials that show anomalous thermal expansion often have light elements where these effects become more pronounced [13–17]. The s-TDEP method has shown adequate representations of atomic densities compared to other path-integral methods even for Hydrogen-gas, but these methods are in need of further testing. Other examples of anomalous thermal expansion behavior system like solid-ice (H_2O) would be strong candidate test materials, both experimentally and computationally.

Another major theme that deserves more attention is changes of lattice dynamics through doping and defects. Doped silicon shows large effects on bulk moduli, and was also found to increase electron-phonon couplings. Comparing how these effects from type of dopant to Fermi level engineering seems to be a good future research direction [18, 19]. Large anharmonic effects were calculated for atoms in close proximity to defects [20, 21]. Anharmonicity was shown to affect the thermal conductivity and the bulk modulus through doping have been studied and great advancements were made through modern DFT methods [22, 23]. But experimental evidence of the microscopic mechanisms is still not available. Significant advancements have been made in understanding the electrical properties of these materials, but the thermal properties and the effects on electronic properties are not as well understood and should be studied.

Other effects of geometry will be vital for understanding advanced materials that are typically in planar, or the so called 2D geometries. Low-dimensional materials such as bismuth-based compounds, and transition metal dichalcogenides show promise due to exotic electronic and transport properties [24–27]. Understanding the thermal properties and inter-planar effects of phonons, and electron-phonon interactions will provide answers to how exotic properties are physically governed. Currently, I am working on understanding the thermodynamics of graphite, single-walled nanotubes, and carbon diamond. We have measured phonon density of states in graphite from 7 to 1400 K and observed large phonon shifts unaccountable by the quasiharmonic model. For graphite in particular, there are reported phonon anharmonicities and electron-

phonon interactions in Raman and IR modes [28, 29]. But an extensive study on the temperature-dependence of all phonon modes is lacking. Surprisingly, the anharmonicities and electron-phonon interactions are avoided in the calculation of thermodynamic free energies and thermal expansion [29]. Accounting for van der Waal forces computationally and understanding the effects on lattice dynamics are also not well understood. Although anharmonic shifts and broadening are observed experimentally, the computational limitations at the moment regarding van der Waals forces need to be addressed passed analytical models.

There are still many open question of how geometry, dimensionality, and bond strength through variations in composition, doping, defects interplaner effects, and many-body interactions contribute to the changes in the thermodynamics, and other materials properties. I am excited in the belief that the community will bring much needed progress in the next decades.

References

- ¹A. A. Maradudin and A. E. Fein, "Scattering of Neutrons by an Anharmonic Crystal", *Phys. Rev.* **128**, 2589–2608 (1962).
- ²H. J. McSkimin and P. Andreatch, "Elastic Moduli of Silicon vs Hydrostatic Pressure at 25.0 C and 195.8 C", **35**, 2161–6 (1964).
- ³H. J. McSkimin, W. L. Bond, E. Buehler, and G. K. Teal, "Measurement of the Elastic Constants of Silicon Single Crystals and Their Thermal Coefficients", *Physical Review* **83**, 1080–1080 (1951).
- ⁴A. R. Ruffa, "Temperature dependence of the elastic shear moduli of the cubic metals", *Physical Review B* **16**, 2504–2514 (1977).
- ⁵R. Perez and P. Gumbsch, "An Ab initio study of the cleavage anisotropy in silicon", *Acta Materialia* **48**, 4517–4530 (2000).
- ⁶B. Redding, S. Shi, T. Creazzo, E. Marchena, and D. W. Prather, "Design and characterization of silicon nanocrystal microgear resonators", *Photonics and Nanostructures - Fundamentals and Applications* **8**, 177–182 (2010).
- ⁷B. N. Jaya, J. M. Wheeler, J. Wehrs, J. P. Best, R. Soler, J. Michler, C. Kirchlechner, and G. Dehm, "Microscale Fracture Behavior of Single Crystal Silicon Beams at Elevated Temperatures", *Nano Letters* **16**, 7597–7603 (2016).
- ⁸J. Kokkedee, "Anharmonic effects in the coherent scattering of neutrons by crystals: A formal treatment of shift and width of the peaks in the scattering spectrum", *Physica* **28**, 374–408 (1962).
- ⁹R. A. Cowley and W. J. L. Buyers, "Asymmetries in the scattering of X-rays and neutrons by crystals", *Journal of Physics C: Solid State Physics* **2**, 2262–2272 (1969).
- ¹⁰V. Ambegaokar, J. M. Conway, and G. Baym, "Inelastic scattering of neutrons by anharmonic crystals", *Solid State Communications* **1**, 172–173 (1963).
- ¹¹H. R. Glyde, "Interference Effects in Neutron and X Ray Scattering", *Can. J. Phys.* **52**, 2281 (1974).
- ¹²W. J. L. Buyers, G. Dolling, G. Jacucci, M. L. Klein, and H. R. Glyde, "Anharmonic phonon response in aluminum: A neutron-scattering test of computer-simulation calculations", *Physical Review B (Condensed Matter)* **20**, 4859–4863 (1979).

- ¹³D. Chandler, "Exploiting the isomorphism between quantum theory and classical statistical mechanics of polyatomic fluids", *The Journal of Chemical Physics* **74**, 4078–19 (1981).
- ¹⁴B. Pamuk, J. M. Soler, R. Ramirez, C. P. Herrero, P. W. Stephens, P. B. Allen, and M. V. Fernandez-Serra, "Anomalous Nuclear Quantum Effects in Ice", *Physical Review Letters* **108**, 193003–5 (2012).
- ¹⁵J. C. Noya, C. P. Herrero, and R. Ramirez, "Thermodynamic properties of c-Si derived by quantum path-integral Monte Carlo simulations", *Physical Review B* **53**, 9869–9875 (1996).
- ¹⁶J. A. Morrone and R. Car, "Nuclear Quantum Effects in Water", *Physical Review Letters* **101**, 017801–4 (2008).
- ¹⁷D. Marx and M. Parrinello, "Ab initio path integral molecular dynamics: Basic ideas", *The Journal of Chemical Physics* **104**, 4077 (1996).
- ¹⁸B. Liao, B. Qiu, J. Zhou, S. Huberman, K. Esfarjani, and G. Chen, "Significant Reduction of Lattice Thermal Conductivity by the Electron-Phonon Interaction in Silicon with High Carrier Concentrations: A First-Principles Study", *Physical Review Letters* **114**, 115901–6 (2015).
- ¹⁹J. J. Hall, "Electronic Effects in the Elastic Constants of Silicon", *Physical Review* **161**, 756–761 (1967).
- ²⁰A. Glensk, B. Grabowski, T. Hickel, and J. Neugebauer, "Breakdown of the Arrhenius Law in Describing Vacancy Formation Energies: The Importance of Local Anharmonicity Revealed by Ab initio Thermodynamics", *Physical Review X* **4**, 011018–9 (2014).
- ²¹A. Glensk, B. Grabowski, T. Hickel, and J. Neugebauer, "Understanding Anharmonicity in fcc Materials: From its Origin to ab initio Strategies beyond the Quasiharmonic Approximation", *Physical Review Letters* **114**, 195901–5 (2015).
- ²²S. Lany and A. Zunger, "Assessment of correction methods for the band-gap problem and for finite-size effects in supercell defect calculations: Case studies for ZnO and GaAs", *Physical Review B* **78**, 235104–25 (2008).
- ²³P. V. C. Medeiros, S. S. Tsirkin, S. Stafstrom, and J. Bjork, "Unfolding spinor wave functions and expectation values of general operators: Introducing the unfolding-density operator", **91**, 041116–5 (2015).

- ²⁴Q. H. Wang, K. Kalantar-Zadeh, A. Kis, J. N. Coleman, and M. S. Strano, “Electronics and optoelectronics of two-dimensional transition metal dichalcogenides”, *Nature* **7**, 699–712 (2012).
- ²⁵X. Zhang, X.-F. Qiao, W. Shi, J.-B. Wu, D.-S. Jiang, and P.-H. Tan, “Phonon and Raman scattering of two-dimensional transition metal dichalcogenides from monolayer, multilayer to bulk material”, *Chemical Society Reviews* **44**, 2757–2785 (2015).
- ²⁶F.-f. Zhu, W.-j. Chen, Y. Xu, C.-l. Gao, D.-d. Guan, C.-h. Liu, D. Qian, S.-C. Zhang, and J.-f. Jia, “Epitaxial growth of two-dimensional stanene”, *Nature Materials* **14**, 1020–1025 (2015).
- ²⁷B. Rasche, A. Isaeva, M. Ruck, S. Borisenko, V. Zabolotnyy, B. Buchner, K. Koepernik, C. Ortix, M. Richter, and J. van den Brink, “Stacked topological insulator built from bismuth-based graphene sheet analogues”, *Nature Materials* **12**, 422–425 (2013).
- ²⁸P. Giura, N. Bonini, G. Creff, J. B. Brubach, P. Roy, and M. Lazzeri, “Temperature evolution of infrared- and Raman-active phonons in graphite”, **86**, 121404–4 (2012).
- ²⁹N. Mounet and N. Marzari, “First-principles determination of the structural, vibrational and thermodynamic properties of diamond, graphite, and derivatives”, **71**, 205214–14 (2005).